

REPUBLIC OF CAMEROON
REPUBLIQUE DU CAMEROUN



DEPARTMENT OF CIVIL ENGINEERING
DEPARTEMENT DE GENIE CIVIL

MINISTRY OF HIGHER EDUCATION
MINISTERE DE L'ENSEIGNEMENT SUPERIEURE



UNIVERSITÀ
DEGLI STUDI
DI PADOVA

DEPARTMENT OF CIVIL, ARCHITECTURAL
AND ENVIRONMENTAL ENGINEERING

**FEM ANALYSIS APPLIED TO THE STUDY
OF STRESS DIFFUSION IN THE BASE PLATE
OF STEEL STRUCTURES: CASE OF A STEEL
WAREHOUSE AT ODZA IN YAOUNDE**

*A thesis submitted in partial fulfilment of the requirement for the degree of Master in
Engineering (Meng) in Civil Engineering*

Curriculum: Structural Engineering

Presented by:

DEFO WABO Jordan Stevy

Student Number: 16TP21080

Supervised by:

Prof. Carmelo MAJORANA

Co-supervised by:

Dr. Eng Guillaume Hervé POH'SIE

Eng. Giuseppe CARDILLO

Eng. Joseph FOTSO

Academic year: 2020 - 2021

DEDICATION

*To my beloved mother,
Mrs KENGNE DEFO Sylvie Bertin*

ACKNOWLEDGEMENTS

This piece of work would not have been completed without the critical efforts of individuals who contributed directly and/or indirectly to its realization. I wish to express my sincere gratitude to:

- The **president of the jury** for the honor of presiding this jury;
- The **Examiner** of the jury for accepting to bring his criticisms and observations to better this work;
- My supervisors **Prof. Eng. Carmelo MAJORANA, Dr. Eng. Guillaume Hervé POH'SIE, Eng. Giuseppe CARDILLO and Eng. Joseph FOTSO** for all the guidance, the advices and the patience towards me throughout the completion of this work;
- **Professor George NKENG and Professor Carmelo MAJORANA** for all their academic and administrative support during these five years under the tutelage of the National Advanced School of Public Works (NASPW) in this Master's in Engineering (Meng) program in partnership with the University of Padua in Italy;
- The vice-director of ENSTP, **Dr. BWEMBA Charles** for his perpetual help and advices during our sojourn in this school;
- **Professor MBESSA Michel**, the head of the Civil Engineering department, for his constant tutoring and counseling;
- The entirety of the teaching staff of the National Advanced School of Public Works and University of Padua for their awesome teaching and study advices they gave us constantly;
- My family and more especially to my mother **KENGNE DEFO SYLVIE BERTIN** for her warm-hearted support, consistent encouragements, education and financial support during these years.
- All my classmates and friends of the 7th batch of Master's in Engineering (Meng) of the National Advanced School of Public Works. They represent a family and were a source of inspiration and motivation.

LIST OF ABBREVIATIONS AND SYMBOLS

SYMBOLS

AISC	American Institute of Steel Construction
CAE	Computer Aided Engineering
CDP	Concrete Damage Plasticity
CEN	European Committee for Standardization
CSI	Computer and Structures Incorporated
EN	European Norm
FEA	Finite Element Analysis
FEM	Finite Element Method
HVAC	Heating, Ventilation and Air Conditioning
LRFD	Load and Resistance Factor Design
NCCI	National Correct Coding Initiative
SAP	Structural Analysis Program
SCI	Steel Construction Info
SCI	Steel Construction Info
SLS	Serviceability Limit State
ULS	Ultimate Limit State

ABBREVIATIONS

A	Area of cross section
A_a	Area of the steel section
A_b	Area of bolt
A_{eff}	Effective area
A_m	Surface area of the member per unit length
A_p	Area of base plate
A_t	Total area of enclosure
A_v	Shear area of the steel profile
A_s	Tensile stress area of the bolt
c_{dir}	Directional factor
$c_e(z)$	Exposure factor
c_{season}	Seasonal factor
$c_o(z)$	Orography factor
$c_r(z)$	Roughness factor
c_{pe}	External pressure coefficient
c_{pi}	Internal pressure coefficient
d	Bolt diameter
d_0	Diameter of bolt holes
d_w	Diameter of the washer or the width across points of the bolt head
E	Young modulus
e_c	Edge distance of the column flange
e_p	Edge distance of the end plate
e_1	End distance from the center of the bolt hole to the adjacent end part measured in the direction of load transfer
e_2	End distance from the center of a bolt to the adjacent edge end, measured at right angles to the direction of load transfer
$F_{b,Rd}$	Bearing resistance
f_{cd}	Design compressive strength of concrete
f_{ck}	Characteristic compressive cylinder strength of concrete

**FEM ANALYSIS APPLIED TO THE STUDY OF STRESS
DIFFUSION IN THE BASEPLATES OF STEEL STRUCTURES**

$F_{c,Rd}$	Resistance of the column web in the compressed zone
$F_{T,1,Rd}, F_{T,2,Rd}, F_{T,3,Rd}$	Design resistances for the failure modes 1,2 and 3
f_{cm}	Cylinder compressive strength
f_y	Yielding strength
f_u	Ultimate tensile strength
f_{ub}	Ultimate tensile strength of the bolt
$F_{t,Rd}$	Traction resistance of the bolt
$F_{v,Rd}$	Shear resistance of the bolt
G_k	Permanent loads
h_w	Height of web
h_p	Height of the plate
H	Height
I_v	Turbulence intensity
i	Radius of gyration
i_s	Influence width
k_T	Terrain factor
k_1	Turbulence factor
l_{eff}	Effective length of the equivalent T-stub
$M_{b,Rd}$	Lateral torsional buckling resistance
$M_{c,Rd}$	Resisting moment of the beam
M_{cr}	Elastic critical moment for lateral torsional buckling
M_{Ed}	Design moment
$M_{el,Rd}$	Elastic resisting moment
$M_{pl,Rd}$	Plastic resisting moment
$M_{j,u}$	Ultimate bending resistance (By Picard and Beaulieu)
$M_{pl,i,Rd}$	Plastic resistance moment of the equivalent T-stub for different modes
$N_{b,Rd}$	Buckling resistance
$N_{c,Rd}$	Resistance to axial compression

N_{Ed}	Design axial load
n_i	Number of bolt rows
$N_{pl,Rd}$	Design plastic resistance of gross cross section
N_{SLS}	Axial force at serviceability limit state
$N_{u,Rd}$	Design ultimate resistance of the net cross section at holes for fasteners
p_1	Spacing between the centers of bolts in a line in the direction of load transfer
p_2	Spacing between the centers of bolts in a line at right angles to the direction of load transfer
q_b	Basic velocity pressure
Q_k	Live loads
$q_p(z)$	Peak velocity pressure
t_f	Thickness of the flange
t_p	Thickness of the plate
t_w	Web thickness
u	Perpendicular distance from the edge of the beam flange to the edge of the column (lever arm)
V_b	Basic wind velocity
$v_m(z)$	Mean wind velocity
V_{Ed}	Design shear
V_{Rd}	Shear resistance of the connectors
$V_{c,Rd}$	Design shear resistance
$V_{pl,Rd}$	Shear resistance of the beam
w_c	Width of column
W_{el}	Elastic section modulus
W_{eff}	Effective section modulus
w_i	Internal pressure coefficient
w_e	External pressure coefficient
W_{pl}	Plastic section modulus
z_e	Reference height for external pressure

***FEM ANALYSIS APPLIED TO THE STUDY OF STRESS
DIFFUSION IN THE BASEPLATES OF STEEL STRUCTURES***

z_{\min}	Minimum height
z_0	Roughness length
χ	Reduction factor for the relevant buckling mode
χ^{LT}	Reduction factor for lateral-torsional buckling
α_{LT}	Imperfection factor for buckling
$\bar{\lambda}$	Non-dimensional slenderness with respect to z-axis
σ	Compression constraint
$\gamma_{M0}, \gamma_{M1}, \gamma_{M2}$	Partial safety factors
γ	Unit weight
ω	Reduction factor to allow for the possible effects of interaction with shear in the column

ABSTRACT

When a steel column is supported by a footing, it is necessary for the column load to be spread over a sufficient area to keep the footing from being overstressed. Column base plates are one of the most crucial components of steel structures that act as a transfer medium for all the forces and moments from the entire building through the steel column to the foundation. The main objective of this thesis is the study of the diffusion of stress on the base plate of steel structures, which serves as a basis for an attempted prediction of the failure mechanism which will ensue. This study is performed with the help of the non-linear analysis tool ABAQUS. To fulfil this objective, an extensive literature review was presented, summarizing an overview on column base plates, their behavior and studies performed on column base plates. Chapter II is dedicated to the creation of a model of the case study in SAP 2000 taking into account the loading conditions necessary to represent the real behavior. The loadings were used to statically verify the structure according to Eurocode norms. Then, in chapter III, using the general-purpose finite element software ABAQUS, an accurate nonlinear analysis of a column base connection sub-model obtained from the global case study model was performed. Concurrently to the static analysis, the column base model was validated with respect to the static design verification performed. A parametric study was performed on the column base connection model to study the stress diffusion on the base plate under different conditions. The parametric study allowed us to have an understanding of the influence of axial load variation, bending moment variation, anchor bolt position variation and base plate thickness variation on the stress diffusion. The results of the parametric study showed that; the distribution of stress in the base plate under different axial loads follow the same pattern and only vary in magnitude with stress concentration points in the flange-web intersection, the closer the anchor bolts are to the center of the plate, the more distributed the stress is uniformly distributed on the plate, the thicker the base plate, the more averagely distributed the stress is. The attempted predictions of the failure mechanisms are; crushing of the concrete due to high axial forces, anchor bolt pull out due to high bending, base plate tearing at its edge due to the proximity of anchor bolts to the edge. These results obtained from these studies are intended to help structural engineers understand the stress diffusion in stiffened base plates.

Keywords: Steel column baseplate, Finite Element Method, Stress diffusion

RESUME

Les pieds de poteaux ont une influence prépondérante sur la stabilité et la rigidité des constructions métalliques agissant comme un moyen de transfert des sollicitations de l'ensemble du bâtiment vers la fondation. L'objectif principal de cette thèse est l'étude de la diffusion des contraintes sur la platine métallique des structures en acier. Cette étude sert de base à une tentative de prédiction du mécanisme de rupture qui s'ensuivra. Cette étude est réalisée à l'aide de l'outil d'analyse non linéaire ABAQUS. Pour atteindre notre objectif, une revue de littérature a été présentée, résumant un aperçu de leur comportement et des études réalisées sur ces platines. Le chapitre II est consacré à la création d'un modèle du cas d'étude dans SAP 2000 prenant en compte les conditions de chargement nécessaires pour représenter le comportement réel. Les chargements ont été utilisés pour effectuer une vérification statique de la structure selon les normes Eurocode. Ensuite, dans le chapitre III, en utilisant le logiciel d'éléments finis ABAQUS, une analyse non linéaire d'un sous-modèle de connexion de poteau – platine de base obtenu à partir du modèle global a été réalisée. Le modèle de pied de poteau a été validé par rapport à la vérification statique effectuée. Une étude paramétrique a été réalisée sur le modèle de connexion poteau – platine de base pour étudier la diffusion des contraintes sur la platine de base sous différentes conditions de chargement. L'étude paramétrique nous a permis d'appréhender l'influence de la variation de la charge axiale, de la variation du moment, de la variation de la position des boulons d'ancrage et de la variation de l'épaisseur de la platine d'assise sur la diffusion des contraintes. Les résultats de l'étude paramétrique ont montré que ; la répartition des contraintes dans la platine de base sous différentes charges axiales suit le même schéma et ne varie qu'en amplitude, avec les points de concentration des contraintes à l'intersection semelle - âme, plus les boulons d'ancrage sont proches du centre de la platine, plus la contrainte est répartie de manière uniforme sur la platine, plus la platine de base est épaisse, plus la contrainte est uniformément répartie. Les tentatives de prédictions des mécanismes de ruine nous ont permis de proposer ces mécanismes ; écrasement du béton dû à des forces axiales élevées, arrachement des boulons d'ancrage en raison d'une forte flexion, déchirure de la plaque de base à son bord en raison de la proximité des boulons d'ancrage avec le bord. Ces résultats obtenus à partir de ces études sont destinés à aider les ingénieurs en structure à comprendre la diffusion des contraintes dans les plaques de base raidies.

Mots clés : Plaque de base d'un poteau en acier, méthode des éléments finis, diffusion des contraintes.

LIST OF FIGURES

Figure 1.1. Column bases: a) Exposed column base, b) Embedded column base..... 3

Figure 1.2. (a) Column baseplate with shear lug and (b) Column base plate with stiffeners... 4

Figure 1.3. Elements of exposed column base plates..... 4

Figure 1.4. Conventional exposed cross-section column bases: (a) unstiffened H-section column base; (b) stiffened H-column base (Kamperidis, 2016)..... 5

Figure 1.5. Conventional exposed tube column bases; (a) unstiffened tube base; (b) stiffened tube base (Kamperidis, 2016)..... 5

Figure 1.6. Types of anchor bolts a) cast-in-situ anchor bolts, b) hooked bars, c) undercut anchor bolts, d) bonded anchor bolts; e) grouted anchor bolts, f) anchoring to grillage beams 7

Figure 1.7. Theoretical behavior of the base plate..... 9

Figure 1.8. Types of base plate behavior (Adapted from Astaneh et al. 1992)..... 10

Figure 1.9. Moment-Rotation diagram defining the joint behavior..... 12

Figure 1.10. Typical plastic hinge in a steel open section (I-beam) 13

Figure 1.11. Anchor bolts failure in tension: (a) Yielding, (b) and (c) Yielding and fracture (d) Close-up of the fractured surface on the anchor shaft (Gomez et al., 2010) 14

Figure 1.12. Internal force distribution under low, medium and high axial force in initial and collapse stage (Grauvilardell et al., 2005)..... 15

Figure 1.13. (a) Grout crushing (b) Pedestal crushing (c) Pedestal splitting (d) Idealized break out cone..... 16

Figure 1.14. Shear key breakout failure of the concrete [after Gomez et al. (2009)] 17

Figure 1.15. Close-up view of crack in a thick base plate (Lai et al., 2015)..... 18

Figure 1.16. Flexural yielding of both the tension and the compression side of the base plate from various loading regimes, with schematics of ideal imposed and resisting forces (Gomez et al., 2010)..... 19

Figure 1.17. Assumed stress distribution under base plates in Cantilever theory 21

Figure 1.18. Assumed stress distribution under base plate in Fling theory..... 22

Figure 1.19. Assumed stress distribution under base plate in Murry-Stockwell theory 22

Figure 1.20. Assumed stress distribution under base plates in Eurocodes theory 23

Figure 1.21. Assumed stress distribution under base plates in T-Stub method..... 23

Figure 1.22. Diffusion of stress under base plates based on different methods 26

Figure 1.23. Column base plate configuration (Lescouarc'h, 1988) 27

Figure 1.24. Main elements composing an exposed column base plate (Amaral, 2014)..... 28

Figure 2.1. Terrain categories and terrain parameters..... 37

Figure 2.2. Illustration of the exposure factor $C_e(z)$ for $C_0 = 1.0$, $k_1 = 1.0$ (BS EN1991-1-4) 38

Figure 2.3. Pressure acting on surfaces 38

Figure 2.4. Beam shear resisting area 44

Figure 2.5. Buckling curves from Eurocode.....	49
Figure 2.6. Spacing of holes on the plate (EN 1993-1-8, 2005).....	51
Figure 2.7. Connection geometry (SCI P398)	53
Figure 2.8. Portal frame eaves connection with bolted end plate (NCCI, 2008).....	54
Figure 2.9. Complete flange yielding (SCI P398)	54
Figure 2.10. Bolt failure with flange yielding (SCI P398).....	55
Figure 2.11. Bolt failure (SCI P398).....	56
Figure 2.12. Portal frame apex connection with bolted extended end plate (NCCI, 2008) ...	58
Figure 2.13. T-stub of the base plate.....	58
Figure 2.14. Tangent lines on the base plate which determine uplift (Morel, 2005).....	60
Figure 2.15. Scheme of distribution of forces and displacements in column base.....	61
Figure 2.16. ABAQUS Stages of a complete simulation.....	64
Figure 3.1. Location of the Case study.....	71
Figure 3.2. Ware house for stockage at Odza.....	73
Figure 3.3. Site plan portraying the ware house	74
Figure 3.4. Structural floor plan of the ware house	74
Figure 3.5. Structural Plan (3D).....	75
Figure 3.6. Portal frame roof dimensions.....	77
Figure 3.7. Roof plan of the ware house	78
Figure 3.8. Roof span considered for load determination	78
Figure 3.9. Roof areas for wind perpendicular to the ridge.....	80
Figure 3.10. Roof areas for wind parallel to the ridge	80
Figure 3.11. Building model from SAP 2000.....	81
Figure 3.12. Baseplate Stress values for columns 1,2 and 3	87
Figure 3.13. Column base connection geometry	92
Figure 3.14. New position of anchor bolts with respect to the Eurocode	98
Figure 2.18. Column base connection.....	103
Figure 2.19. Interactions in the column base plate	104
Figure 2.20. Anchor embedded region.....	105
Figure 2.21. Axial Force application on column base.....	106
Figure 3.15. Result of stress distribution in the overall model when subjected to design axial force.....	109
Figure 3.16. stress distribution in the IPE column.....	110
Figure 3.17. Stress distribution in stiffeners.....	111
Figure 3.18. The most stressed point of the stiffener.....	111

Figure 3.19. Stress distribution in the anchor bolts of the connection.....	112
Figure 3.20. 2D Stress distribution on the concrete base.....	112
Figure 3.21. 3D stress distribution in the concrete base.....	113
Figure 3.22. Cone Stress distribution in the concrete base.....	114
Figure 3.23. Von-mises stress distribution on the base plate	114
Figure 3.24. Central path under study	115
Figure 3.25. Mises stress variation along the central path	115
Figure 3.26. Stress distribution along the geometrical central line of the base plate.....	117
Figure 3.27. Variation of mises peak stress with axial force.....	118
Figure 3.28. Rotation of the IPE column with respect to its strong axis.....	122
Figure 3.29. Stress distribution on a base plate subjected to bending.....	123
Figure 3.30. Stress distribution in anchor bolts when subjected to bending	123
Figure 3.31. Stress distribution in stiffeners subjected to bending	124
Figure 3.32. Stress distribution in concrete under bending moment action of column base connection.....	124
Figure 3.33. Paths considered for the stress diffusion study under bending action.....	125
Figure 3.34. Variation of stress along line 1 under different bending conditions	126
Figure 3.35. Variation of stress along line 2 under different bending conditions	126
Figure 3.36. Variation of stress along line 3 under different bending conditions	127
Figure 3.37. Stress variation along line 1 in model 2.....	127
Figure 3.38. Stress variation along line 2 in model 2.....	128
Figure 3.39. Stress variation along line 3 in model 2.....	128

LIST OF TABLES

Table 2.1. Eurocodes	34
Table 3.1. Steel material properties (S235JR)	76
Table 3.2. Concrete and reinforcing steel properties.....	76
Table 3.3. Building Data.....	78
Table 3.4. Vertical loads.....	81
Table 3.5. Internal moment and shear force	82
Table 3.6. Properties of IPE 120	82
Table 3.7. Classification of the purlin cross section.....	83
Table 3.8. Design verification of the purlin.....	83
Table 3.9. Moments and Forces on rafter	83
Table 3.10. Properties of IPE 300	84
Table 3.11. Classification of the rafter cross section	84
Table 3.12. Design verifications of the rafter	84
Table 3.13. Column loadings	85
Table 3.14. Critical columns.....	86
Table 3.15. Design verifications of the IPE 300 column.....	87
Table 3.16. Properties of IPE 120	88
Table 3.17. Classification of the IPE 120 column.....	88
Table 3.18. Design verification of the IPE 120 column	88
Table 3.19. Axial force on braces	89
Table 3.20. Properties of L60×60×5	89
Table 3.21. Design verification of the horizontal braces.....	90
Table 3.22. Internal moments and forces in the rafter to column connection	90
Table 3.23. Design verifications of the rafter-column connection.....	90
Table 3.24. Internal actions on rafter to rafter connection	91
Table 3.25. Design verifications of the rafter-rafter connection.....	91
Table 3.26. Axial forces in the beam to beam connection.....	92
Table 3.27. Design verifications of the brace connection	92
Table 3.28. Column base design forces.....	93
Table 3.29. Column Details	93
Table 3.30. Base plate details.....	93
Table 3.31. Anchor details.....	93
Table 3.32. Concrete base details.....	93
Table 3.33. Steel details.....	93

Table 3.34. Tension and compressive lever arms	94
Table 3.35. Design forces in T-stubs.....	94
Table 3.36. Concrete base bearing strength under left hand flange – EN1992-1-1 Section 6.7	94
Table 3.37. Concrete base bearing strength under right hand flange – EN1992-1-1 Section 6.7.....	95
Table 3.38. Equivalent T-stub in compression under right hand flange – Section 6.2.5	95
Table 3.39. Equivalent T-stub in compression under left hand flange – Section 6.2.5.....	95
Table 3.40. Concrete in compression under right hand flange – Section 6.2.6.9	95
Table 3.41. Concrete in compression under left hand flange – Section 6.2.6.9	96
Table 3.42. Bending resistance of column – EN1993-1-1 Section 6.2.5	96
Table 3.43. Column bases subjected to axial forces and bending moments – Section 6.2.8.....	396
Table 3.44. Design moment resistance of column base	96
Table 3.45. Frictional shear resistance	96
Table 3.46. Shear weld resistance	96
Table 3.47. Limitations for bolt spacings and distances.....	97
Table 3.48. Components of the column base connection	99
Table 3.49. Concrete cylinder compression test performed on ABAQUS.....	100
Table 3.50. Concrete main properties in compression and tension.....	101
Table 3.51. Concrete damaged plasticity parameters.....	101
Table 3.52. Column base components with assigned properties	102
Table 3.53. Stress diffusion results along central path.....	116
Table 3.54. Effect of baseplate thickness variation on the stress diffusion (2 cm and 1.5 cm)	119
Table 3.55. Effect of baseplate thickness variation on the stress diffusion (1.5 cm and 1.0 cm)	120
Table 3.56. Stress diffusion disparity between model 1 and 2	129
Table 3.57. Failure mechanisms under axial loads	131
Table 3.58. Failure mechanisms under bending moment.....	132

TABLE OF CONTENTS

DEDICATION.....	i
ACKNOWLEDGEMENTS.....	ii
LIST OF ABBREVIATIONS AND SYMBOLS	iii
ABSTRACT.....	viii
RESUME	ix
LIST OF FIGURES.....	x
LIST OF TABLES	xiii
TABLE OF CONTENTS	xv
GENERAL INTRODUCTION.....	1
CHAPTER 1 : LITERATURE REVIEW.....	2
Introduction.....	2
1.1. Background Information.....	2
1.2. Structural Description of Column Base Connections.....	3
1.2.1. Baseplate.....	6
1.2.2. Mortar Layer	6
1.2.3. Concrete Block.....	6
1.2.4. Anchor Bolts	6
1.3. Theoretical Behavior of a Column Baseplate Connection	7
1.4. Column Baseplate Classification	9
1.4.1. Classification According to Base Plate Behavior	9
1.4.2. Classification According to Amount of Restraint provided	11
1.4.3. Classification According to Steel Failure Mode	12
1.4.4. Classification According to Concrete Failure Mode.....	14
1.4.5. Classification According to Energy Dissipation Capacity	15
1.4.6. Classification According to Type of Frame.....	20
1.5. Precursory Experimental and Theoretical Studies	20
1.5.1. Experimental Studies.....	20
1.5.2. Theoretical Studies.....	21
1.6. Previous analytical studies.....	24
1.6.1. Picard and Beaulieu (1985).....	24
1.6.2. Stamatopoulos and Ermopoulos (2011)	24
1.6.3. Abdollahzadeh and Ghobadi (2013).....	25
1.7. Limitations of Previous Studies and the Necessity of the Subject Matter.....	25
1.8. Column Base Connection Design Provisions	27

**FEM ANALYSIS APPLIED TO THE STUDY OF STRESS
DIFFUSION IN THE BASEPLATES OF STEEL STRUCTURES**

1.8.1. Elastic design methods	27
1.8.2. Design method EN 19993-1-8: Component method.....	27
1.9. The Finite Element Method	29
1.9.1. Principle of FEM.....	29
1.9.2. Methods used to perform FEM analysis.....	30
1.9.3. Meshing	30
1.9.4. Sources of errors in FEM.....	31
1.9.5. Finite Element Analysis Steps in Computers	31
Conclusion	32
CHAPTER 2 : METHODOLOGY	33
Introduction.....	33
2.1. General Site Recognition	33
2.2. Site visit	33
2.3. Data collection	33
2.3.1. Structural data	33
2.3.2. Material properties	34
2.4. Codes and Specifications	34
2.5. Loading conditions on the structure	34
2.5.1. Permanent loads G	34
2.5.2. Variable loads Q.....	34
2.6. Limit states.....	39
2.6.1. Ultimate limit states.....	40
2.6.2. Serviceability limit states.....	40
2.7. Load combinations	40
2.8. Structural design method and verification of steel structures	41
2.8.1. Presentation of the FEA software SAP 2000.....	41
2.8.2. Static Analysis Modelling.....	42
2.8.3. Verification of the global model	42
2.9. Numerical sub-model for stress-diffusion analysis.....	62
2.9.1. Presentation of the numerical software Abaqus.....	62
2.9.2. Model definition.....	64
2.10. Stress diffusion analysis.....	68
2.10.1. Determination of the critical column base connection to be studied.....	69
2.10.2. Stress analysis of the column base plate subjected to the design axial load	69
2.10.3. Parametric study of the stress on base plate with respect to the Axial load	69

2.10.4. Parametric study of the stress on base plate with respect to the baseplate thickness	69
Conclusion	69
CHAPTER 3 : RESULTS AND INTERPRETATIONS	70
Introduction	70
3.1. General presentation of the site	70
3.1.1. Physical parameters	70
3.1.2. Socio-economical parameters	72
3.2. Physical description of the site	73
3.3. Presentation of the project	73
3.3.1. Presentation of the structural data	74
3.3.2. Characteristics of the materials	75
3.4. Loads determination	77
3.4.1. Vertical loads	81
3.4.2. Horizontal loads	81
3.5. Design verifications of the steel structure	81
3.5.1. Purlin design verification	82
3.5.2. Rafter design verifications	83
3.5.3. Column design verification	85
3.5.4. Braces design verifications	89
3.5.5. Connection design verifications	90
3.6. Results Obtained from the Sub-model Study in ABAQUS	98
3.6.1. Parts module results	98
3.6.2. Property module results	99
3.6.3. Assembly module	102
3.6.4. Step module	103
3.6.5. Interactions	104
3.6.6. Load module	105
3.6.7. Mesh	107
3.7. Stress analysis of the column base plate connection subjected to the design axial loads	109
3.7.1. Parametric study of the stress diffusion in a stiffened baseplate	115
3.7.2. Prediction of possible failure mechanisms with respect to stress concentrations observed	131
Conclusion	132
GENERAL CONCLUSION	134
BIBLIOGRAPHY	136
ANNEXES	141

***FEM ANALYSIS APPLIED TO THE STUDY OF STRESS
DIFFUSION IN THE BASEPLATES OF STEEL STRUCTURES***

Annex 1: Comprehensive summary of column base connection studies	141
Annex 2: Building usage categories.....	145
Annex 3: Safety factors for permanent and variable actions.....	146
Annex 4: Recommended values of Ψ factors for buildings	147
Annex 5: Classification of steel cross section	148
Annex 6: Imperfection factor and buckling curve's selection tables.....	149
Annex 7: Effective length of the T-stub	150
Annex 8: Real view of the column base connection.....	151

GENERAL INTRODUCTION

The twenty-first century witnessed the evolution and widespread of steel construction technologies. This is because it combines a number of unique features that makes it an ideal solution for many applications in the construction industry. Steel provides unbeatable erection speed, off-site fabrication and has less environmental impact. Within the scope of steel structures, there exists particular elements which are of great importance known as steel joints. Steel joints are structural members that link different elements of the steel structure such as beams, columns, foundations. The mechanical properties of these joints have a big influence on the global behavior of the structure, thus, their characterization is very important. Column bases are one of the most important structural joints in steel constructions, owing their worth to their critical role of transferring the acting loads of the superstructure to the foundation system which greatly affects the stability and durability of the overall structure. However, they are still one of the least studied structural connections compared to other joints like; beam-to-column or beam-to beam. Moreover, within existing studies carried out in the scope of column bases, little to none provide explicit results regarding the stress diffusion in baseplates. Consequently, it is very difficult to predict the stress diffusion in baseplates subjected to loading. Thus, it is of paramount importance to have a correct analysis of the stress diffusion and a valid estimate of the properties and loading conditions which affect this diffusion. For this reason, the main objective of this work is to provide a visible stress diffusion pattern in stiffened baseplates subjected to different loading conditions. From this, propose a prediction of the failure mechanism which could incur. Thus, the work presented in this dissertation was divided into the following tasks; Chapter 1 which welcomes us with a literature review including a background overview of column bases, structural description of column bases, design provisions, failure modes and the use of FEM software in stress diffusion analysis. The limitation of the existing studies regarding stress diffusion in base plates appears to be evident at the end of this chapter, as such a study pertaining to this subject matter appears to be necessary. Chapter 2 comprises of a methodology displaying the codes and standards, numerical modelling procedure of the column baseplate connection, FEM analysis of the baseplate and concluding remarks. Chapter 3 contains the results of the work carried out and interpretations relative to it. Lastly, a conclusion of the work and useful recommendations for future work are presented.

CHAPTER 1 : LITERATURE REVIEW

Introduction

Column base plates are one of the most critical and influential elements on steel structures. This is because their efficiency and performance strongly affect the whole behavior of the structure. The main function of this type of connection is to transfer to the foundation the self-weight and the loads applied to the structure, representing a great influence on the stability and durability of the overall structure. Hence, the paramount importance of this connection is not questionable. Thus, the present chapter aims to describe column bases, their components and a succinct explanation of the behavior of column base plate connections. In addition, the chapter covers early-stage research efforts on column base plate connections as well as the most recent research performed within the scope of study. Firstly, a brief overview of column base plate connections is provided followed by a brief review of experimental research conducted on column base plate connections. In addition, different types of failure modes of column base plates are discussed. Furthermore, a brief presentation of design codes pertaining to column base plates has been made available. Lastly, a rundown into finite element methods in relation to column base plates has been explored.

1.1. Background Information

Column base plates were the subject of first studies in 1971 carried by Delesques in France. At the time, the calculation was made based on elastic methods used for reinforced concrete structures. Seventeen years later, Lescouarc'h adopted the same model for the development of the methodology presented in his article (Lescouarc'h, 1988) for column base plates subjected to biaxial bending moment. In addition, in 1987, Colson developed two and three-dimensional models to investigate the nonlinear bending flexibility of column base plates. In 1986, David Thambiratnam analyzed by means of an experimental program the behavior of column base plates subjected to eccentric axial loads and bending moment. Later, Krishnamurthy and Thambiratnam (1990) made great advances studying the column base plates behavior. The same way in 1992, Astaneh and Nakashima studied the parameters which play a major influence on the behavior of several column base plate configurations.

In the United States, before the Northridge earthquake, the design of column base plates under bending moments was based on published works by DeWolf and Sarisley (1980), DeWolf

(1982), Ballio and Mazzolani (1983), Thambiratnam and Paramasivam (1986) and AISC Design Guide No. 1 “Column Base Plates” (DeWolf and Ricker, 1990; Lee et al., 2008a). However, the earthquake that occurred in 1994 allowed researchers to conclude that the performance of column base plates did not fulfill the requirements, exhibiting considerable and irreversible damages. Thus, the necessity of furthering the knowledge of column base plates was evident.

1.2. Structural Description of Column Base Connections

A column base connection is a special type of steel joint that connects the steel column to its foundation whose function is to transfer loads from the supported members to the supporting members. Conventional column bases are classified into two main categories: (a) the exposed column bases (or column bases with exposed base plates) (Figure 1.1a) and (b) embedded column bases (see Figure 1.1b). According to Grauvilardell et al. (2005), this distinction is determined by the position of the base plate in relationship to the foundation of the structure. Exposed column base plates are of the main interest in this research work because they represent the most common practice for steel buildings.

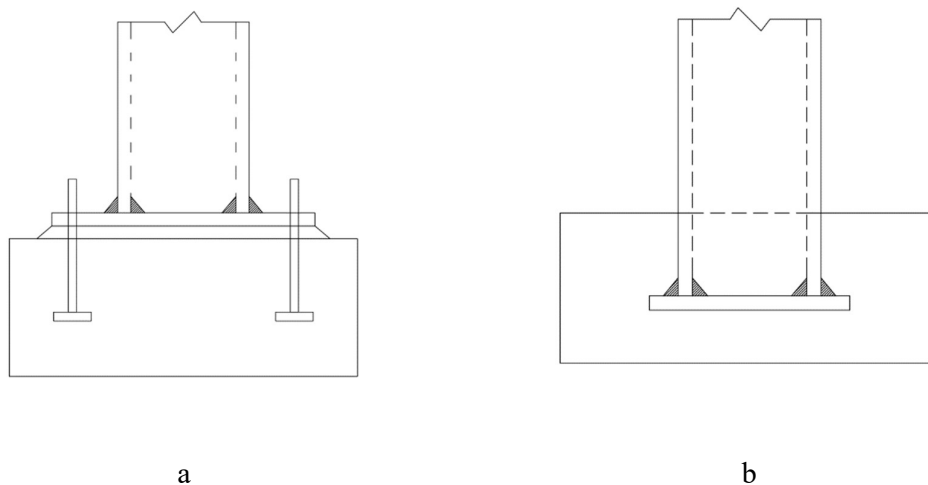


Figure 1.1. Column bases: a) Exposed column base, b) Embedded column base

The main elements of exposed column base plates, also known as anchored baseplates are; the column foot, the base plate welded to the column foot, the mortar layer, the anchor bolts and

FEM ANALYSIS APPLIED TO THE STUDY OF STRESS DIFFUSION IN THE BASEPLATES OF STEEL STRUCTURES

the concrete block (foundation). Sometimes, the joint can be reinforced using stiffeners. Also, it could be stiffened with a shear-resisting key (shear lug).

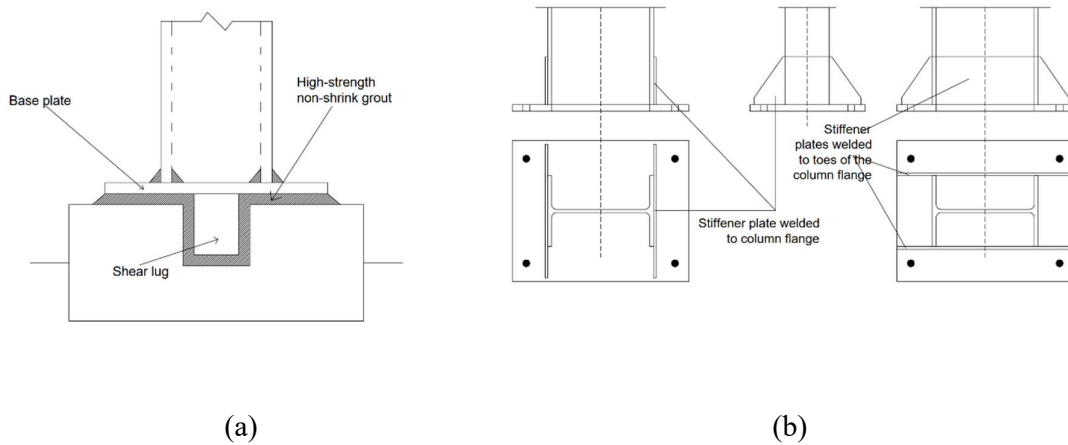


Figure 1.2. (a) Column baseplate with shear lug and (b) Column base plate with stiffeners

Figure 1.3 is a clear representation of elements of an exposed column base plate.

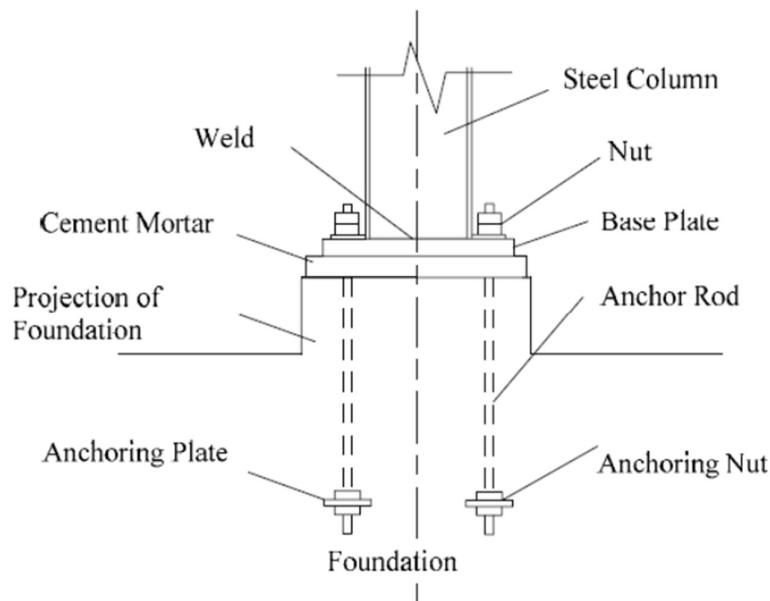


Figure 1.3. Elements of exposed column base plates

Also, exposed column base plates could have an open cross section or a closed/tube cross section.



Figure 1.4. Conventional exposed cross-section column bases: (a) unstiffened H-section column base; (b) stiffened H-column base (Kamperidis, 2016)

In practice, a thicker base plate is more economical than a thinner base plate with additional stiffeners or other reinforcements (DeWolf 1990).



Figure 1.5. Conventional exposed tube column bases; (a) unstiffened tube base; (b) stiffened tube base (Kamperidis, 2016)

A concise description of each component of a column base plate connection is given in this subchapter.

1.2.1. Baseplate

A base plate is a steel sheet that is welded to the column. Its main purpose is to increase the contact area between the column and the concrete block, which will decrease the stress in case of compression and prevent crushing of the concrete. Its other function is to transfer the possible tension in the column to the anchor bolts.

1.2.2. Mortar Layer

The contact between the steel plate and the concrete block is provided by the mortar layer which allows the transition of shear forces from the column to the concrete footing by the friction between themselves. In the construction process of exposed steel column bases, this element is usually the last to be materialized.

1.2.3. Concrete Block

The concrete block is the foundation of the column whose function is to transfer the loads to the ground. The bearing strength of concrete is calculated with respect to the design value of compressive strength, f_{cd} to ensure the efficient support and transfer of loads.

1.2.4. Anchor Bolts

The main purpose of the anchor bolts is to hold down the column by transferring the tensile loads to the corresponding foundations. These loads may appear in the form of pure tension in one side of the column caused by a bending moment. There are various types of anchor bolts, as shown in Figure 1.6, and they should be chosen according to the appropriate conditions. The most common ones are the cast-in-situ anchor bolts and hooked bars, since they are the most economic ones. Anchoring to grillage beams embedded in the concrete foundations are designed only for column bases loaded by large bending moment, because it is very expensive.

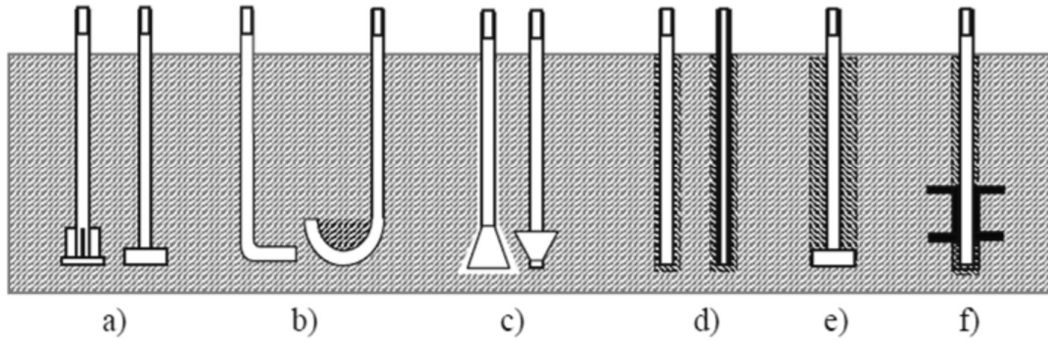


Figure 1.6. Types of anchor bolts a) cast-in-situ anchor bolts, b) hooked bars, c) undercut anchor bolts, d) bonded anchor bolts; e) grouted anchor bolts, f) anchoring to grillage beams

1.3. Theoretical Behavior of a Column Baseplate Connection

A typical column base connection between the column of a steel moment-resisting frame and its concrete foundation consists of an exposed steel base plate supported on unreinforced grout and secured to the concrete foundation using steel anchor bolts. This moment resisting connection is generally subjected to a combination of high bending moments, axial and shear forces. A number of steel buildings, particularly low-rise moments resisting frame systems developed failure at the column base plate connection during the 1995 Kobe, Japan, and the 1994 Northridge and 1989 Loma Prieta, California earthquakes due to severe load combinations. It was found by (Bertero et al. 1994, Youssef et al. 1995) that the rotational stiffness and strength of the base plate assemblages affected the damage these structures suffered not only directly in the column bases, but also in other parts of their lateral load-resisting frames. The theoretical behavior of an exposed base plate connection is explained in the following lines.

In a base plate connection, column axial forces are transmitted to the base plate through the gross cross-section area of the column, where both flanges and web are effective. Depending on the base plate flexural stiffness, the bearing stress on the supporting concrete foundation can vary from a uniform distribution throughout the entire base plate for thick plates, to an irregular distribution with stress concentrations under the column flanges and web for thin plates, where only part of the plate area is effective in transmitting compressive loads to the concrete foundation.

As lateral loads due to wind pressure or earthquake ground motion increases, the compression stress bulb on the supporting concrete foundation shifts from the center of the column towards

the edges of the plate. Due to plate bending in the case of thin base plates, the bearing stress concentration is located under column flanges in compression. As concrete fibers reach their ultimate capacity, the resulting stress distribution in both cases (axial load and lateral load case) flattens and becomes more uniform. In most design methods, the stress distribution is approximated for simplicity as an equivalent rectangular distribution, similar to the Whitney compression block used in reinforced concrete load resistant factor design (LRFD) (ACI 318, 2002). On the other side of the column, the tension in the column flange induces tensile forces in the anchor bolts, necessary to maintain vertical force and moment equilibrium in the case of moderate to large eccentricities.

The column bending moment is resisted by coupled tension-compression force, with a lever arm equal to the distance between the resultant of the concrete bearing stresses on the compression side of the base plate and the centerline of the anchor bolts on the tension side. The maximum bending demand in the base plate is the greater of the effects of the cantilever bending on the tension side of the plate caused by tensile forces in the column flange and in anchor bolts, or cantilever bending due to bearing stress distribution on the compression side (Drake, Elkin 1999). In the center of the plate, in the transition zone between tension and compression, the plate is subjected to high shear stresses.

The shear resistance and the horizontal force equilibrium of the column base connection is provided by a combination of three mechanisms: friction along the contact area between the concrete surface and the steel base plate, which can be taken as the effective bearing area resisting compressive loads; bending and shear in the anchor bolts; and bearing of shear lugs installed underneath the base plate (or the side of the base plate if it is embedded) against the adjacent concrete or grout. The behavior of a column base plate is expressed in figure 1.7.

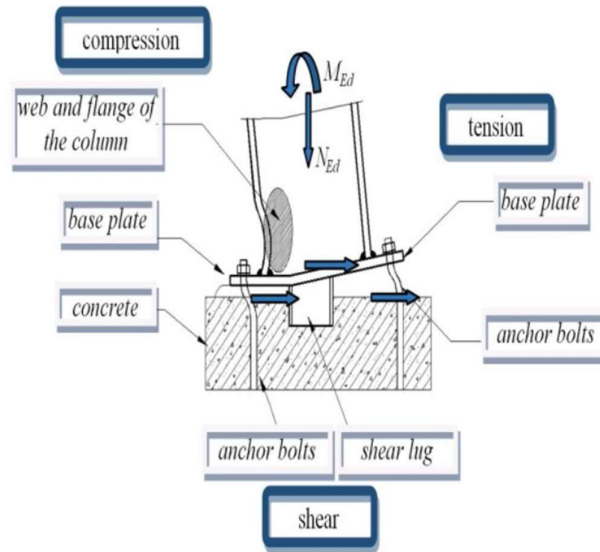


Figure 1.7. Theoretical behavior of the base plate

1.4. Column Baseplate Classification

As aforementioned, column base plate connections can be broadly classified as exposed and embedded, based on their position with respect to the foundation element that traditionally represent pinned and fixed supports, respectively. Researchers have classified exposed column base connections based on several criteria such as base plate behavior, amount of restraint provided, steel failure mode, concrete failure mode, energy dissipation and type of frame.

1.4.1. Classification According to Base Plate Behavior

Astaneh et al. (1992) and Fahmy (1999) classified base plate connection according to the thickness required to form a plastic hinge in the base plate. Figure 1.8 illustrates a schematic representation of three types of column base plate connections based on the base plate behavior and their deformed shapes.

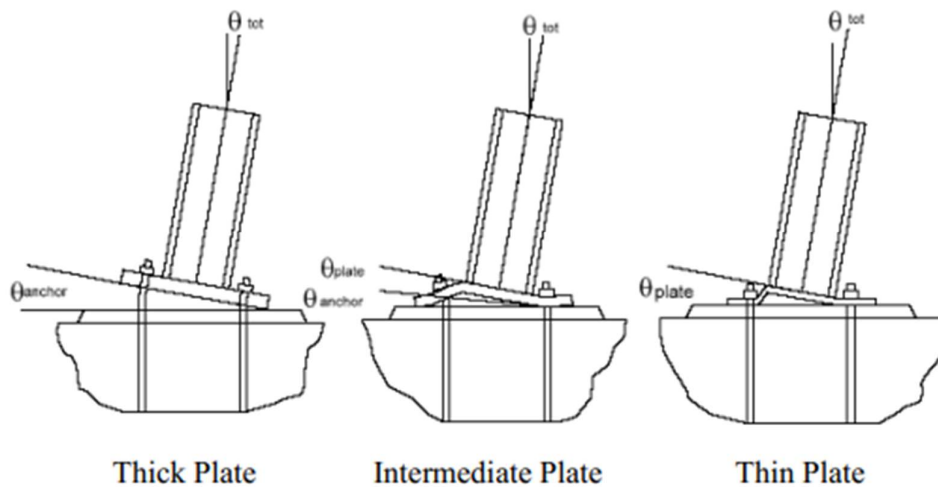


Figure 1.8. Types of base plate behavior (Adapted from Astaneh et al. 1992)

1.4.1.1. Thick/Rigid Plate

A rigid base plate is a plate whose load distribution is simplified by assuming that the plate itself does not deform analogously to Euler-Bernoulli's beam theory. Column base connections with thick base plates are considered as the most rigid among the three types of classification summarized in this section. Although rigid, these types of column base plate connections very often experience a non-ductile behavior due to fracture of anchor rods or crushing and spalling of the grout during large rotations (Grauvilardell et al., 2005).

1.4.1.2. Intermediate/Semi-rigid Plate

Lee and Goel (2001) expressed their concerns about designing the base plate following AISC provisions stating that it might not behave as expected due to yielding of the base plate. They suggested that the failure of anchor rods in tension needed to be considered, which might be the governing case. Basically, the failure of semi-rigid plates is initiated by both the anchor rods and base plates.

1.4.1.3. Thin/Flexible Plate

Column base connections associated with thin base plates are specified as flexible where ductile behavior is achieved through the inelasticity in the base plate itself. Yield lines are expected to form along the flanges of the column. However, very thin base plates can form 45° yield lines at the corners of the base plate (Grau Vilardell et al., 2005). The rest of the components of column base plate connections such as anchor rods, grout, and concrete

foundation are considered as elastic. This type of inelastic deformation of the base plate may help to lessen seismic response by acting as an isolator for the structure during any seismic event.

1.4.2. Classification According to Amount of Restraint provided

Three types of classification such as pinned, fixed and partially restrained exist under this category of column base plate connection.

1.4.2.1. Pinned

These connections have a relatively low rotational stiffness and consequently have a high capacity of transferring bending moments.

1.4.2.2. Fixed

Fixed column base plate connections can be closely compared with the rigid connection. They are connections which are not designed for transferring bending moments due to their high rotational stiffness.

1.4.2.3. Partially Restrained

Column base connections for structures with gravity and moderate lateral loads may present typical simple classifications “fixed” or “pinned.” However, Astenah et al. (1992) reported that column base plate connections, when subjected to inelastic cycles, could act as a “semi rigid” connection. Yamada and Akiyama (1997) as well as Kawano and Matsui (1998) had shown through analytical studies that partially restrained column bases distributed the story drift and formation of plastic hinges more evenly than perfectly fixed ones. Figure 1.9 expresses the classification of different joint restraints with respect to moment and rotation.

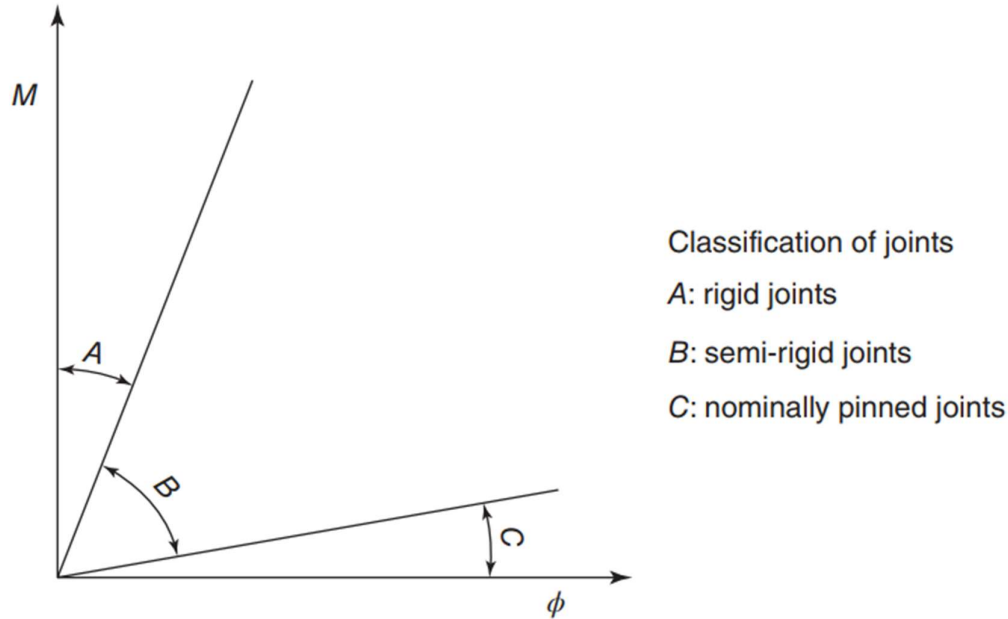


Figure 1.9. Moment-Rotation diagram defining the joint behavior

1.4.3. Classification According to Steel Failure Mode

Fahmy (1999) classified three types of steel failure modes based on three regions on the moment–rotation diagram through experimental and numerical investigation. The first region is considered where the behavior remains elastic. The second one is a transition region where the behavior is inelastic and material hardening takes place. The third one is the softening region after the maximum moment of the connection has been reached and rupture occurs at the end. The three types of connections are as follows:

1.4.3.1. Weak Column-Strong Connection:

These types of connections are specified by the formation of a plastic hinge at the base of the column while the rest of the components of the column base plate connection remains elastic or exhibit incipient yielding. Fahmy (1999) and Adany et al. (2000) conducted experimental investigation on this type of connection and found plastic hinges only in the column, when all the other components of column base plate connections reached yield stress. They also reported that welds could play an important role in this type of connection. Figure 1.10 displays a plastic hinge development at the base of a weak column-strong connection.



Figure 1.10. Typical plastic hinge in a steel open section (I-beam)

1.4.3.2. Strong Column-Weak Connection:

Strong column-weak connections can resemble a pinned condition as long as the connection is in the nonlinear range (Grau Vilardell et al., 2005). It has been reported that the performance of this type of connection is characterized by the inelastic deformation of one or more components of the column base plate connection as well as potential brittle failures such as concrete crushing, anchor rod fracture (DeWolf and Sarsley, 1980). Figure 1.11 expresses the possible failures that a strong column-weak connection may suffer.

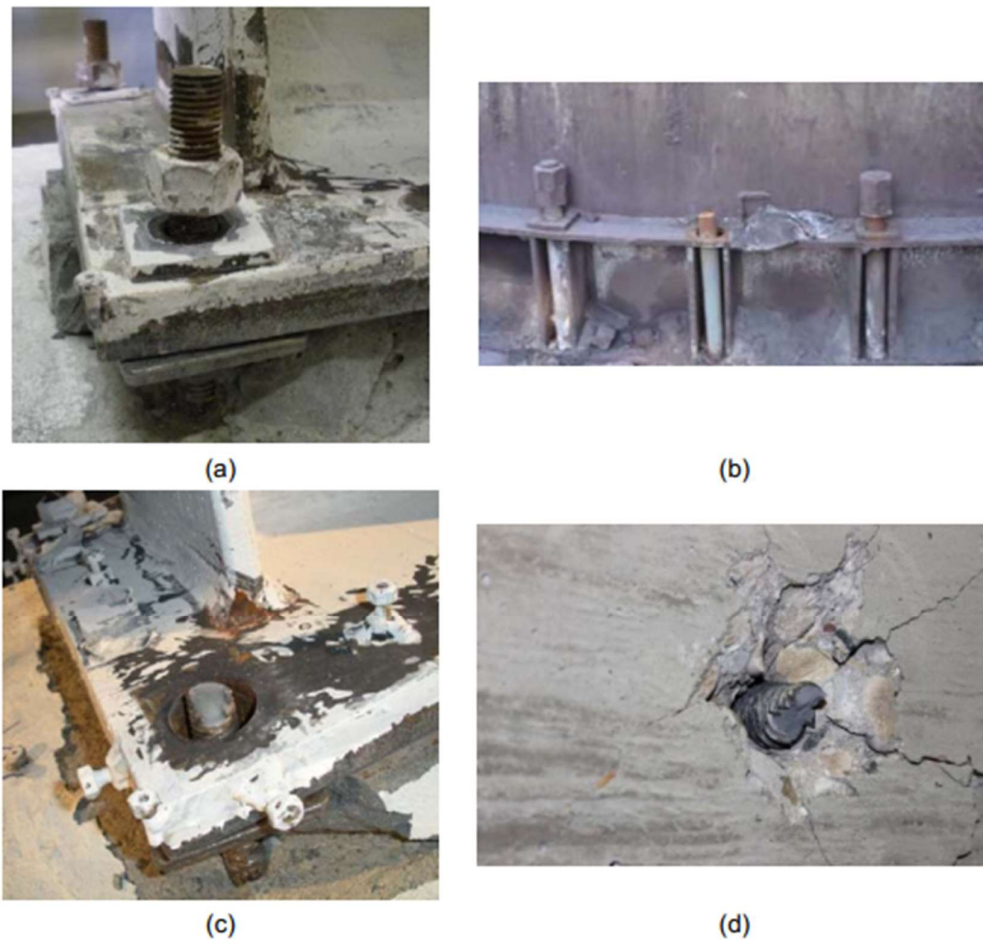


Figure 1.11. Anchor bolts failure in tension: (a) Yielding, (b) and (c) Yielding and fracture (d) Close-up of the fractured surface on the anchor shaft (Gomez et al.,2010)

1.4.3.3. Balanced Mechanism

This type of connection can be characterized as an intermediate mechanism where simultaneous and concurrent behavior can be achieved in between the two types of connections discussed above. In this type of connection, the column yields at approximately the same time as one or more of the components of the connection, meaning that not only one component is subjected to extreme deformations but all the components undergo inelastic behavior.

1.4.4. Classification According to Concrete Failure Mode

Several researchers (Wald et al.,1995), (Balut and Moldovan,1997), (Stamatopoulos and Ermopoulos,1997) assumed an elastic plastic stress distribution in the concrete to define

bearing stresses that develop under the base plate. Three types of failure modes can be classified according to the level of bearing stresses as shown in Figure 1.12 and are characterized by the level of compressive axial force with respect to the ultimate bearing stress in the concrete.

1.4.4.1. Low Axial Load

The bearing capacity of the concrete is never reached when the axial load is low. Here, collapse occurs either by yielding of anchor rods or by formation of a plastic mechanism, in the base pate.

1.4.4.2. Medium Axial Load

During a medium axial loading mechanism, the behavior is characterized by anchor rod yielding and concrete attaining its bearing strength relatively at the same time.

1.4.4.3. High Axial Load

In case of high axial loads, only the concrete bearing capacity is reached at the time of failure.

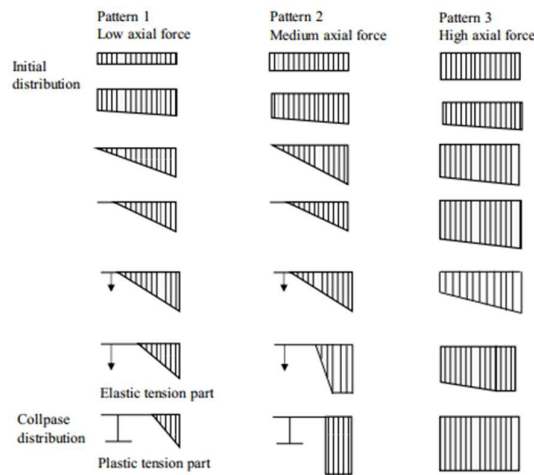


Figure 1.12. Internal force distribution under low, medium and high axial force in initial and collapse stage (Grauvilardell et al., 2005)

1.4.5. Classification According to Energy Dissipation Capacity

Fahmy (1999) classified column base plate connections according to energy dissipation characteristics. This type of classification becomes important when a capacity design of the column base plate connection is carried out.

1.4.5.1. Non-dissipative Mechanism:

These types of failure mechanisms do not provide significant energy dissipations. These mechanisms provide brittle behavior such as; cracking of welds, fracture of anchor rods, fracture of base plates, and crushing of the concrete or grout. For mechanisms that show some form of ductility, excessive local buckling of the column flange is observed which in turn leads to a lower strength capacity in the connection than expected. Some illustrations of non-dissipative failure mechanisms are provided in figures 1.13, 1.14 and 1.15.

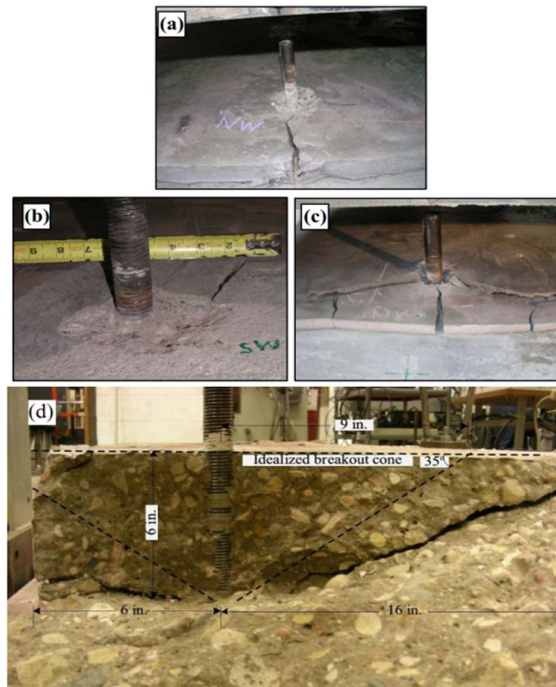


Figure 1.13. (a) Grout crushing (b) Pedestal crushing (c) Pedestal splitting (d) Idealized break out cone.

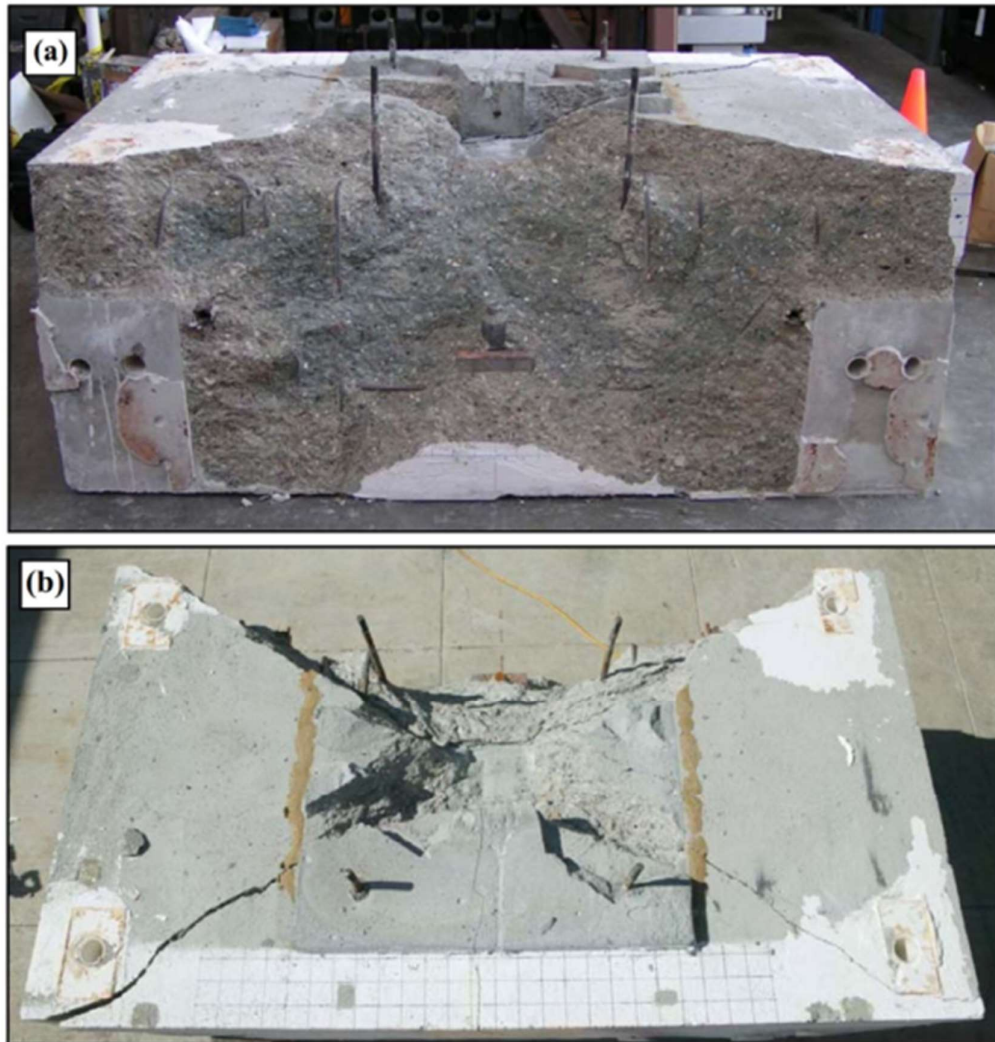


Figure 1.14. Shear key breakout failure of the concrete [after Gomez et al. (2009)]



Figure 1.15. Close-up view of crack in a thick base plate (Lai et al., 2015)

1.4.5.2. Dissipative Mechanism:

Dissipative mechanisms provide considerable energy dissipation through yielding of one or more components of column base plate connections such as yielding of the base plate, yielding of the anchor rods and plasticization of the base of the column by forming a plastic hinge. Some illustrations of dissipative failure mechanisms are provided below. An illustration of the hinge plasticization which is a dissipative mechanism is expressed in figure 1.10. Figure 1.16 expresses some dissipative mechanisms undergone by the column base connection.

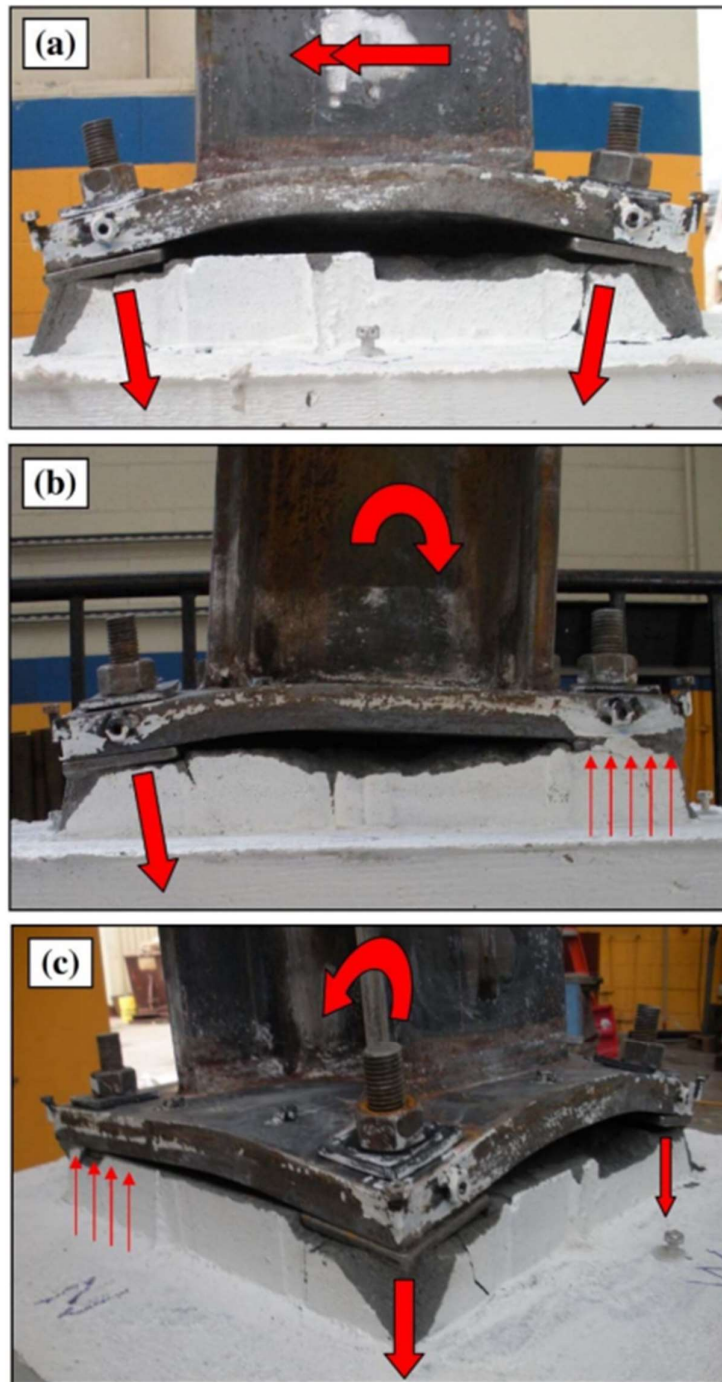


Figure 1.16. Flexural yielding of both the tension and the compression side of the base plate from various loading regimes, with schematics of ideal imposed and resisting forces (Gomez et al., 2010)

1.4.6. Classification According to Type of Frame

The variation of overall behavior, as well as the nature of acting forces on the exposed column base plate connections largely depends on the attachment of the column base with the type of structure. Two types of attachments are viable such as column bases attached with moment resisting frames and column bases attached with braced frames.

1.4.6.1. Column Bases Attached to Moment Resisting Frames:

This type of column base plate connection experiences moments in addition to axial forces and shear. Researchers have focused mainly on this type of connection because it is a common practical scenario. These types of column base plate connections are challenging when lateral forces are significant with low gravity loads at the sides of the frames.

1.4.6.2. Column Bases Attached to Braced Frames:

No significant research effort was found in the literature dealing with column bases attached to braced frames. Goldman (1983) and Tronzo (1984) have addressed the design of this type of connection analytically focusing on the design of the anchor rods, shear lug, and the gusset plate. However, none of them accounted to the contribution of the gusset plate attached to the base plate.

1.5. Precursory Experimental and Theoretical Studies

1.5.1. Experimental Studies

During the past years, the uncertainty related to the behavior of column base plates led researchers to study them with more detail. The analytical and numerical works described in annex 1 represent the most renowned studies on column base plates under loading developed all over the world. Moreover, test campaigns were carried out on column base plates in order to have a better understanding about the behavior of such connections subjected to different loading conditions. In some cases, experimental tests represented the starting point to the development and validation of new calculation procedures.

The table in annex 1 provides a comprehensive summary of the literature in terms of investigations performed all around the world by different researchers regarding exposed column base connections under different loading scenarios.

1.5.2. Theoretical Studies

Many studies have been done in order to design base plates as well as to predict their behavior and to know the stress distribution under them. The few existing stress distribution theories on base plates are the; Cantilever theory, the Fling theory, the Murry-Stockwell theory, the Eurocode theory and the T-stub theory. These theories will be explained in this section.

1.5.2.1. The Cantilever Theory

This theory is centered on the stress diffusion on a baseplate initiated by an H-steel column. It assumes that the stress distribution in the baseplate operates in an area equal to $0.95d_c \times 0.8b_{fc}$ as shown in figure 1.17.

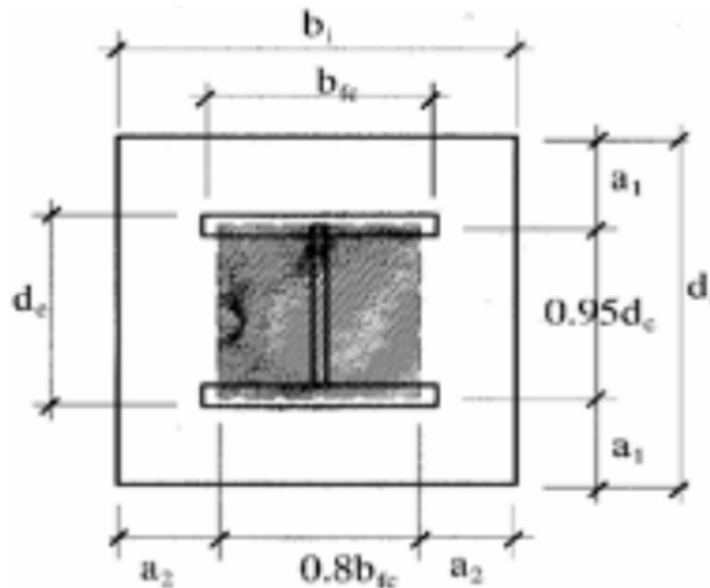


Figure 1.17. Assumed stress distribution under base plates in Cantilever theory (CWE Journal Stress distribution)

1.5.2.2. The Fling Theory

The Fling theory suggests that the stress distribution is uniform along the web and it's both sides such that the stress distribution intervenes by an angle from the flange edges into the plate inside. Also, it is assumed that the flange edges bear no stress. The Fling stress distribution is shown in figure 1.18.

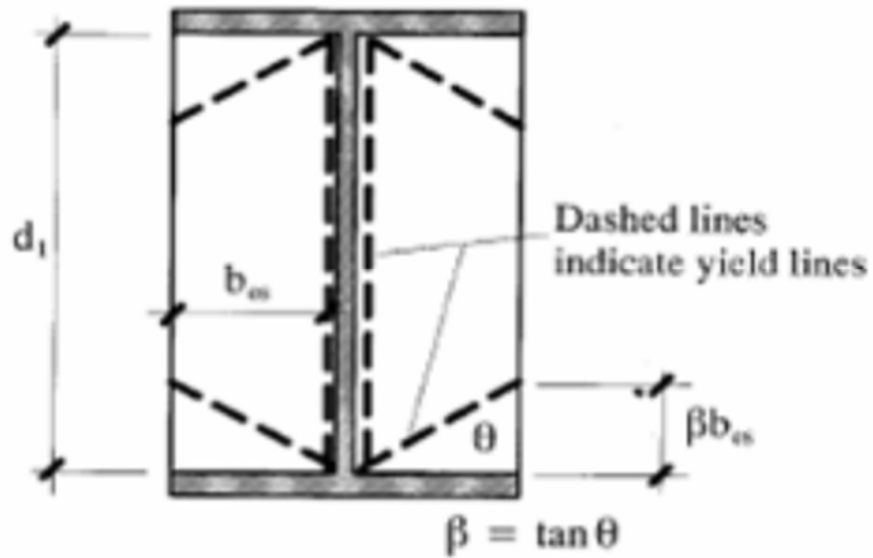


Figure 1.18. Assumed stress distribution under base plate in Fling theory (CWE Journal Stress distribution)

1.5.2.3. The Murry-Stockwell Theory

In this theory, the stress distribution is considered as an H-shaped region inside an H-shaped cross section. Figure 1.9 displays this stress distribution.

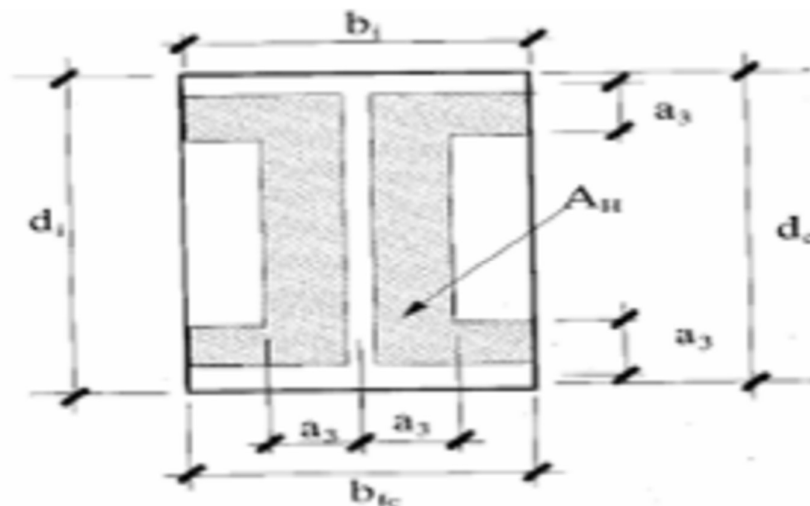


Figure 1.19. Assumed stress distribution under base plate in Murry-Stockwell theory (CWE Journal Stress distribution)

1.5.2.4. Eurocodes Theory

In the Eurocode theory, the stress distribution is considered to be initiated in a space outside of an H-shape cross section perimeter and then developed inside the of H-shaped cross section perimeter. Figure 1.2 displays the Eurocode stress distribution.

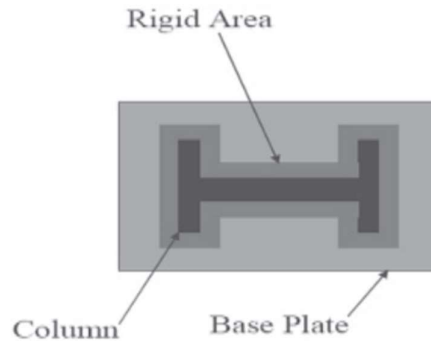


Figure 1.20. Assumed stress distribution under base plates in Eurocodes theory (CWE Journal Stress distribution)

1.5.2.5. T-stub theory

In this theory, the web and flanges are constituted from H-shape profiles separately, then equivalent stress distributions are drawn for each one. Afterwards stress distribution for the T-stub method is obtained by adding distributed stresses for both web and flanges of an H-shape cross-section. It should be noted that there is high stress at the interface of the web and flange due to the addition of the web stress and flange stress. The T-stub distribution is presented on figure 1.21.



Figure 1.21. Assumed stress distribution under base plates in T-Stub method (CWE Journal Stress distribution)

1.6. Previous analytical studies

Analytical findings expressed as equations or formulas are always a direct result of experimental and numerical studies which have been carried out. In the following lines, an outline of some analytical expressions and their evolution across time is shown below.

1.6.1. Picard and Beaulieu (1985)

Picard and Beaulieu proposed the following equation for the ultimate bending resistance:

$$M_{j,u} = 0.85\alpha f_{ck} d_{eff} b_{bp} [0.5(h_{bp} - x_c)] + n A_s f_{ub} (0.5h_{bp} - e) \quad (1.1)$$

with

α : coefficient that considers the concrete confinement,

f_{ck} : compressive strength of concrete,

d_{eff} : depth of the rectangular stress block,

h_{bp} : base plate depth,

b_{bp} : base plate width,

n : number of anchor bolts in the tensile zone,

A_s : tensile stress area of an anchor bolt,

f_{ub} : ultimate tensile stress of anchor bolt,

e : distance from the base plate edge to the axis of the anchor bolt.

1.6.2. Stamatopoulos and Ermopoulos (2011)

Stamatopoulos and Ermopoulos performed tests on eight specimens and developed finite element models to evaluate the moment-rotation curves of column base plates. Experimental moment-rotation curves were compared with the analytical formula proposed by the authors that relates the moment M with the rotation of the connection θ_j :

$$M = \alpha M_0 \frac{\theta_j}{\theta_0 + \theta_j} \quad (1.2)$$

with

α : curve fitting coefficient,

M_0, θ_0 : moment and rotation corresponding to the yield point.

1.6.3. Abdollahzadeh and Ghobadi (2013)

Abdollahzadeh and Ghobadi proposed a model similar to that of Stamatopoulos and Ermopoulos to predict the moment-rotation curves $M - \theta$ of column base plates subjected to monotonic loading. Their work was based on the study of Stamatopoulos and Ermopoulos above. The proposed equation is:

$$M = M_n \left(1 + \left(\frac{M_y}{M_n} - 1 \right) \frac{\theta}{\theta_y} \right) \left(1 - e^{-\left(1 + 0.25 \frac{\theta}{\theta_y} \right) \frac{\theta}{\theta_y}} \right) \quad (1.3)$$

with

$$M_n = 0.8025 M_{j,u}$$

M_y, θ_y : moment and rotation corresponding to the yield point.

1.7. Limitations of Previous Studies and the Necessity of the Subject Matter

From the aforementioned experimental and numerical studies, it can be noticed that most of the studies carried out with respect to column base plates are centered on their behavior when subjected to different loading regimes (axial load, eccentric axial load and bending moment). The common objectives these studies had included; the definition of the rigidity of the connection with the use of moment-rotation diagrams, determination of the design strength resistance and analysis of various failure modes. Upon observation of this existing literature, the absence or the very limited existence of studies regarding stress diffusion in column base plates is quite noticeable.

Due to the complex nature of steel-concrete interactions, simple assumptions of the stress distributions are usually employed for designing the connection. Less complex assumptions of compressive stress distribution in the base plate and concrete layer may accelerate the design procedure, but they may lead to overdesigned results. The existing theories, literatures and design codes provide us with stress diffusion schemes within the column base plates portrayed in section 1.5.2 which are concurrent to the stress distributions displayed on figure 1.22.

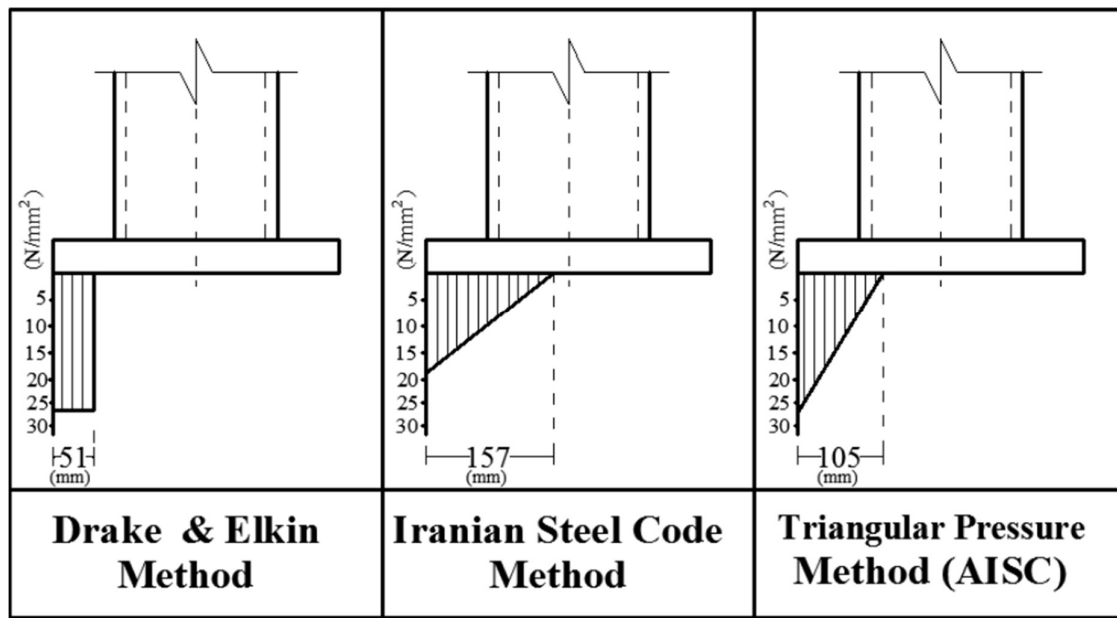


Figure 1.22. Diffusion of stress under base plates based on different methods

These stress diffusions provided by different design codes are proven to be simplifications and not being an exact representation of the real diffusion of stress in base plate. Additionally, these design codes-based stress diffusions were obtained by considering the base connection to be either pinned or rigid whereas most recent researches have put to light the fact that the real behavior of a column base plate is neither pinned nor rigid but instead exhibit a semi-rigid behavior.

In accordance with the previous stated facts, it is quite clear that the real stress diffusion is not considered in existing design codes. Faced with this difficulty, it is of paramount importance to perform a stress diffusion analysis on base plates. With the advance of modern technology, the aid of cutting-edge technology of remarkable precision such as finite element analysis (FEA) software is of great use.

To carry out a stress diffusion analysis, loads from the column are to be distributed to the concrete foundation via the column base plate. The base plate must be of defined geometry and its resistance should be known. On the other hand, to design a base plate, applied loads should be known. This means primary design and stress analysis are related and an iterative procedure could be employed to achieve an economical and safe design.

As a logical consequence of the preceding paragraph, the next part of this chapter shall briefly elaborate on the design provisions with respect to base plates.

1.8. Column Base Connection Design Provisions

The calculation procedure to predict the resistance and stiffness of column base plates nowadays available for engineers in EN 1993-1-8 resulted from the evolution and improvement of several researchers that in the past, throughout their work, provided numerical and experimental data, proposing also analytical models based on the most diverse assumptions. This subchapter presents the previous elastic design methods used before and the current design procedure of EN 1993-1-8.

1.8.1. Elastic design methods

Lescouarc'h (1988) proposed a calculation procedure for the evaluation of the resistance of column base plates subjected to the combination of axial force and biaxial bending. The model was developed for rigid column base plates configuration with four anchor bolts, subjected to a combination of axial force N , bending moment M_y and M_z and shear forces V_y and V_z as shown in figure 1.23.

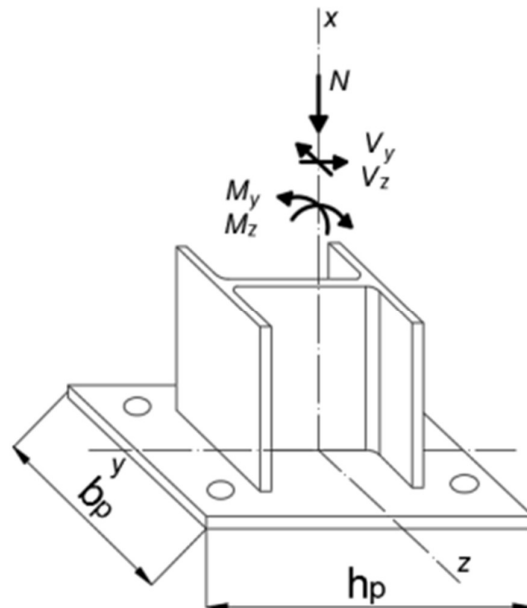


Figure 1.23. Column base plate configuration (Lescouarc'h, 1988)

1.8.2. Design method EN 1993-1-8: Component method

Eurocode introduces the concept of plasticity in the evaluation of the resistance of elements and this concept can be applied to column base plates in the presence of axial forces and in-plane bending moments.

The component method design procedure allows us to calculate the resistance and stiffness of column base plates. This model is valid for exposed column base plates, as shown in Figure 1.24 composed of the following elements:

- stiffened/unstiffened steel column (HEA, HEB, IPE steel profiles),
- Steel base plate welded to the column
- Grout layer
- Anchor bolts
- Concrete foundation

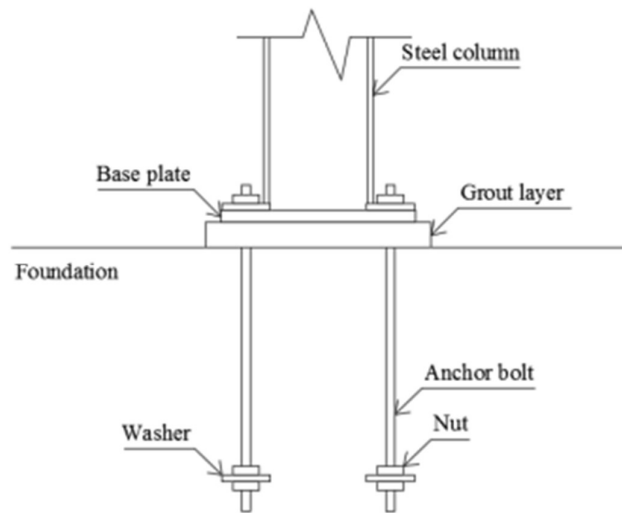


Figure 1.24.Main elements composing an exposed column base plate (Amaral, 2014)

The component method consists in the evaluation of the complex non-linear response through the subdivision into basic joint components, determining each individual resistance and stiffness in order to obtain the overall structural behavior. The procedure of this method is as follows:

- Identification of the basic components
- Characterization of the mechanical properties of each individual component (resistance and stiffness)
- Assembly of the individual components properties to obtain the overall properties of the connection
- Classification of the connection in terms of resistance and stiffness
- Modeling

A more detailed literature of the component method could be obtained from: N1993-1-8:2006, Eurocode 3, Design of steel structures, Part 1-8, Design of joints, CEN, Brussels, 2006.

Another design provision with respect to column base plates is that proposed by the American Institution of Steel Construction (AISC) which is mostly centered with the use of the Load and Resistance Factor Design (LRFD) method and the Allowable Stress Design (ASD) method. A detailed explanation of this design methods can be found in the design guide published by the AISC.

1.9. The Finite Element Method

The Finite Element Method is a general discretization procedure of continuum mechanics posed by mathematically defined statements (Zienkiewicz et al., 2013). It is widely used in engineering to solve practical engineering problems.

Many physical phenomena in engineering and science can be described in terms of partial differential equations. In general, solving these equations by classical analytical methods for non-conventional shapes is almost impossible. Numerical approaches such as the Finite Element Method (FEM) can be used to give approximate solutions to these partial differential equations. From an engineering standpoint, the FEM is a method used for solving engineering problems such as stress analysis, heat transfer, fluid flow and electromagnetic works by computer simulation.

1.9.1. Principle of FEM

The principle of the Finite Element Method is to divide a complicated model into a finite number of elements for which stresses and strains can be solved numerically. FEM is a technique to find appropriate numerical solutions for partial differential equations as well as for integral equations. This can be done by eliminating differential equations completely or rendering it to ordinary differential equations which can then be solved by other techniques (such as the Euler method for example). Basically, in the finite element method the object is divided into many smaller bodies or elements and are interconnected at common points called nodes or boundary lines. Each of the small elements is solved separately using algebraic equations and the unknowns are calculated. The result of all the elements is unified to obtain the solution of the object under study.

1.9.2. Methods used to perform FEM analysis

The basic problem in any engineering design is to evaluate displacements, stresses and strains in any given structure under different loads and boundary conditions. To meet the needs of specific applications, several approaches to finite element analysis have been developed among which the Displacement Method, the Forced Method, the Mixed Method and the Mixed Method.

1.9.2.1. The Displacement Method

This is the most common and suitable method for solving practical engineering problems. Here, the structure is subjected to applied loads and/or specified displacements. The primary unknowns are the displacements, obtained by inversion of the stiffness matrix, and the derived unknowns are stresses and strains (Hsu, 2017).

1.9.2.2. The Forced Method

Here, the structure is subjected to loads and/or specified displacements. The primary unknowns are member forces, obtained by inversion of the flexibility matrix, and the derived unknowns are stresses and strains. Calculation of the flexibility matrix is possible only for discrete structural elements (such as trusses, beams and pipes) hence, this method is limited to the early analysis of discrete structures and piping analysis.

1.9.2.3. The Mixed Method

Here, the structure is subjected to applied loads and/or specified displacements. The method deals with large stiffness coefficients as well as very small flexibility coefficients in the same matrix. Analysis by this method leads to numerical errors and is not possible except in some special cases.

1.9.2.4. The Hybrid Method

Here, the structure is subjected to applied loads and stress boundary conditions. This deals with special cases such as; airplane door frame which should be designed for stress-free boundary, so that the door can be opened during flight in cases of emergencies.

1.9.3. Meshing

Every continuous object has infinite degrees of freedom and it is not possible to solve in this case. As mentioned before, the basic idea of FEM is to divide the body into finite elements

connected by a number of joints called nodes and obtain an approximate solution. This is called the finite element mesh and the process of making the mesh is called mesh generation (Fish & Belytschko, 2007). The meshes generated could be 1,2 or 3 dimensional elements based on their geometrical size and shape (Gokhale et al., 2008). The 1-D element is used when one of the dimensions is very large in comparison to the rest of the two. The 1-D Element shape is the line. Examples: rod, bar, beam, pipe and axisymmetric shell.

The 2-D element is used when two of the dimensions are very large in comparison to the third. Examples include: thin shells, plates, membrane, plane stress, plane strain, axisymmetric solid.

The 3-D element is used when all dimensions are comparable. Element shapes are: tetra, hex, pyramid, Penta and the element type is solid.

1.9.4. Sources of errors in FEM

Finite Element Analysis (FEA) based on the FEM is a simulation applied to a mathematical model. This simulation may be prone to errors which may occur during the modelling and analysis process either due to the limitation of the software or user error. Some common sources of errors in the use of FEA are modelling errors, discretization errors and numerical errors.

1.9.4.1. Modelling error

This error is associated with approximations that are made to the real problem. These approximations to the real world usually fail to consider the real behavior of the model.

1.9.4.2. Discretization error

Discretization error is related to parameters such as the size and shape of the finite elements. This error can be reduced by modifying the mesh size and shape.

1.9.4.3. Numerical error

This error is based on the algorithm used and the finite precision of numbers used to represent data in the computer. Most software uses double precision to reduce numerical errors.

1.9.5. Finite Element Analysis Steps in Computers

The steps followed by a FEA commercial software can be narrowed down to 3.

1.9.5.1. Pre-processing

This step involves modelling of the structure, meshing and application of the boundary conditions. The subdivision of the problem domain into finite elements in today's computer aided engineering (CAE) environment is performed by an automatic mesh generator but given instructions concerning the type of element and the mesh density desired.

1.9.5.2. Processing

This step involves the development of equations for each element and solving the system of equations. Here, the software automatically generates matrices that describe the behavior of each element, combines these matrices into a large matrix equation that represents the overall model and solves this equation to determine values of fields at nodes. Substantial additional calculations are performed if the behavior is non-linear or time dependent.

1.9.5.3. Post Processing

This step involves the display of FEA solution, calculation of various variables that do not emanate directly from the solution, determining quantities of interest such as stresses and strains, viewing simulations of the response. It involves verifications, conclusions and thinking about what steps could be taken to improve the design.

In the early use of finite element methods, only specific structures were analyzed, mainly in the aerospace and civil engineering industries. However, with the evolution of finite element methods and the increased application of computers in the engineering design environments, emphasis in research and development was placed in making use of finite element methods an integral part of the design process in mechanical, civil and aeronautical engineering.

Conclusion

The aim of this chapter was to illustrate the concept of column base plates and get accustomed to its behavior and studies performed with respect to it. The information presented above provides enough insight for the identification of gaps or limitations of the existing literature. The main limitation that was highlighted from this extensive literature review was the inexact nature of the stress diffusion in base plates used in different design codes. In an attempt to resolve this issue, a solid and comprehensive finite element analysis applied to a column base plate is required. The next chapter will deal with the procedure followed in order to perform this study.

CHAPTER 2 : METHODOLOGY

Introduction

The previous chapter enabled us to have an understanding of column base plates and their behavior under various actions. This chapter will focus in the description of the methodology of the work. The methodology is the part of the study that establishes the research procedure after the definition of the problem, so as to achieve the set of objectives. It is presented following a logical procedural outline starting with the general recognition of the site done by a documentary research. This is followed by data collection that will ease the modelling and analysis of the case study. The objective of this chapter is to display the static verification procedure of an existing building in compliance with Eurocode 3, the modeling of the sub-model and finally the stress analysis procedure of the sub-model with the software Abaqus/CAE.

2.1.General Site Recognition

The recognition of the site will be based on the documentary research on the study site. It allows physical parameters like the geographical location, the climate and the hydrology of the site to be known. Also, to a greater extent, information pertaining to socio-economic parameters to be known.

2.2.Site visit

The site visit is the phase that consists in going down to the site in order to discover it. The site visit will be done in two phases, the first phase for direct observation of the site and the second for inquiries related to specific aspects of the site.

2.3.Data collection

The data collected are the structural plans and the data concerning the different properties of the materials used on site.

2.3.1. Structural data

The structural data contains the structural plans that shows the disposition of the different structural elements of the building and their geometrical dimensions. They are collected using the software AutoCAD. These data are composed of structural details and they contain the sections of different elements used in the construction of the building.

2.3.2. Material properties

This is the data that characterizes the materials that were used for the implementation of the structure. Knowing the material properties will help us to during the determination of the resisting forces and resisting moments of sections under study.

2.4. Codes and Specifications

The codes and the different types of loads acting on the steel ware house will be presented in this section. This study will focus on two main types of actions which acts on steel buildings. They are; permanent and variable loads.

The building will be described according to EN1991-1-1 (2002), clause 6.3.2 which is a part of Category E1 as shown in annex 2 since it is used for storage. Depending on the location of the building and the government accepted standards, design codes are used for the definition of loads and calculations. European codes that will be used in this study are reported in table 2.1.

Table 2.1. Eurocodes

Codes	Abbreviation
Eurocode 0: Basis of design	EN1990_E_2002
Eurocode 1: Actions on structures	EN1991_E_2002
Eurocode 2: Design of concrete structures	EN1992_E_2004
Eurocode 3: Design of steel structures	EN1993_E_2005

2.5. Loading conditions on the structure

In the following lines, the actions and loads considered in the study are explained detailly.

2.5.1. Permanent loads G

Equally known as static or dead loads, they are actions that act during the whole nominal life of the structure with a negligible variation of their intensity in time. These include the self-weight of the structural elements and the self-weight of the non-structural elements present during the nominal life of the structure but do not take part in the load bearing mechanism.

2.5.2. Variable loads Q

These are actions on the structure for which their variation in magnitude with time is non-negligible. These actions include; imposed loads and wind loads.

2.5.2.1. Imposed loads

These are loads other than the weight of the structure like loads due to the weight of people, objects, vehicles, etc. They depend on the building occupancy and maintenance (such as HVAC installations). According to Eurocode 1, the appropriate load with respect to the building occupancy is selected. The steel portal frame belongs to the category E1, pertaining to storage area as shown in annex 2.

2.5.2.2. Wind loads

Wind actions fluctuate with time and act directly as pressures on the external surfaces of enclosed structures. Also, due to the porosity of the external surface, wind pressures act indirectly on internal surfaces. The pressure created inside a building due to the access of wind through openings could be termed suction (negative) or pressure (positive) and have the same order of intensity while those outside could also vary in magnitude with possible reversals. Thus, the design value shall be taken as the algebraic sum of the two in a considered direction. The response of the building to high wind pressures depends not only on the geographical location and proximity to airflow obstructions but also on the characteristics of the structure like the size, shape and dynamic properties of the structure.

a. Basic wind velocity

EN 1991-1-4 (2002) specifies that the fundamental value of the basic wind velocity, $v_{b,0}$ is the characteristic mean wind velocity irrespective of the wind direction and time of the year. It is taken at 10m above the ground level in an open country terrain with low vegetation such as grass. This basic wind velocity will be calculated from equation (2.1).

$$v_b = C_{dir} \times C_{season} \times v_{b,0} \quad (2.1)$$

Where C_{dir} and C_{season} are respectively the directional and seasonal factors. EN 1991-1-4 (2005) recommends these values to be taken as 1.

b. Basic and peak velocity pressure

The basic velocity will be calculated as shown in equation (2.2).

$$q_b = \frac{1}{2} \times \rho_{\text{air}} \times v_b^2 \quad (2.2)$$

Where $\rho_{\text{air}} = 1.25 \text{ kg/m}^3$ (air density)

The peak velocity pressure $q_p(z)$ at height z , which includes mean and short-term velocity fluctuations shall be determined as presented on equation (2.3).

$$q_p(z) = [1 + 7I_v(z) + 12 \times \rho \times v_m(z)^2] \quad (2.3)$$

Where:

I_v is the turbulence intensity;

ρ is the density;

$v_m(z)$ is the mean wind velocity as shown in equation (2.4).

$$v_m(z) = C_r(z) \times C_0(z) \times v_b \quad (2.4)$$

Where:

$C_0(z)$ is the orography factor;

$C_r(z)$ is the roughness factor as calculated in equation (2.5) or (2.6).

$$C_r(z) = k_r \times \ln\left(\frac{z}{z_0}\right) \quad \text{for } z_{\min} \leq z \leq z_{\max} \quad (2.5)$$

$$C_r(z) = C_r(z_{\min}) \quad \text{for } z \leq z_{\min} \quad (2.6)$$

Where:

z_0 is the roughness length;

k_T is the terrain factor, depending on the roughness length z_0 as shown in equation (2.7).

$$k_T = 0.019 \times \left(\frac{z_0}{z_{0,II}}\right) \times 0.07 \quad (2.7)$$

Where:

$z_{0,II} = 0.05$ (terrain category IV, taken from table 2.2);

z_{\min} is the minimum height;

z_{\max} is to be taken as 200m.

Table 2.2. Terrain categories and terrain parameters

Terrain category	z_0 m	z_{min} m
0 Sea or coastal area exposed to the open sea	0,003	1
I Lakes or flat and horizontal area with negligible vegetation and without obstacles	0,01	1
II Area with low vegetation such as grass and isolated obstacles (trees, buildings) with separations of at least 20 obstacle heights	0,05	2
III Area with regular cover of vegetation or buildings or with isolated obstacles with separations of maximum 20 obstacle heights (such as villages, suburban terrain, permanent forest)	0,3	5
IV Area in which at least 15 % of the surface is covered with buildings and their average height exceeds 15 m	1,0	10

NOTE: The terrain categories are illustrated in A.1.

Figure 2.1. Terrain categories and terrain parameters

The turbulence intensity $I_v(z)$ at height z is defined as the standard deviation of the turbulence divided by the mean wind velocity. It is calculated as represented in equation (2.8) and (2.9).

$$I_v = k_1 C_0(z) \times \ln\left(\frac{z}{z_0}\right) \quad \text{for } z_{min} \leq z \leq z_{max} \quad (2.8)$$

$$I_v = I_v(z_{min}) \quad \text{for } z < z_{min} \quad (2.9)$$

Where k_1 the turbulence factor and the recommended value for is k_1 is 1.0.

The peak velocity pressure $q_p(z)$ can also be calculated as shown in equation (2.10).

$$q_p(z) = C_e(z) \times q_b \quad (2.10)$$

Where $C_e(z)$ is the exposure factor illustrated in figure 2.1 as a function of height above terrain and the terrain category.

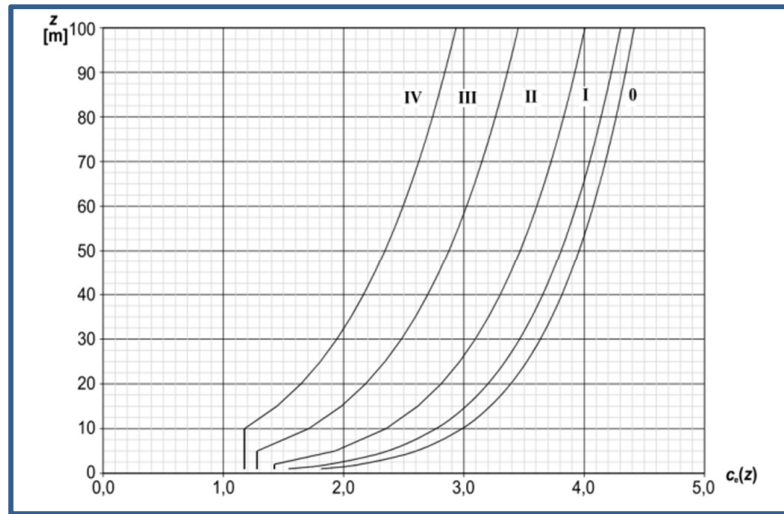


Figure 2.2. Illustration of the exposure factor $C_e(z)$ for $C_0 = 1.0$, $k_1 = 1.0$ (BS EN1991-1-4)

c. Wind pressure on surfaces

The effect of wind on the structure as whole is determined by the combined action of external and internal pressures acting upon it. A positive wind load stands for pressure whereas a negative wind load indicates suction. This definition applies for the external wind action as well as for the internal wind action. The pressure distribution is shown in figure 2.3.

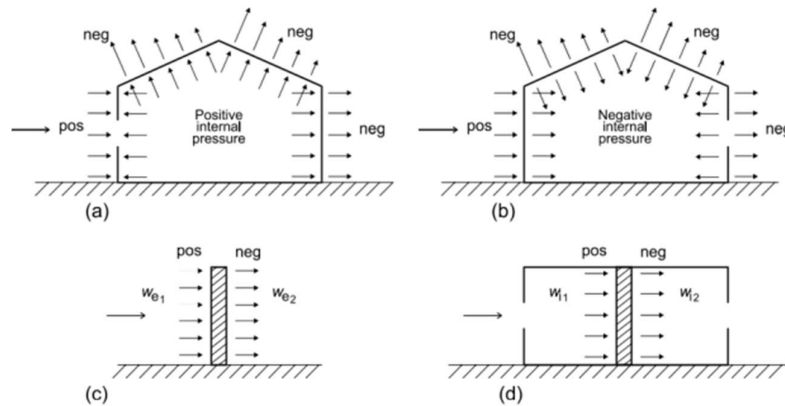


Figure 2.3. Pressure acting on surfaces

i. External wind pressure

The wind pressure acting on the external surfaces, w_e , should be obtained from the equation (2.11).

$$w_e = q_p(z_e) \times c_{pe} \quad (2.11)$$

Where:

$q_p(z_e)$ is the peak velocity pressure;

z_e is the reference height for the external pressure;

C_{pe} is the pressure coefficient for the external pressure depending on the size of the loaded area.

ii. Internal wind pressure

The internal pressure coefficient depends on the size and distribution of the openings in the building. The wind pressure acting on the internal surfaces of a structure, w_i will be obtained from equation (2.12).

$$w_i = q_p(z_i) \times C_{pi} \quad (2.12)$$

Where:

z_i is the reference height for the internal pressure;

C_{pi} is the pressure coefficient for the internal pressure

The net pressure on a wall, roof or element is the difference between the pressures on the opposite surfaces taking due account of their signs. The wind loadings per unit length, w for an internal frame are calculated using the influence width (spacing between the columns) i_s , as presented in equation (2.13). The worst combination of external and internal pressures are to be considered for every combination during the analysis.

$$w = (c_{pe} - c_{pi}) \times q_p \times i_s \quad (2.13)$$

2.6.Limit states

A structure is designed according to the corresponding limit states in such a way that it sustains all actions acting upon it during its intended life. This implies it will be designed having adequate structural stability (ultimate limit states) and remain fit for the use it is required (serviceability limit states).

2.6.1. Ultimate limit states

According to EN 1990 (2002), ultimate limit states (ULS) corresponds to the loss of structural capacity of the whole structure or one of its fundamental elements (for example structural collapse). It concerns the safety of people and/or the safety of the structure. The loss of structural capacity includes; loss of equilibrium of the whole structure or one of its fundamental parts, excessive displacements or deformations, reaching the maximum strength capacity of parts of structures, joints, foundations, reaching the maximum strength capacity of the entire structure and reaching the failure mechanisms in the soils.

2.6.2. Serviceability limit states

Serviceability limit state (SLS) is the inability of the structure to meet the specific service requirement for which it was built. This include mainly; functioning of the structure or structural members under normal use, comfort of people, the appearance of the construction works.

2.7. Load combinations

A combination of actions defines a set of values used for the verification of the structural reliability for a limit state under the simultaneous influence of different actions. For the verification of the structure at ultimate limit state (ULS), the load combinations used were given by equation (2.14) and (2.15).

$$ULS1 : \gamma_{G,1}G_1 + \gamma_{G,2}G_2 + \gamma_{Q,m}Q_m + \gamma_{Q,w}\Psi_{0,w}Q_w \quad (2.14)$$

$$ULS2 : \gamma_{G,1}G_1 + \gamma_{G,2}G_2 + \gamma_{Q,w}Q_w + \gamma_{Q,m}\Psi_{0,m}Q_m \quad (2.15)$$

Where:

Q_m is the maintenance load on the roof;

Q_w are the wind loads acting on the roof, windward and leeward side;

G_1 are the self-weight of the structural components;

G_2 is the self-weight of the aluminium roof;

$\gamma_{i,j}$ is the safety factor for permanent and variable loads and its values are obtained from annex 3.

$\Psi_{i,j}$ are the combination coefficients and their values are given in annex 4.

In a general design and verification-oriented work, load envelopes of the ULS combinations are obtained and used to size structural members. Also, for the verification of the structure at serviceability limit state (SLS), load combination used is given in equations (2.16), (2.17), and (2.18).

$$\text{SLS1(Characteristic combination)} : G_1 + G_2 + Q_m + \Psi_{0,w}Q_w \quad (2.16)$$

$$\text{SLS2(Characteristic combination)} : G_1 + G_2 + \Psi_{1,w}Q_w + \Psi_{2,m}Q_m \quad (2.17)$$

$$\text{SLS3(quasi – permanent combination)} : G_1 + G_2 + \Psi_{2,m}Q_m + \Psi_{2,w}Q_w \quad (2.18)$$

Without neglecting the necessity of this procedure, the methodology will give priority to the static analysis of the building and the loads acting on each member, particularly loads acting on the steel column which is the main object of the study.

2.8. Structural design method and verification of steel structures

The structural design process involves the static analysis of the steel structure and the verification of members at ULS and SLS. It is performed firstly by creating a numerical model of the structure to determine the structural response to loading and other actions in terms of internal forces and moments, stresses, deformations, strains or vibrations. This is done by setting up appropriate numerical models that represent the real structure. This section shall incorporate a static analysis of a steel structure performed with respect to the ULS loading combinations described earlier. This global analysis model shall be represented and analyzed using the FEA software SAP 2000.

2.8.1. Presentation of the FEA software SAP 2000

SAP 2000 is a powerful analysis and design program that was introduced for over 30 years ago by CSI (Computer and Structures INC). SAP 2000 can be used to handle simple 2D exercises to complex 3D structures. The goal when making the program was to simplify the engineer's calculation process in the form of modelling, design and optimization with help from a powerful analysis engine and a versatile interface.

SAP 2000 is known for its flexibility between international borders, multiple sets of standards, sectional dimensions and material qualities can be used.

The program can also perform different loading analysis such as: static linear/non-linear analysis, buckling analysis, influence lines analysis, p-delta analysis, accidental load analysis

and vibration analysis. All the capacity checks are based on the given standard chosen and the program compares the acting analysis forces to the sectional capacities.

2.8.2. Static Analysis Modelling

The model is based on drawings received from the designers of the structural system. Modelling include; creating the appropriate materials, section properties, loads and load combinations. The steel elements shall be drawn according to the plans and the support conditions assigned with respect to the restraint condition. The load combinations will be defined prior to the analysis to satisfy the ULS and SLS conditions discussed in section 2.5. The case study will be loaded and a static linear analysis will be performed to obtain the forces acting on each member, particularly compressive axial forces and bending moments acting on the steel columns.

2.8.2.1. Grids

The first step of modelling the structure is to define grids. When laying out the grid, it is important that the geometry defined accurately represents the major geometrical aspects of the model.

2.8.2.2. Materials

Materials are chosen from the Eurocode databases integrated in the software, to ensure correct values for the different material properties. The main properties that will be defined are the concrete and steel resistances.

2.8.2.3. Sections

The various elements are modelled differently depending on the section type. The beams, columns, purlins and braces are modeled as frames with dimensions according to the information gathered from the received drawings.

2.8.3. Verification of the global model

After completion of the static analysis, the internal forces, moments and stresses are known. A verification of these elements with respect to Eurocode 3 is performed. Before any element is verified, it needs to be classified according to its capacity to develop plastic hinges and rotation deformations.

2.8.3.1. Classification of sections

The classification of a section depends on geometric characteristics. The sections of the members to be designed are going to be classified as class 1, 2, 3 or 4. Eurocode defines these classes as follows:

- Class 1 cross-sections are those which can form a plastic hinge with the rotation capacity required from plastic analysis without reduction of the section's resistance.
- Class 2 cross-sections are those which can develop their plastic moment resistance, but have limited rotation capacity because of local buckling.
- Class 3 cross-sections are those on which the stress in the extreme compression fiber of the steel member assuming an elastic distribution of stresses can reach the yield strength, but local buckling is liable to prevent development of the plastic moment resistance.
- Class 4 cross-sections are those in which local buckling will occur before the attainment of yield stress in one or more parts of the cross-section.

Classification of the sections will be done with respect to annex 5.

2.8.3.2. Members in bending

The ULS design verification procedure of the members in bending will consider; uniaxial bending, shear resistance and lateral torsional buckling.

a. Uniaxial bending

The design value of the bending moment M_{Ed} at of each cross-section shall satisfy the equation

$$\frac{M_{Ed}}{M_{c,Rd}} \leq 1 \quad (2.19)$$

Where M_{Ed} is the design moment and $M_{c,Rd}$ is the resisting moment.

The design resistance for bending about one principal axis of a cross-section is determined using the equations;

$$M_{c,Rd} = M_{pl,Rd} = \frac{W_{pl} f_y}{\gamma_{M0}} \quad \text{for class 1 or 2 cross sections} \quad (2.20)$$

$$M_{c,Rd} = M_{el,Rd} = \frac{W_{el,min} f_y}{\gamma_{M0}} \quad \text{for class 3 cross sections} \quad (2.21)$$

$$M_{c,Rd} = \frac{W_{eff,min} f_y}{\gamma_{M0}} \quad \text{for class 4 cross sections} \quad (2.22)$$

Where:

f_y is the yielding strength;

W_{pl} is the plastic section modulus;

W_{elmin} is the elastic modulus;

$W_{eff,min}$ is the effective section modulus.

b. Shear resistance

The design value of the shear force V_{Ed} at each cross section shall satisfy equation 2.19.

$$\frac{V_{Ed}}{V_{c,Rd}} \leq 1.0 \quad (2.23)$$

Where $V_{c,Rd}$ is the design shear resistance.

For plastic design $V_{c,Rd}$ is the design plastic shear resistance $V_{pl,Rd}$ as given in equation

$$V_{pl,Rd} = \frac{A_v (f_y / \sqrt{3})}{\gamma_{M0}} \quad (2.24)$$

Where A_v is the shear area as illustrated in figure 2.4.

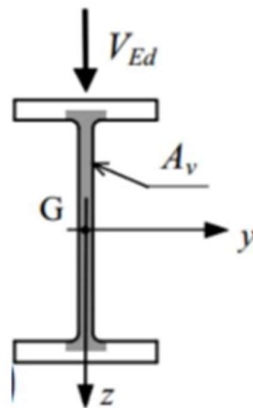


Figure 2.4. Beam shear resisting area

For rolled I and H sections with load parallel to the web, the shear area A_v may be taken as showed in equation ..

$$A_v = A - 2bt_f + (t_w + 2r) \text{ but not less than } \eta h_w t_w \quad (2.25)$$

In addition, the shear buckling resistance for webs without intermediate stiffeners should be verified according to section 5 of EN 1993-1-5 (2006), if equation 2.26 is true.

$$\frac{h_w}{t_w} = 72 \frac{\varepsilon}{\eta} \quad (2.26)$$

Where:

h_w is the height of the web;

t_w is the thickness of the web.

$$\varepsilon = \sqrt{\frac{235}{f_y}}$$

According to EN 1993-1-5 (2006), the value $\eta = 1.20$ is recommended for steel grades up to and including S460. For higher steel grades, $\eta = 1.00$ is recommended.

Shear and bending moment may interact if present at the same time on the member due to the loading condition. Provided that the design value of the shear force does not exceed 50% of $V_{pl,Rd}$, no reduction of resistances defined for the bending and axial force need to be made. If V_{Ed} exceeds 50% of $V_{pl,Rd}$, the reduced plastic shear resistance is calculated using a reduced yield strength given by equation (2.27)

$$f'_y = (1 - \rho)f_y \quad (2.27)$$

$$\text{Where } \rho = \left(\frac{2V_{Ed}}{V_{pl,Rd}} - 1 \right)^2$$

c. Lateral torsional buckling

A laterally unrestrained member subjected to major axis bending should be verified against lateral-torsional buckling using the equation (2.28)

$$\frac{M_{Ed}}{M_{b,Rd}} \leq 1.0 \quad (2.28)$$

Where:

M_{Ed} is the design value of the moment;

$M_{b,Rd}$ is the design buckling resistance moment.

The design buckling resistance moment of a laterally unrestrained beam is calculated using equation (2.29).

$$M_{b,Rd} = \chi_{LT} W_y \frac{f_y}{\gamma_{M1}} \quad (2.29)$$

Where:

W_y is the appropriate section modulus as follows:

$W_y = W_{pl,y}$ for class 1 or 2 cross-sections

$W_y = W_{pl,y}$ for class 3 cross-sections

$W_y = W_{eff,y}$ for class 4 cross-sections

χ_{LT} is the reduction factor for lateral-torsional buckling, which will be calculated as shown in equation (2.30)

$$\chi_{LT} = \frac{1}{\phi_{LT} + \sqrt{\phi_{LT}^2 - \bar{\lambda}_{LT}^2}} \quad \text{But } \chi_{LT} \leq 1.0 \quad (2.30)$$

Where :

$$\phi_{LT} = 0.5[1 + \alpha_{LT}(\bar{\lambda}_{LT} - 0.2) + \bar{\lambda}_{LT}^2]$$

α_{LT} is an imperfection factor

$$\bar{\lambda}_{LT} = \sqrt{\frac{W_y f_y}{M_{cr}}}$$

M_{cr} is the elastic critical moment for lateral torsional buckling.

Beams with sufficient restraint to the compression flange are not susceptible to lateral-torsional buckling. In addition, beams with certain types of cross-sections, such as square or circular hollow sections are susceptible to lateral-torsional buckling.

2.8.3.3. Members in tension

For members in axial tension, at ULS the design resisting value of the tensile force $N_{t,Rd}$ at each cross-section shall satisfy equation (2.31).

$$\frac{N_{Ed}}{N_{t,Rd}} \leq 1.0 \quad (2.31)$$

Where, N_{Ed} is the design tension load and $N_{t,Rd}$ is the resisting tensile force of the element and it is the minimum between $N_{pl,Rd}$ and $N_{u,Rd}$ given in equations (2.32) and (2.33)

$$N_{pl,Rd} = \frac{A f_y}{\gamma_{M0}} \quad (2.32)$$

$$N_{u,Rd} = \frac{0.9 A_{net} f_u}{\gamma_{M2}} \quad (2.33)$$

Where:

$N_{pl,Rd}$ is the design plastic resistance of the gross cross-section;

$N_{u,Rd}$ is the design ultimate resistance of the net cross-section at holes for fasteners;

f_y is the yield strength of steel;

A_{net} is the net cross section area;

γ_{M2} is the safety coefficient with value 1.25

These verifications with respect to the Eurocode are performed using SAP 2000 since the verification code is chosen before analysis.

2.8.3.4. Members in compression

For members in compression, the element is verified at ULS for pure compression and buckling resistance.

a. Pure compression

For pure compression, the design resistance value of the compressive force $N_{c,Rd}$ at each cross-section shall satisfy equation (2.34)

$$\frac{N_{Ed}}{N_{c,Rd}} \leq 1.0 \quad (2.34)$$

Where $N_{c,Rd}$ should be determined by equations (2.35) and (2.36)

$$N_{c,Rd} = \frac{Af_y}{\gamma_{M0}} \quad \text{for class 1, 2 or 3 cross sections} \quad (2.35)$$

$$N_{c,Rd} = \frac{A_{eff}f_y}{\gamma_{M0}} \quad \text{for class 1, 2 or 3 cross sections} \quad (2.36)$$

b. Buckling resistance

A compression member should be verified against buckling using equation (2.37)

$$\frac{N_{Ed}}{N_{b,Rd}} \leq 1.0 \quad (2.37)$$

Where:

N_{Ed} is the design value of the compression force;

$N_{b,Rd}$ is the buckling resistance force and is given by equation (2.38) and (2.39)

$$N_{b,Rd} = \frac{\chi Af_y}{\gamma_{M1}} \quad \text{for class 1, 2 and 3 cross sections} \quad (2.38)$$

$$N_{b,Rd} = \frac{\chi A_{eff}f_y}{\gamma_{M1}} \quad \text{for class 4 cross sections} \quad (2.39)$$

Where χ is the reduction factor for the relevant buckling mode. The value of χ for the appropriate non-dimensional slenderness, $\bar{\lambda}$, should be determined from equation (2.40).

$$\chi = \frac{1}{\phi + \sqrt{\phi^2 - \bar{\lambda}^2}} \quad \text{but } \chi \leq 1.0 \quad (2.40)$$

Where $\Phi = 0.5[1 + \alpha_{LT}(\bar{\lambda}_{LT} - 0.2) + \bar{\lambda}_{LT}^2]$

With α the imperfection factor obtained from annex 6.

The non-dimensional slenderness $\bar{\lambda}$ is given by the equation (2.41) and (2.42)

$$\bar{\lambda} = \sqrt{\frac{Af_y}{N_{cr}}} = \frac{L_{cr}}{i} \frac{1}{\lambda_1} \quad \text{for class 1,2 and 3 cross – sections} \quad (2.41)$$

$$\bar{\lambda} = \sqrt{\frac{A_{eff}f_y}{N_{cr}}} = \frac{L_{cr}}{i} \frac{\sqrt{\frac{A_{eff}}{A}}}{\lambda_1} \quad \text{for class 4 cross – section} \quad (2.42)$$

Where:

L_{CR} is the buckling length in the buckling plane considered;

i is the radius of gyration about the relevant axis, determined using the properties of the gross cross-section;

$$\lambda_1 = \pi \sqrt{\frac{E}{f_y}} = 93.9\varepsilon ;$$

$$\varepsilon = \sqrt{\frac{235}{f_y}} \quad (f_y \text{ in N/mm}^2).$$

N_{CR} is the elastic critical force for the relevant buckling mode based on the gross cross-sectional properties.

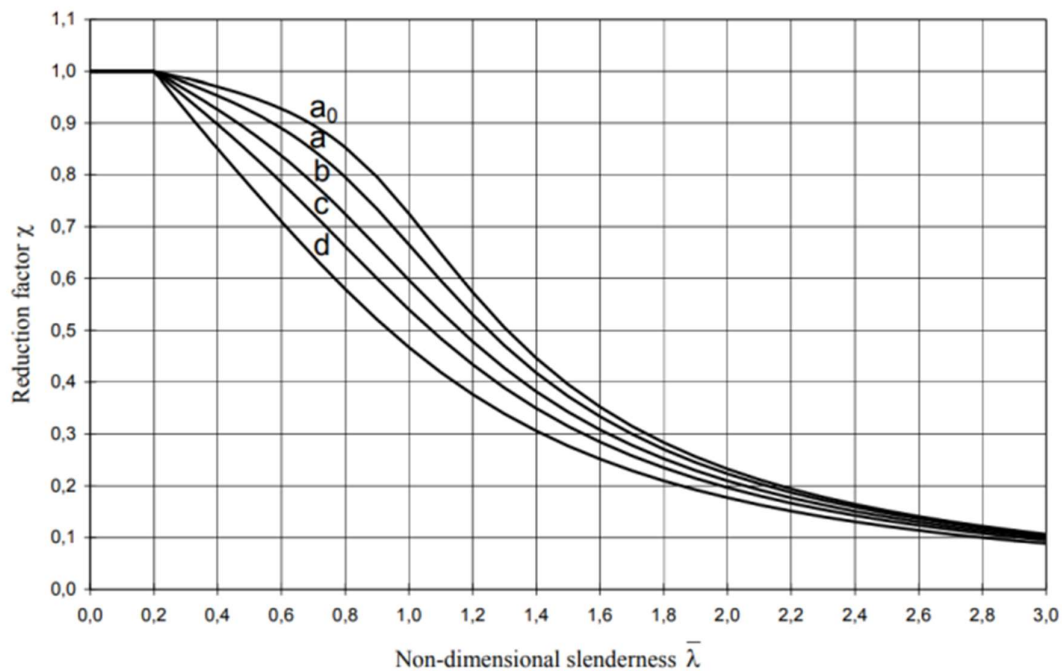


Figure 2.5. Buckling curves from Eurocode

When an element is subjected to axial and flexural load, equation (2.43) should be verified.

$$\frac{N_{Ed}}{N_{c,Rd}} + \frac{M_{Ed}}{M_{c,Rd}} \leq 1.0 \quad (2.43)$$

In which N_{Ed} is the design axial force and M_{Ed} the design moment acting on the element at the cross-section under consideration, $N_{c,Rd}$ is the cross-section axial resistance, and $M_{c,Rd}$ is the cross-section moment resistance.

For doubly symmetrical I and H-sections or other flanges' sections, allowance need not be made for the effect of the axial force on the plastic resistance moment about the y-y axis when both the criteria of equations (2.44) and (2.45) are satisfied.

$$N_{Ed} \leq 0.25N_{pl,Rd} \quad (2.44)$$

$$N_{Ed} \leq \frac{0.5h_w t_w f_y}{\gamma_{M0}} \quad (2.45)$$

Where:

h_w is the height of the web;

t_w is the thickness of the web;

f_y is the yield strength of steel;

γ_{M0} is the safety coefficient with value 1.25.

2.8.3.5. Connection design

The connection between the structural members are done using bolted connections and they are to be analyzed at ULS based on EN1993-1-8 (2005). The connection is a bearing type bolted connection using non-preloaded bolts.

a. Beam-column connection

The beam to column connection present in this work is an eave moment connection connecting a rafter with a column since the building is made of a portal frame with eave haunches.

i. Shear resistance

The shear resistance of the bolts are going to be verified according to the equations (2.46) and (2.47).

$$F_{v,Rd} = 0.6f_{ub} \frac{A_b}{\gamma_{M2}} \quad \text{for class 4.6, 5.6 and 8.8} \quad (2.46)$$

$$F_{v,Rd} = 0.5f_{ub} \frac{A_b}{\gamma_{M2}} \quad \text{for class 4.8, 5.8.6.8 and 10.9} \quad (2.47)$$

Where;

A_b is the cross sectional area of the bolt at the shear plane determined by equation (2.48)

f_{ub} is the ultimate strength of the bolt;

γ_{M2} is a safety factor whose recommended value is 1.25.

$$A_b = \frac{\pi d^2}{4} \quad (2.48)$$

ii. Bearing resistance

The bearing resistance of the bolt on the plate is going to be verified according to equations (2.49).

$$F_{b,Rd} = \frac{k_1 a_b f_u d t}{\gamma_{M2}} \quad (2.49)$$

Where:

d is the diameter of the bolts;

f_u is the yielding strength of the plate;

a_b is the smallest of α_b ; $\frac{f_{ub}}{f_u}$ or 1;

α_b equals $\frac{e_1}{3d_0}$ for end bolts and $\frac{p_1}{3d_0} - \frac{1}{4}$ for inner bolts;

k_1 is the smallest of $2.8 \frac{e_2}{d_0} - 1.7$ or 2.5 for edge bolts;

k_1 is the smallest of $1.4 \frac{p_2}{d_0} - 1.7$ or 2.5 for inner bolts;

d_0 is the diameter of the bolts' holes on the plate;

e_1 , e_2 , p_1 , p_2 are shown in figure 2.6.

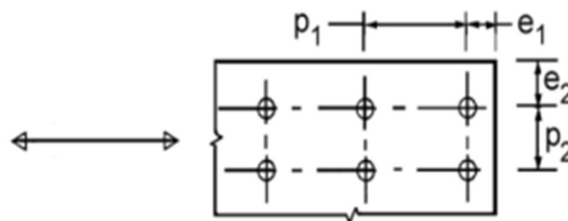


Figure 2.6. Spacing of holes on the plate (EN 1993-1-8, 2005)

iii. Traction resistance

The resistance to traction of each bolt is given by equation (2.50).

$$F_{t,Rd} = \frac{k_2 f_{ub} A_s}{\gamma_{M2}} \quad (2.50)$$

Where:

A_s is the tensile stress area of the bolt;

k_2 is equal to 0.9

iv. Simultaneous traction and shear

Simultaneous traction and shear will be verified as shown in equation (2.51)

$$\frac{F_{v,Ed}}{F_{v,Rd}} + \frac{F_{t,Ed}}{1.4F_{t,Rd}} \leq 1.0 \quad (2.51)$$

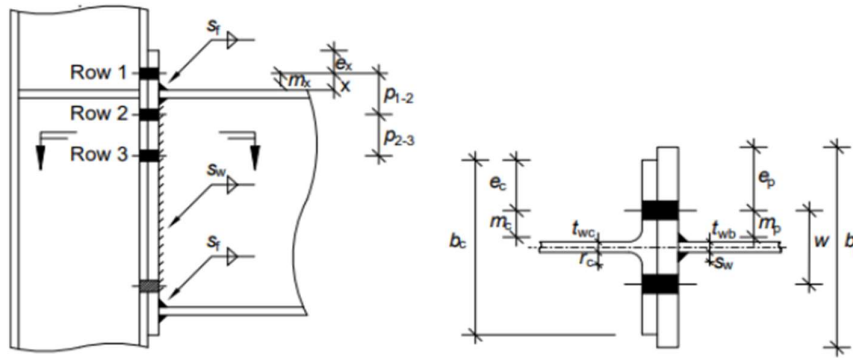
With $F_{v,Ed}$ and $F_{t,Ed}$ are respectively the shear and traction forces.

v. Resistances of bolt rows in the tension zone

The effective design tension resistance for each row of bolts in the tension zone is limited by the least resistance of bending in the column flange, tension in the column web, bending in the end plate and tension in the rafter web. In bolted connections. An equivalent T-stub in tension may be used to model the design resistances for the endplate and the column flange separately.

vi. Column flange in bending

The connection geometry for an end plate connection is shown in figure 2.7. The geometry for a haunched connection in a portal frame would be similar although the beam would usually be at a slope and there will be more bolts rows as shown in figure 2.8 which provides information to identify its basic joint components.



For the end plate:

$$m_p = \frac{w}{2} - \frac{t_{wb}}{2} - 0.8s$$

$$e_p = \frac{b_p}{2} - \frac{w}{2}$$

For the column flange:

$$m_c = \frac{w}{2} - \frac{t_{wc}}{2} - 0.8r_c$$

$$e_c = \frac{b_c}{2} - \frac{w}{2}$$

For the end plate extension only:

$$m_x = x - 0.8s_f$$

Adjacent to a flange or stiffener:

m_2 is calculated in a similar way to m_x , above. m_2 is the distance to the face of the flange or stiffener, less 0.8 of the weld leg length.

Note: dimensions m and e , used without subscripts, will commonly differ between column and beam sides

where:

w is the horizontal distance between bolt centrelines (gauge)

b_p is the end plate width

b_c is the column flange width

t_{wb} is the beam web thickness

t_{wc} is the column web thickness

s is the weld leg length ($s = \sqrt{2}a$, where a is the weld throat) (subscripts f and w refer to the flange and the web welds respectively)

r_c is the fillet radius of the rolled section (for a welded column section use s , the weld leg length)

Figure 2.7. Connection geometry (SCI P398)

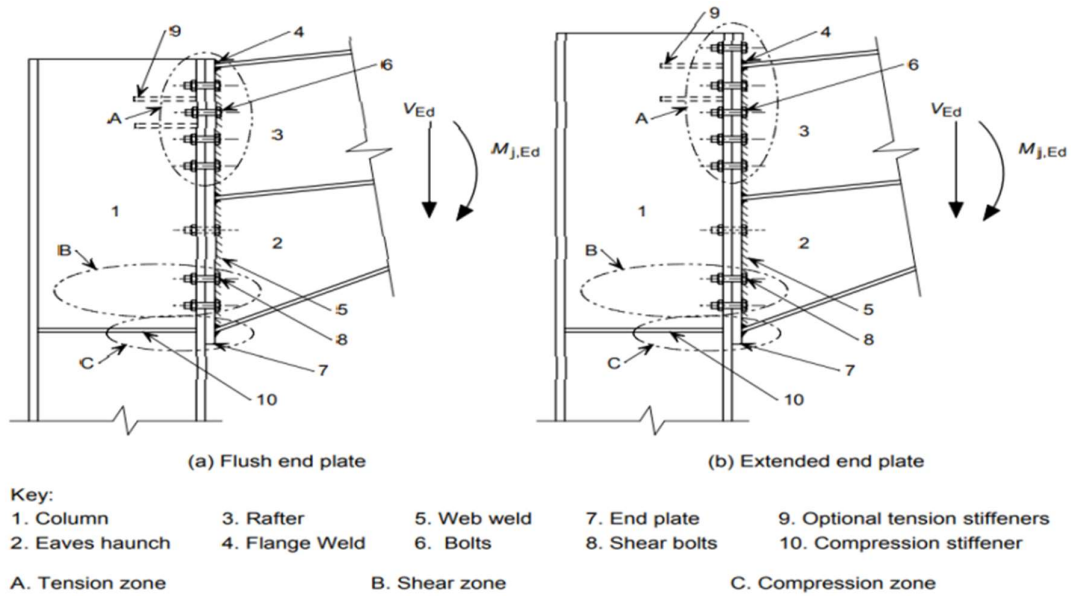


Figure 2.8. Portal frame eaves connection with bolted end plate (NCCI, 2008)

The resistances are calculated for three possible modes of failure and the least value is taken as shown in equation (2.52).

$$F_{t,fc,Rd} = \min(F_{T,1,Rd}; F_{T,2,Rd}; F_{T,3,Rd}) \quad (2.52)$$

- Mode 1

For the failure mode 1, the failure is due to the plate as shown in figure 2.9.

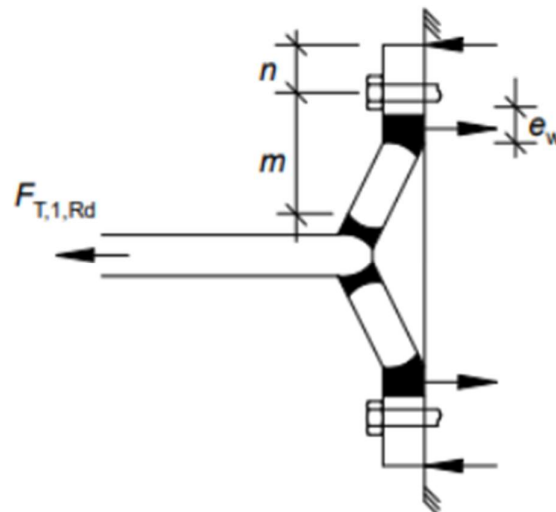


Figure 2.9. Complete flange yielding (SCI P398)

Using “Method 2” in Table 6.2 of EN 1993-1-8 (2005), the design resistance of the T-stub flange is calculated as shown in equation (2.53).

$$F_{T,1,Rd} = \frac{(8n - 2e_w)M_{pl,1,Rd}}{2mn - e_w(m + n)} \quad (2.53)$$

Where:

$M_{pl,1,Rd}$ is the plastic resistance moment of the equivalent T-stub for mode 1 as calculated in equation (2.54).

$$M_{pl,1,Rd} = \frac{0.25 \sum l_{eff,1} t_p^2 f_y}{\gamma_{M0}} \quad (2.54)$$

m is defined in figure 2.7.

$$e_w = \frac{d_w}{4};$$

d_w is the diameter of the washer or the width across points of the bolt head. Washers are not necessarily provided and it is conservative to assume washers are not used;

$\sum l_{eff,1}$ is the effective length of the equivalent T-stub for mode 1 (see annex 7)

$t_{w,b}$ is the web thickness of the beam;

n is the $\min(e_c; e_p; 1.25m)$

e_c is the edge distance of the column flange;

e_n is the edge distance of the end plate

e_p is the edge distance of the end plate.

- Mode 2

For the failure mode 2, the failure is due to the local yielding of the plate and bolts failure as shown in figure 2.10.

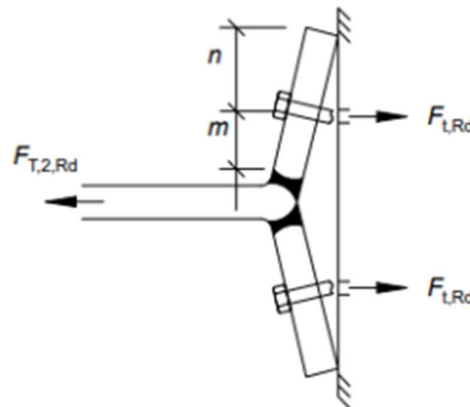


Figure 2.10. Bolt failure with flange yielding (SCI P398)

The design resistance of the T-stub flange is calculated as shown in equation (2.55).

$$F_{T,2,Rd} = \frac{2M_{pl,2,Rd} + n \sum F_{t,Rd}}{m + n} \quad (2.55)$$

Where:

$\sum F_{T,Rd}$ is the total tension resistance for the bolts in the T-stub (it is equal to $2 \times F_{t,Rd}$ for a single row)

$M_{pl,2,Rd}$ is the plastic resistance of the equivalent T-stub for mode 2 as calculated in equation (2.56).

$$M_{pl,2,Rd} = \frac{0.25 \sum l_{eff,2} t_p^2 f_y}{\gamma_{M0}} \quad (2.56)$$

$\sum l_{eff,2}$ is the effective length of the equivalent T-stub for mode 2 (annex 7).

- Mode 3

In mode 3, the failure is due to the bolts as shown in figure 2.11.

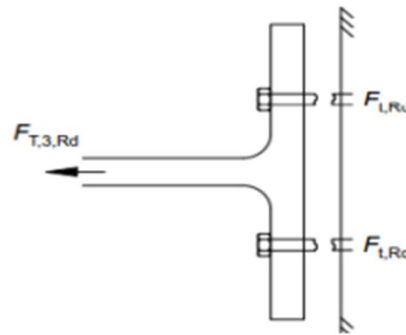


Figure 2.11. Bolt failure (SCI P398)

The design resistance of the T-stub flange is given by equation (2.57).

$$F_{T,3,Rd} = \sum F_{t,Rd,u} \quad (2.57)$$

vii. Column web in transverse tension

The transverse tension resistance for a column web is given in equation (2.58).

$$F_{t,wc,Rd} = \frac{\omega b_{eff,t,wc} t_{wc} f_{y,wc}}{\gamma_{M0}} \quad (2.58)$$

Where:

ω is the reduction factor to allow for the interaction with shear in the column web panel as calculated in equation (2.59).

$$\omega = \frac{1}{\sqrt{1 + 1.3 \left(\frac{b_{\text{eff},c,wc} t_{wc}}{A_{vc}} \right)^2}} \quad (2.59)$$

A_{vc} is the shear area of the column. For rolled I and H sections it can be conservatively taken as $h_w t_w$;

$b_{\text{eff},t,wc}$ is equal to l_{eff} .

viii. End plate in bending

The design resistance and failure mode of an end-plate in bending, together with the associated bolts in tension can be determined following the methodology used for column flange and using equation (2.60).

$$F_{t,ep,Rd} = \min(F_{t,1,Rd}; F_{T,2,Rd}; F_{T,3,Rd}) \quad (2.60)$$

ix. Rafter web in tension

The resistance of the rafter web in tension can be calculated as shown in equation (2.61).

$$F_{t,wb,Rd} = \frac{b_{\text{eff},eb} t_{wb} f_{y,wb}}{\gamma_{M0}} \quad (2.61)$$

Where $b_{\text{eff},t,wb}$ is equal to l_{eff}

x. Total resisting moment

The total resisting moment is obtained from the sum of the products of the traction resistance in each bolt row in the tension zone times with their respective distances d_i from the center of resistance of the compression zone (neutral axis of the compression flange) as shown in equation (2.62).

$$M_{Rd} = \sum F_{t,Rd,i} \times d_i \quad (2.62)$$

b. Beam-beam connection

This connection is done between two rafters of the portal frame as shown in figure ... The verification procedure will be done as for the beam to column connection.

The shear resistance per bolt is computed using equation (2.46) or equation (2.47) depending on the bolt grade. Bearing resistance per bolt, traction resistance per bolt and total moment resistance will be verified using equation (2.49), (2.50) and (2.62) respectively.

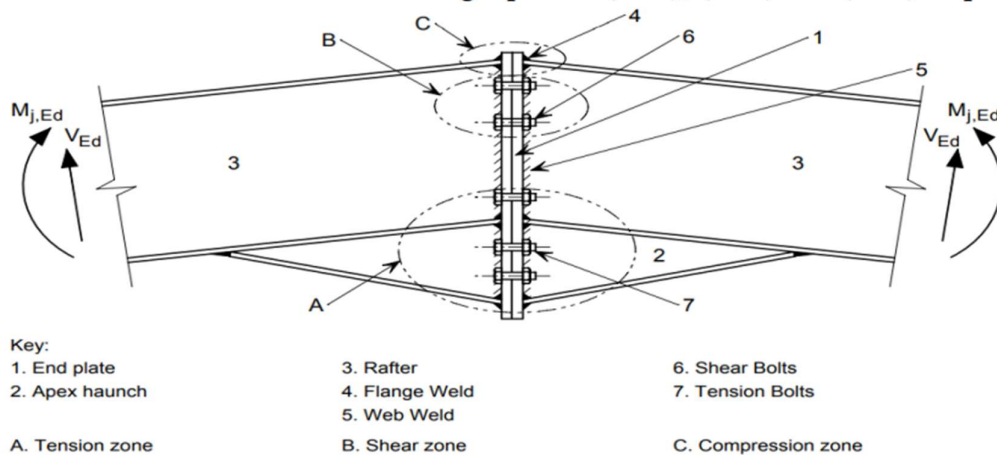


Figure 2.12. Portal frame apex connection with bolted extended end plate (NCCI, 2008)

c. Brace connection

The presence of the brace is mainly to take horizontal loads and these loads are transmitted through the brace connections. This connection is a simple one with no moment. The shear resistance per bolt is computed using equation (2.46) or equation (2.47) depending on the bolt grade and the bearing resistance will be verified using equation (2.49).

d. Design of the column base plate

The verification of the column base connection is done by verifying the concrete base and the thickness of the plate. A basic component for more elaborated joints is the T-stub joint. The T-stub joint have bolts on two sides and are appropriate for connections with I-sections as in the case considered.

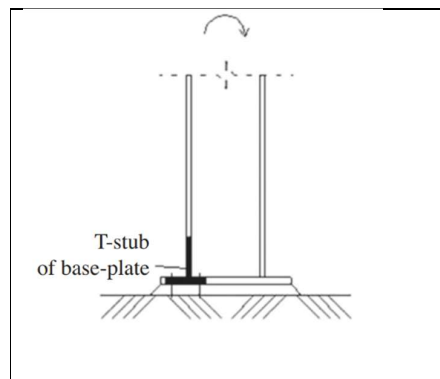


Figure 2.13. T-stub of the base plate

For this connection, the resistance of each T-stub must be calculated independently and the final resistance be determined as the minimum value between the two T-stubs.

i. Concrete footing

Firstly, the bearing capacity is verified using equation (2.63).

$$\sigma_{sol} \leq \sigma_{adm} \quad (2.63)$$

Where σ_{sol} is the pressure exerted by the footing on the ground and it is calculated using the equation (2.64).

$$\sigma_{sol} = \frac{N_{SLS} + \gamma \times A \times B \times H}{A \times B} \quad (2.64)$$

Where:

N_{SLS} is the axial force exerted at the column in SLS conditions;

A and B are the dimensions of the section of the concrete footing;

H is the height of the concrete footing;

γ is the unit weight of concrete.

Afterwards, the compressive resistance of the concrete block is verified with the help of equation (2.65).

$$\sigma < f_{ck} \quad (2.65)$$

Where:

f_{ck} is the characteristic compressive cylinder strength of concrete;

σ is the compressive stress exerted on the concrete block calculated using the equation (2.66)

$$\sigma = \frac{N}{ab} \quad (2.66)$$

ii. Plate

Admitting that part of the plate at the edge of the columns will be subjected to an uplift due to the reactions from the foundations, it will bend according to the tangent lines 1 and 2 shown in figure ...

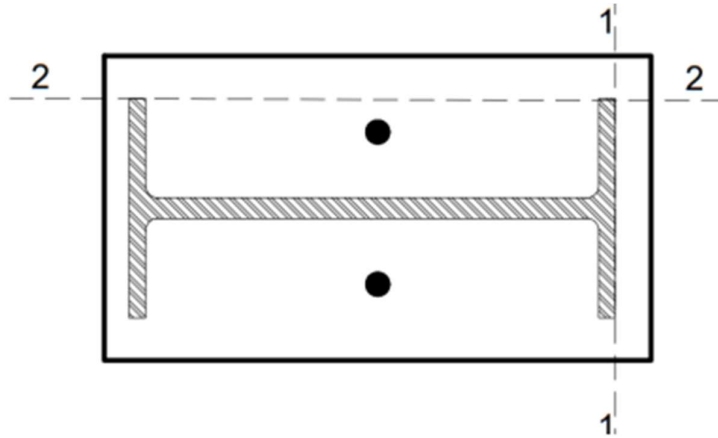


Figure 2.14. Tangent lines on the base plate which determine uplift (Morel, 2005)

The thickness of the plate is verified using the equation (2.67).

$$t \geq u \sqrt{\frac{3\sigma}{f_y}} \quad (2.67)$$

Where:

u is the perpendicular distance from the edge of the beam flange to the edge of the column (lever arm).

Afterwards the shear resistance, bearing resistance and traction resistance of the anchors will be verified using equation (2.46) or (2.47), (2.49) and (2.50) respectively.

When the force transferred to the foundation is significant, a single base plate is insufficient, so vertical stiffeners on the base plates are required. The actual code (Eurocode) does not provide guidelines for calculations of column bases with such complex geometry.

A calculation procedure to determine the bending resistance of steel column bases with stiffeners considering plastic stress distribution based on the Eurocode proposed by Marcin Gorski was proposed for the design of a stiffened baseplate. This method is based on a scheme of distribution of forces as shown in figure 2.15.

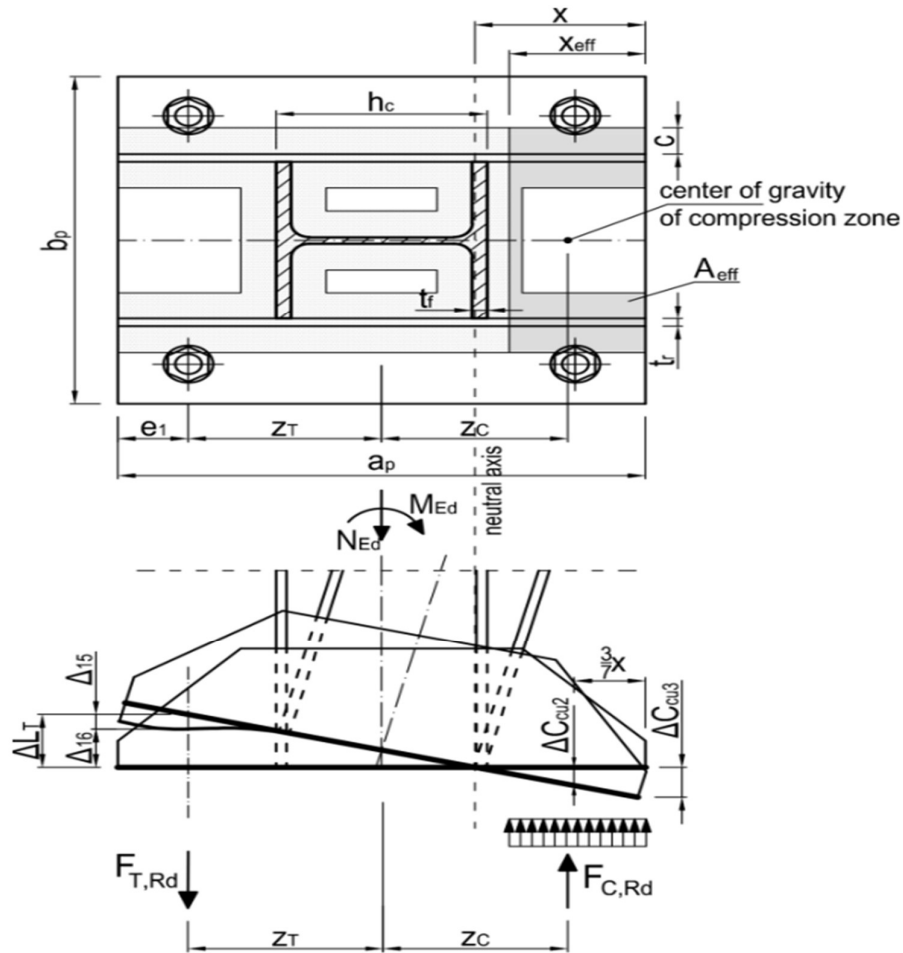


Figure 2.15. Scheme of distribution of forces and displacements in column base

This procedure to compute the bending resistance of the column base consists of the following steps:

Step 1: Calculation of the resistance of the tension zone $F_{T,Rd}$ and the associated necessary displacement $\Delta_{L_{T,Rd}}$.

Step 2: If necessary, the assumption of the reduced resistance of the tension zone $F_{T,Rd,red}$ due to insufficient displacement in this zone is considered.

Step 3: Calculation of the required resistance of the compression zone using equations (2.68) or (2.69):

$$F_{C,Rd} = F_{T,Rd} + N_{Ed} \quad (2.68)$$

$$F_{C,Rd} = F_{T,Rd,red} + N_{Ed} \quad (2.69)$$

Step 4: Determining the range of the compression zone x_{eff} and x .

Step 5: Calculation of the vertical displacement of the tension zone ΔL_T and comparison with $\Delta L_{T,Rd}$.

Step 6: If necessary, calculation of the actual resistance of the tension zone $F_{T,Rd,red}$ and comparison with the assumed value in step 2. In case of discrepancies repeating steps 2 – 6 is performed until satisfactory compatibility is reached.

Step 7: Calculation of the bending resistance using equations (...) or (...):

$$M_{j,Rd} = F_{C,Rd} \cdot (z_c + z_r) - N_{Ed} \cdot z_T \quad (2.70)$$

$$M_{j,Rd} = F_{C,Rd} \cdot z_C + F_{T,Rd,red} \cdot z_T \quad (2.71)$$

2.8.3.6. Serviceability limit states check for steel members

For the structure, it shall be verified that the maximum deflection of each elements is less than its maximum value according to Eurocodes. For beam elements, the maximum vertical deflection should be less than $l/200$, where l is the length of the beam in millimeters. For columns, the maximum horizontal deflection should be less than $h/300$, where h is the height of the column.

2.9. Numerical sub-model for stress-diffusion analysis

Important parts of a structure could be modeled separately from the global structure for optimization purposes and local analysis. Local analysis models generally collaborate with the global model. Analysis is performed on the global model in order to determine global deformations, internal forces and moments. Subsequently the area of interest is separated and a more refined local model is built. The load effects as determined in the global model are introduced at the boundaries of the local model for a detailed study of the area. Such technique will be implemented in this methodology to study the stress diffusion in a column base plate. The FEA software that will be used to perform this local analysis is Abaqus CAE.

2.9.1. Presentation of the numerical software Abaqus

ABAQUS is a set of finite element analytical programs originally developed by Hibbit, Karlsson & Sorenson, Inc. and currently maintained by SIMULIA Corp. ABAQUS is a

general-purpose simulation tool, and can solve a wide range of engineering problems, including stress analysis problems. ABAQUS has extensive elements and material libraries capable of modelling a variety of geometries and material constitutive laws.

ABAQUS consists of three main products: ABAQUS/Standard, ABAQUS/Explicit and ABAQUS/CAE. While ABAQUS/Standard and ABAQUS/Explicit perform analysis, ABAQUS/CAE provides a graphical environment for pre and post-processing. ABAQUS/Standard is a general-purpose analysis program for solving linear, non-linear, static and dynamic problems. ABAQUS/Explicit is a special-purpose analysis program that uses an explicit dynamic finite element formulation. It is suitable for modelling brief, transient dynamic events, such as impact and blast problems. ABAQUS/Standard and ABAQUS/CAE are used in this thesis for stress analysis.

In general, a complete ABAQUS simulation consists of 3 distinct stages: preprocessing, simulation and postprocessing as shown in Figure...

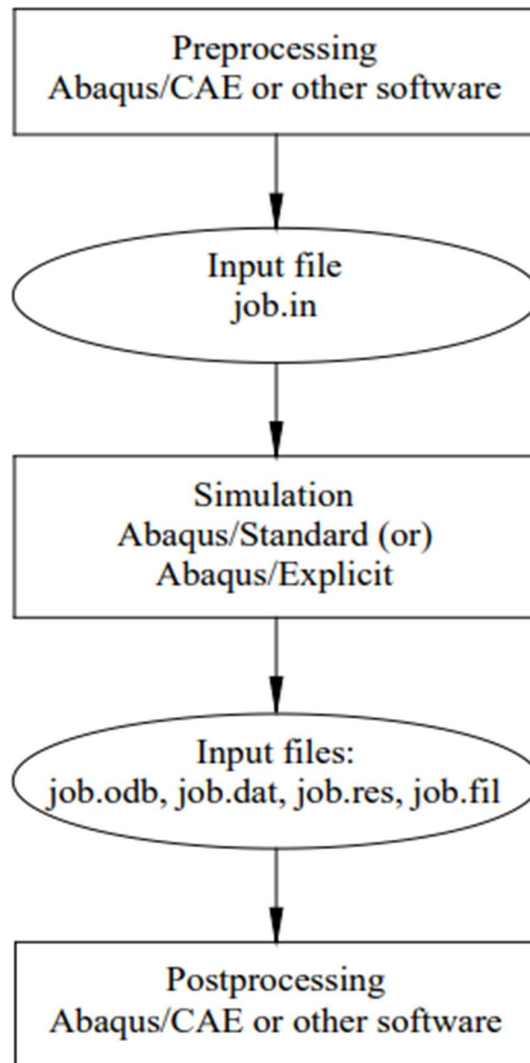


Figure 2.16. ABAQUS Stages of a complete simulation

2.9.2. Model definition

The ABAQUS model will be created following procedural modules provided in the software. They are; the part module, property module, assembly module, step module, interaction module, load module, mesh module, job module and the visualization module where the results will be visualized.

2.9.2.1. Part module

Here, connection components (base-plate, column, concrete, anchors and stiffeners) will be modelled as three-dimensional deformable solids using eight-node linear brick elements. The

actual dimensions of the real column base plate connection will be considered in the finite elements model.

2.9.2.2. Property module

In order to obtain numerical results with higher accuracy, the material non-linearity will be considered during the analysis. Information regarding the characteristic strength of different elements are provided which allows the evolution of steel resistance with time to be considered.

a. Steel

For steel elements such as the IPE column, baseplate and anchor bolts, the material characteristics obtained from the construction documents will be used.

b. Concrete

An estimate of the evolution of maximum compressive strength in concrete will be considered based on results from a standard cylinder test. The concrete behavior law considered here is taken from EN 1992-1-1 and expressed by equation 2.72.

$$\frac{\sigma_c}{f_{cm}} = \frac{k\eta - \eta^2}{1 + (k - 2)\eta} \quad (2.72)$$

With

$$f_{cm} = f_{ck} + 8$$

$$\eta = \varepsilon_c / \varepsilon_{c1},$$

$$k = 1.05 E_{cm} \times \frac{|\varepsilon_{c1}|}{f_{cm}}$$

A Concrete Damaged Plasticity model will be used to model the concrete material behavior. CDP model allows us to define the plasticity by damage parameters as well as the behavior in tension and compression of the concrete. Nominal values suggested in EN 1992-1-1 will be used to define the stress-displacement law in tension. The characteristics of concrete will be detailed with the help of compressive stress-strain diagrams and tensile stress-displacement diagram as shown in figure 2.17.

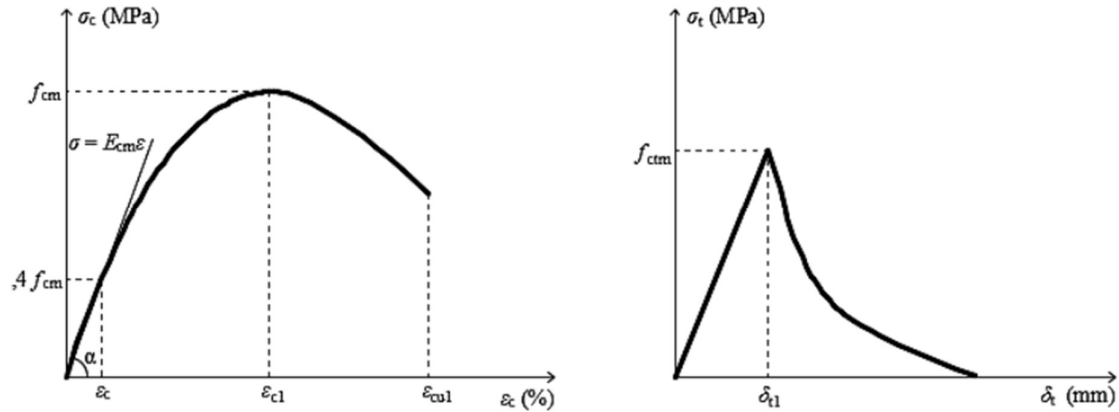


Figure 2.17. Concrete stress-strain law for compression and stress-displacement law for tension

The parameters that will be used to define the CDP model for all models are the dilation angle, the eccentricity, the strength ratio between the biaxial state and the uniaxial state and the viscosity parameter.

2.9.2.3. Assembly module

This module involves the combination of all the parts created to obtain the column base connection model.

2.9.2.4. Step module

The analysis will be performed in two subsequent steps. The initial step is defined to set the contact interactions between the elements and the boundary conditions. The second step is used to reproduce the loading conditions obtained from the static global analysis performed. For that, a vertical force parallel to the center line of the column steel profile is applied at the top of the column. In addition, the moments in the x (Mx) and y (My) directions could be considered in the model depending on the study performed.

2.9.2.5. Interactions

In order to represent the real behavior of the column base plate, a special attention will be given to the interactions between the different components of the column base connection. Contact interactions between elements strongly affect the computing process (time, convergence, accuracy). For the same model and depending on the applied loading, the contact conditions

between elements can vary widely and consequently affect the internal force distribution. Interactions in ABAQUS are characterized as step dependent and thus, must be defined in the correct analysis steps. To create it, a contact pair between two rigid or deformable three-dimensional surfaces has to be defined. Although it is not necessary to guarantee matching meshes on the connected surfaces, the establishment of a “master” and “slave” surface is required. As master surfaces, analytical rigid surfaces and rigid-element-based surfaces, smaller surfaces in case of contact with a larger surface, stiffer body surface, and coarser mesh surface should be considered. Several contact interactions between elements will be created in the model. The types of contact interactions are listed below:

- “rigid body” constraint: this type of constraint is used to create a rigid cross-section at the top of the column where the load is applied. The reference point is located at the geometric center of the column cross-section for all models. This constraint allows to guarantee the uniformity of imposed loads throughout the section
- “tie” constraint: this type of constraint is used to tie two surfaces in contact during the simulation. Constraints involving two surfaces connected by a weld as shown in figure... are created using “tie” constraints.
- steel-steel interaction: to model the contact between two steel surfaces, a surface to surface discretization method with finite sliding formulation is considered with a friction coefficient equal to 0.35. For normal behavior, the hard contact is selected allowing separation and preventing penetration of surfaces in contact,
- steel-concrete interaction with a friction coefficient equal to 0.35.

2.9.2.6. Load module

In this module, the loads will be applied as well as the boundary conditions to be able to simulate the real loading condition of the model.

2.9.2.7. Mesh

In order to reduce the computing time needed for the simulation, different mesh sizes are usually adopted according to the importance of the elements. Since the scope of this study focuses on the stress distribution in the base plate and the existing literature suggests that the

anchoring system has a heavy influence on the base plate behavior, these two elements are chosen as the most important of the model. As a consequence, a particular attention is given to the discretization of these elements. To produce reasonable and physically sound stress distributions at the interface between the anchor bolts and the concrete, a smaller mesh size will be selected for the layer of concrete material in contact with the anchor bolts. For the remaining concrete material, a coarser mesh will be considered as this zone is of little interest. In areas with high stress concentrations such as welds, mesh size needs to be reduced. Similarly, in regions where buckling and/or bending are expected such as column flanges and base/end plates mesh sizes should be reduced. Typically, this limits inaccuracies in the results and convergence problems due to severe change of stresses and strain distributions during the simulation.

2.10. Stress diffusion analysis

The stress analysis is performed using ABAQUS and it is initiated in the job module. It is performed by resolving the principal von-mises-stress equations which are used depending on the type of loading. The equations used to obtain the von-mises stress are;

$$\sigma = \sqrt{\sigma_1^2 + \sigma_2^2 + \sigma_3^2 - \sigma_1\sigma_2 - \sigma_2\sigma_3 - \sigma_3\sigma_1} \quad (2.73)$$

OR

$$\sigma = \sqrt{\frac{(\sigma_1 - \sigma_2)^2 + (\sigma_2 - \sigma_3)^2 + (\sigma_3 - \sigma_1)^2}{2}} \quad (2.74)$$

And to avoid the failure,

$$\sigma = \sqrt{\frac{(\sigma_1 - \sigma_2)^2 + (\sigma_2 - \sigma_3)^2 + (\sigma_3 - \sigma_1)^2}{2}} < \sigma_{yt} \quad (2.75)$$

Where, $\sigma_1, \sigma_2, \sigma_3$ are the principal stresses

The stresses obtained are then analyzed to study the stress diffusion. The stress diffusion study shall be performed on the column base plate subjected to the design axial load so as to verify and validate the model with respect to the design standards. Prior to the stress diffusion, the selection of the column base model which will be the subject of study is done based on a criteria.

2.10.1. Determination of the critical column base connection to be studied

The most critical column is the one which induces more stresses in the base plate. This is the criteria of choice that will be used for the selection of the column which will be designed.

The analysis of the models for the selection will be performed on Abaqus, the von mises stress values will be obtained and subsequently the choice will be made.

In addition to this, stress diffusion studies shall be conducted on the column base plate subjected to the following loading conditions; axial loading, bending moment, biaxial loading. This shall be done during the parametric studies which shall be performed.

2.10.2. Stress analysis of the column base plate subjected to the design axial load

After completing the model definition as the methodology clearly explains, the column base model will be subjected to the design axial load obtained from the static global analysis. This load will be used to perform a stress analysis of the overall model from which various stress distributions of the different components shall be obtained. In this section, these resulting stress distributions shall be presented for each component with more attention portrayed to the diffusion of stress in the base plate.

2.10.3. Parametric study of the stress on base plate with respect to the Axial load

In this section, a study will be performed to evaluate the stress diffusion under five different axial loading conditions and subsequently the pattern of stress diffusion will be observed.

2.10.4. Parametric study of the stress on base plate with respect to the baseplate thickness

Here, the thickness of the base plate will be varied with respect to different axial loads. The different von mises stresses will be obtained and the variation pattern observed.

Conclusion

The aim of this chapter was to describe the different steps followed in order to achieve the objectives of this work. Primarily, the procedures for obtaining the design parameters are described supported by the corresponding norms used. Secondly, a description of the static design procedure is provided and finally, the key points of the stress diffusion study are highlighted.

CHAPTER 3 : RESULTS AND INTERPRETATIONS

Introduction

This chapter will portray the results of the procedure described in chapter two. It consists of the presentation of results obtained from the general site recognition and site visit, the data collected and the results from the static verification of the steel structural elements.

In addition to this, the results of the local sub model stress analysis of the column base connection performed in ABAQUS is presented, considering the results from the different loading conditions under which the column base is subjected.

3.1.General presentation of the site

The case study is located in the center region of Cameroon, Yaoundé, precisely at the area known as Terminus Odza. Here, a general overview of Yaoundé will be done, showing its physical and socio-economical parameters.

3.1.1. Physical parameters

The case study's physical parameters will be outlined such as its; geographical location, climate and hydrology.

3.1.1.1. Location

The city of Yaoundé whose coordinates are 3°52'N 11°31'E is found in the center region of Cameroon. The case study is located at Odza street precisely at the area known as "Terminus Odza". Figure 3.1 shows the location of the case study.

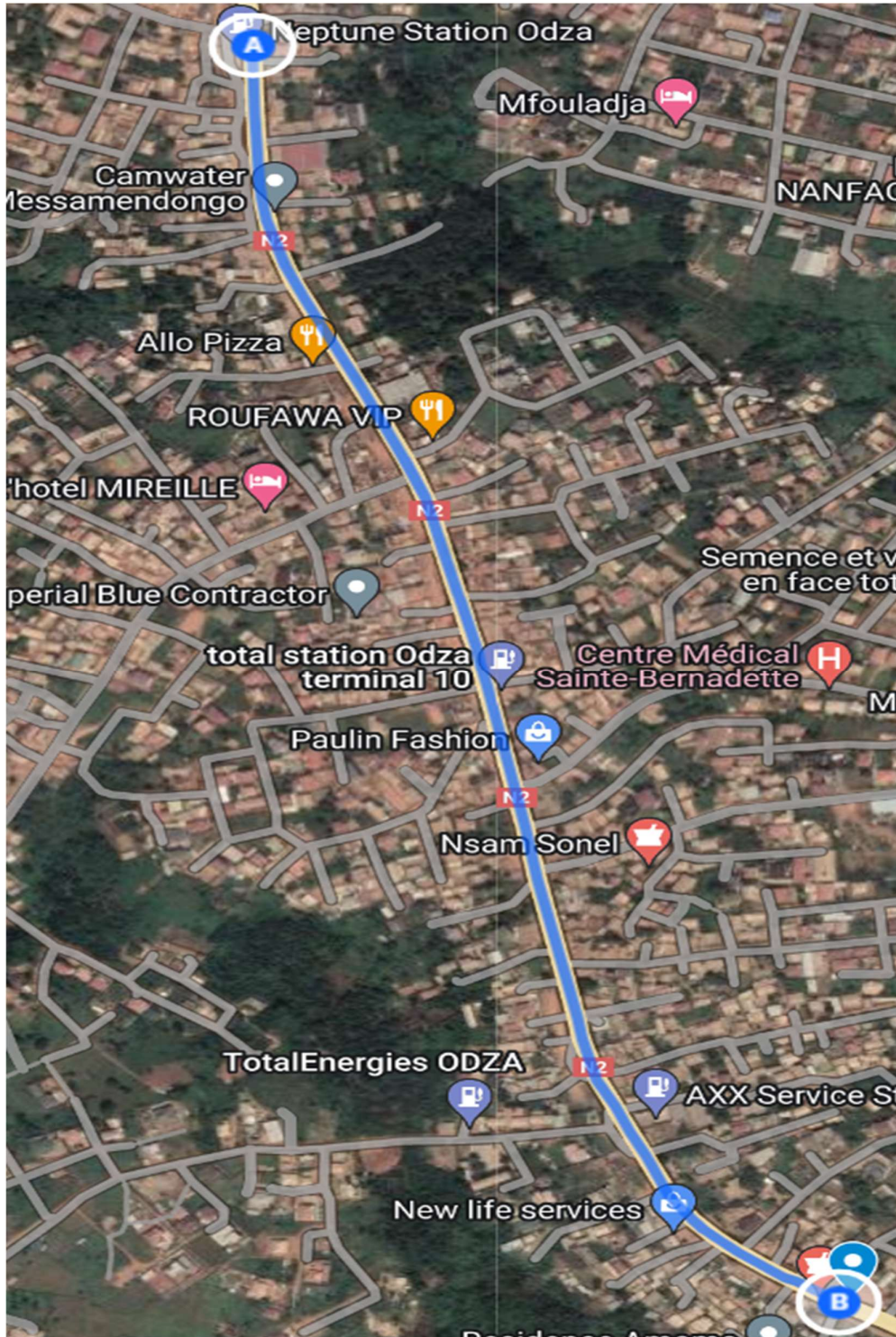


Figure 3.1. Location of the Case study

3.1.1.2. Climate and Hydrology

Yaoundé features a tropical wet and dry climate with constant temperatures throughout the course of the year. Figure 3.2 shows the climate chart of Yaoundé which expresses the variation

amount of rainfall with respect to the different periods of the year. A dry season from December to February and a rainy season from March to November. The rains decrease a bit in July and August, although the sky remains often cloudy.

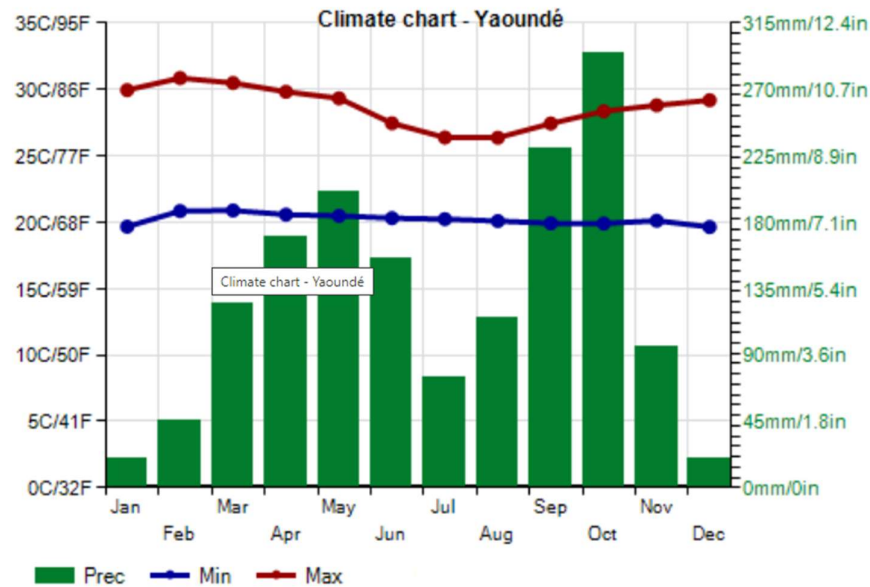


Figure 3.2. Yaoundé Ombrothermic diagram (climatestotravel.com)

The city of Yaoundé is situated slightly above the equator between Latitude 3° 47'-3° 56' North and between Longitude 11° 10'-11° 45' East. It is a Sub-equatorial city and records an average precipitation of 1600mm/year, average temperature of 23°C and four seasons.

The hydrographic network of Yaoundé is very dense and composed permanent rivers such as the Mfoundi river which crosses the city from North to South, a few creeks and lakes.

3.1.2. Socio-economical parameters

The socio-economical parameters used to characterize Yaoundé in this section are; population, transport and economic activities carried out in this area.

3.1.2.1. Population

Yaoundé has a population estimated to be 4336670 in 2022 with a growth rate of 4.14% from the previous year's estimate (source: worldpopulationreview.com).

3.1.2.2. Economy

Yaoundé's economy is centered on the administrative structure but industries performing in other sectors exist such as; tobacco, dairy products, beer, clay, glass goods and timber.

3.1.2.3. Transport

The transportation means available in Yaoundé include railways, roadways, waterways, pipelines and airlines. These transport means are used by citizens for personal transportation, by businesses for transporting goods and by tourists for both accessing the country and traveling while within the country.

3.2. Physical description of the site

The case study is located at Odza in Yaoundé precisely at “Terminus Odza”. The area is not an industrial zone and based on the percentage of residential buildings around the area it is safe to consider the area a residential area.

Though being in a residential area, the case study is not destined for residential use. It is a steel warehouse destined for storage uses whose construction is still on going as shown in figure.



Figure 3.3. Ware house for stockage at Odza

3.3. Presentation of the project

The project is a five span-single-story steel warehouse comprising of a series of unbraced transverse portal frames. The primary steel work consists of columns and rafters which form the portal frames and bracings in-between the purlins found on the roof. The warehouse was

FEM ANALYSIS APPLIED TO THE STUDY OF STRESS DIFFUSION IN THE BASEPLATES OF STEEL STRUCTURES

built on an area of approximately 8000m². The shed width of each span is 24.75m but they do not have the same length nor the same number of portal frames. A presentation of the site is done in figure 3.2.

3.3.1. Presentation of the structural data

The project is a multiple portal frame ware house with no lateral brace system. The spans in-between are imbued with masonry infills. Figure 3.2 materializes the building and specifies its external boundaries. Figure 3.3 illustrates the structural system considered.

ODZA WAREHOUSE : GROUND FLOOR PLAN

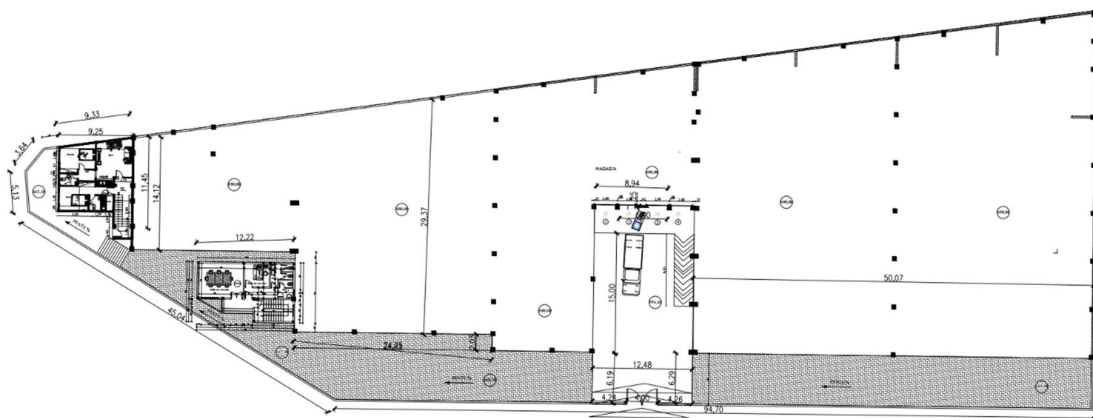


Figure 3.4. Site plan portraying the ware house

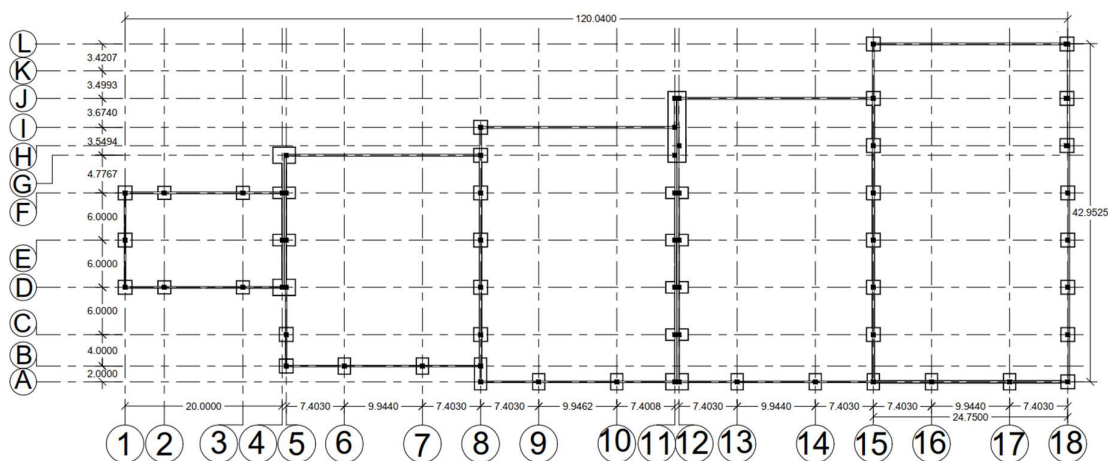


Figure 3.5. Structural floor plan of the ware house

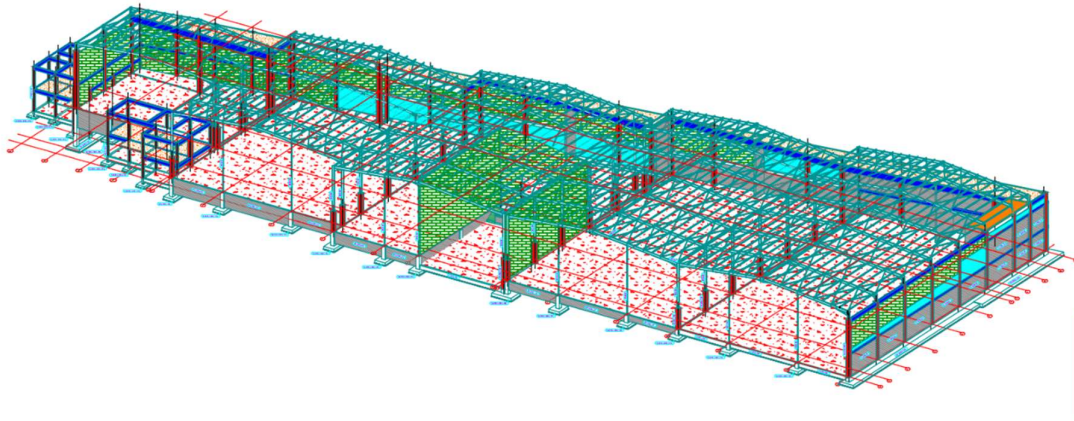


Figure 3.6. Structural Plan (3D)

The building consists of the following elements:

- Five portal frame spans with a shed width of 24.75m each
- The portal frames are separated by a distance of 6m each, also this value varies and becomes lower when we go towards the portal frames at the ends.
- The portal frames are made up of two IPE 300 columns deriving their support from concrete base columns. The total height of these columns is 8.8m (eave height) from the ground.
- Each frame has two IPE 300 rafter beams forming a half-range punch. Also, haunches at the rafter to column and rafter to rafter connection.
- Each frame has IPE 120 gable columns at the front faces
- IPE 120 steel profiles as purlins spaced at 1.2m from each other;
- L60x5-steel profile used for the bracing system

3.3.2. Characteristics of the materials

The structure is composed of steel and concrete materials but predominantly steel. The steel grades used here are S275 JR for the structural sections and S235JR for additional steel elements like stiffeners; material specifications with respect to the steel grades are given in tables 3.1. The concrete class used is C25/30 and specifications related to this are presented in table 3.2.

Table 3.1. Steel material properties (S235JR)

Property	Value	Unit	Definition
Steel grade	S235JR	-	Characteristic strength of steel
f_y	235	N/mm ²	Yield strength of steel
f_u	360	N/mm ²	Ultimate strength of steel
E	210000	N/mm ²	Young's modulus
G	80769.23	N/mm ²	Shear modulus
ν	0.3	-	Poisson's ratio
γ_{M0}	1	-	Coefficient of safety for all sections
γ_{M1}	1	-	Coefficient of safety for unstable members
γ_{M2}	1.25	-	Coefficient of safety for cross sections in tension.
f_{yb}	640	N/mm ²	Yield strength of bolt grade
f_{ub}	800	N/mm ²	Ultimate strength of anchor

Also, S275JR steel profiles have been used in this structure,

Table 3.2. Concrete and reinforcing steel properties

Property	Value	Unit	Definition
Concrete class	C25/30	N/mm ²	Concrete class
f_{ck}	25	N/mm ²	Cylindrical crushing strength
f_{ctk}	2.5	N/mm ²	Characteristic tensile strength
E_{cm}	31000	N/mm ²	Secant modulus of elasticity of concrete
ϵ_{cu2}	0.35%	-	Ultimate compressive strain of concrete
γ_c	1.5	-	Safety coefficient of concrete

Reinforcing steel	B450C	-	Reinforcement steel type
f_{yk}	450	N/mm ²	Characteristic yield strength of reinforcing steel
E_s	210000	N/mm ²	Modulus of elasticity of reinforcing steel
γ_s	1.15	-	Safety factor for steel

3.4.Loads determination

The building is constructed for storage purposes implying that it automatically falls under the category E1 as shown in annex 2. The wind loads acting on the structure were determined using equations from EN 1991-1-4: 2005. The net pressures acting on the windward and leeward roofs are calculated using the internal and external pressure coefficients. A presentation of the geometrical data of the roof span considered is shown in figure 3.7. Figure 3.8 illustrates a detailed roof plan of the ware house.

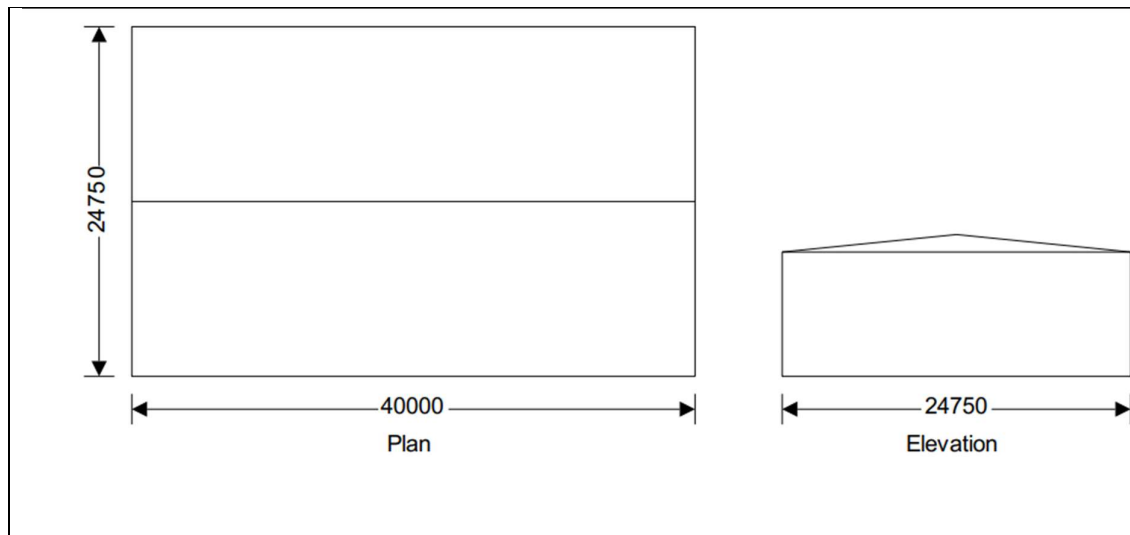


Figure 3.7. Portal frame roof dimensions

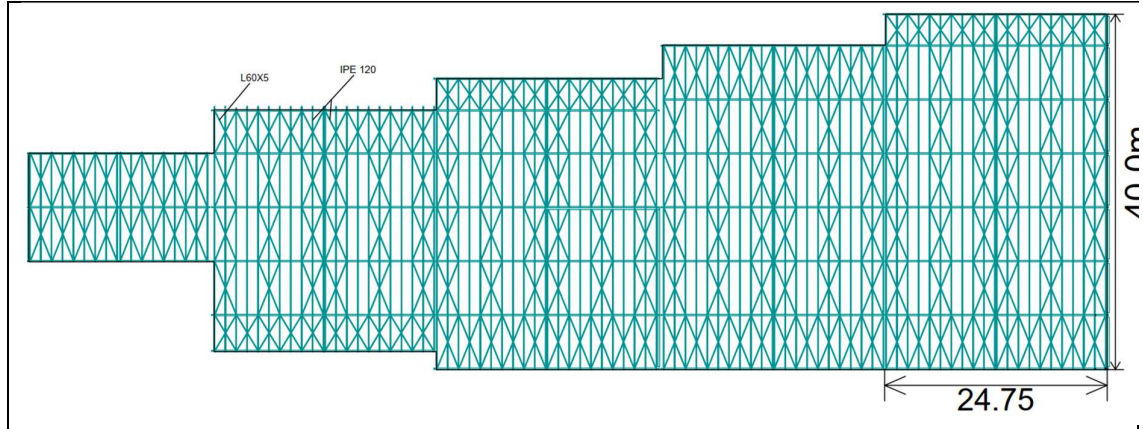


Figure 3.8. Roof plan of the ware house

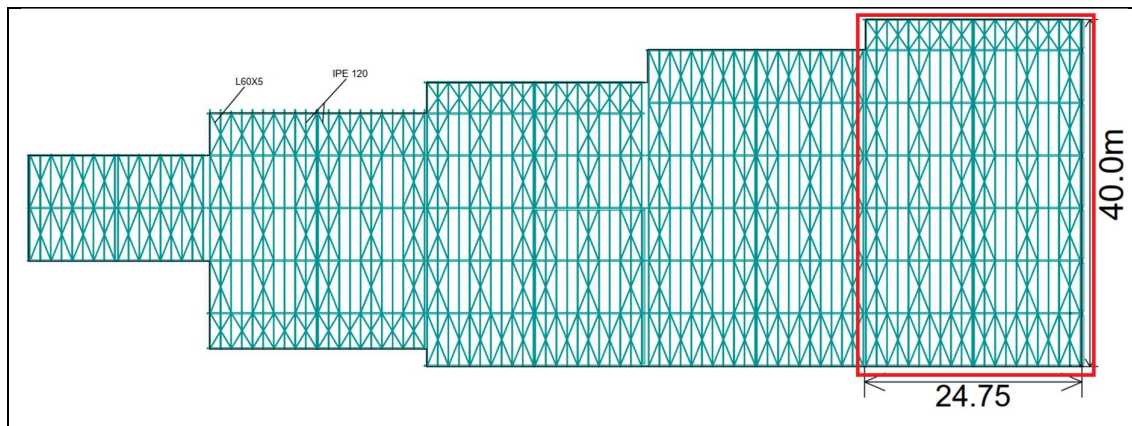


Figure 3.9. Roof span considered for load determination

Table 3.3. Building Data

Type of roof	Duopitch
Length of building	L=40m
Width of building	W=24.75m
Height to eaves	H=8.8m
Pitch of roof	$\alpha_0 = 5.72^\circ$
Total height	h=10.4m
Basic values	
Fundamental basic wind velocity	$V_{b,0} = 22.0\text{m/s}$
Season factor	$C_{season} = 1.00$
Direction factor	$C_{dir} = 1.00$
Shape parameter K	$K = 0.2$
Exponent n	$n = 0.5$
Air density	$\rho = 1.250\text{kg/m}^3$

**FEM ANALYSIS APPLIED TO THE STUDY OF STRESS
DIFFUSION IN THE BASEPLATES OF STEEL STRUCTURES**

Probability factor	$C_{prob} = \left[\frac{1 - K \times \ln(-\ln(1 - \rho))}{1 - K \times \ln(-\ln(0.98))} \right]^n = 1.00$
Basic wind velocity	$V_b = C_{dir} \times C_{season} \times V_{b,0} \times C_{prob} = 22.0m/s$
Reference mean velocity pressure	$q_b = 0.5 \times \rho \times V_b^2 = 0.303kN/m^2$
Orography	
Orography factor not significant	$C_0 = 1.0$
Terrain category	II
Reference height (When wind is perpendicular to ridge)	$Z = 8800mm$
Roughness length (Table 4.1)	$z_0 = 50mm$
Roughness length (Category II)	$z_{0,II} = 50mm$
Minimum height	$z_{min} = 2000mm$
Maximum height	$z_{max} = 200000mm$
Terrain factor	$k_r = 0.19 \times \left(\frac{z_0}{z_{0,II}} \right)^{0.07} = 0.190$
Roughness factor	$C_r = k_r \times \ln \left(\frac{Z}{z_0} \right) = 0.98$
Mean wind	$V_m = C_r \times C_0 \times V_b = 21.6m/s$
Turbulence factor	$k_I = 1.0$
Turbulence intensity	$I_v = \frac{k_I}{c_0 \times \ln \left(\frac{Z}{z_0} \right)} = 0.193$
Peak velocity pressure	$q_b = (1 + 7 \times I_v) \times 0.5 \times \rho \times V_m^2 = 0.69kN/m^2$
Structural factor	
Building type	Steel
Structural factor (Annex D of Eurocode)	$c_s c_d = 0.857$
Reference height (When wind is parallel to ridge)	$Z=10040mm$
Terrain factor	$k_r = 0.19 \times \left(\frac{z_0}{z_{0,II}} \right)^{0.07} = 0.190$
Roughness factor	$c_r = k_r \times \ln \left(\frac{Z}{z_0} \right) = 1.01$
Mean wind speed	$V_m = c_r \times c_0 \times V_b = 22.2m/s$
Turbulence factor	$k_I = 1.0$
Peak velocity pressure	$q_p = (1 + 7 \times I_v) \times 0.5 \times \rho \times V_m^2 = 0.71kN/m^2$

With the peak velocity gotten, it is possible to determine the net pressures acting on the roof and the column using the external pressure coefficients c_{pe} and internal pressure coefficient c_{pi} .

**FEM ANALYSIS APPLIED TO THE STUDY OF STRESS
DIFFUSION IN THE BASEPLATES OF STEEL STRUCTURES**

The Eurocode specifications allow us to take into considerations specific surface areas for the determination of distributed and punctual wind loads. The areas taken into consideration depend on the direction of the wind. These areas are shown on figure 3.7 and figure 3.8.

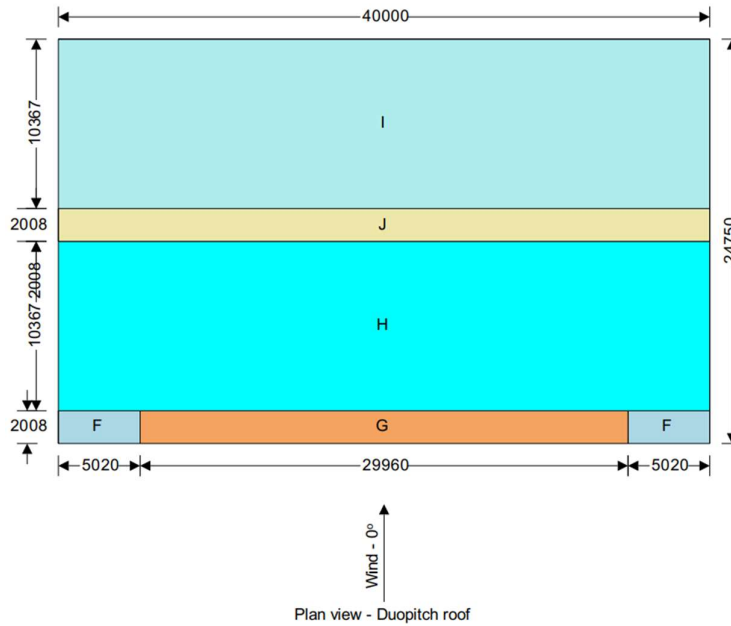


Figure 3.10. Roof areas for wind perpendicular to the ridge

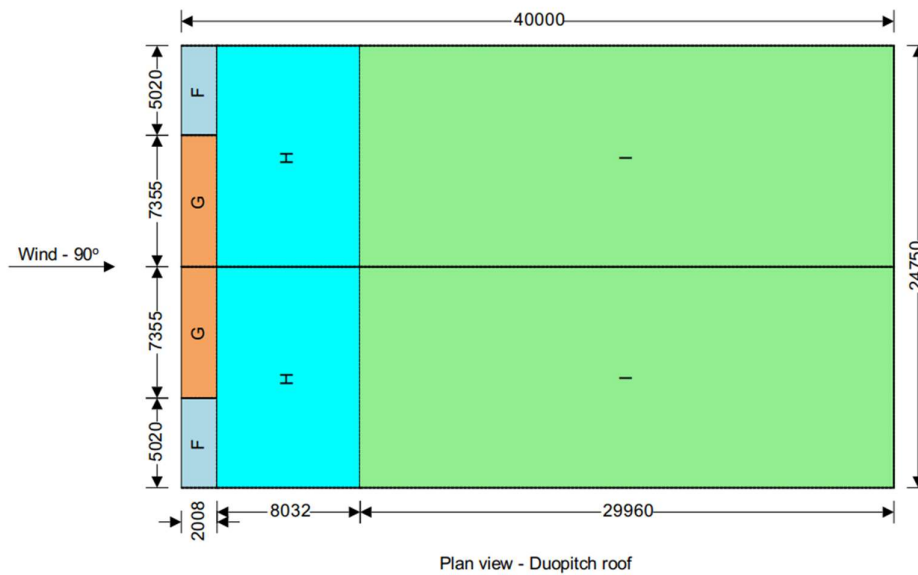


Figure 3.11. Roof areas for wind parallel to the ridge

Upon analysis of the net pressures acting on each surface (determined by considering the internal and external pressure coefficients), it has been observed that the maximum wind load was obtained when the wind surface load corresponds to the peak velocity pressure q_p .

3.4.1. Vertical loads

The vertical loads acting on the structure are generated due to the self-weight of the structural elements, self-weight of the roof, imposed load of the roof and the and the wind load acting on the roof. These loads are presented in table 3.4.

Table 3.4. Vertical loads

Nature	Description	Value	Unit
G_1	Self-weight of structural component	γA	kN/m
G_2	Self-weight of metal roof	0.038	kN/m^2
$Q_{w(roof)}$	Wind force per unit area on the roof	0.71	kN/m^2

3.4.2. Horizontal loads

The horizontal loads on the structure are generated due to the wind loads applied on the structure were considered on the roof.

3.5. Design verifications of the steel structure

The design verifications of the building are done under the different actions acting on the building. It consists in obtaining the internal forces and moments in the members of the structure after the model has been created in SAP 2000 as shown in figure 3.12. The results of the design verifications will be discussed in this section.

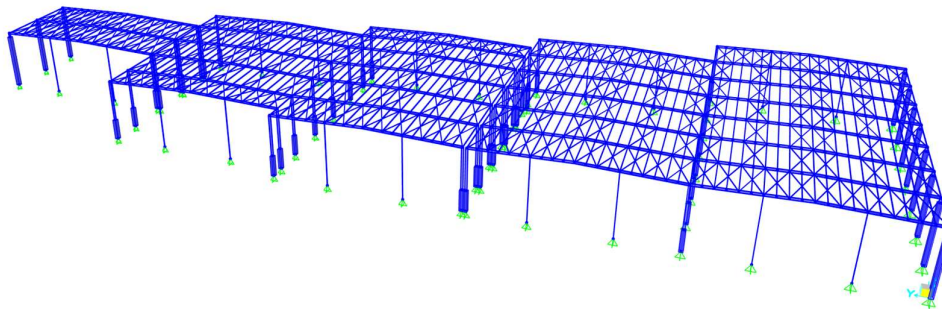


Figure 3.12. Building model from SAP 2000

3.5.1. Purlin design verification

The internal forces and moments acting on the purlin gotten from the static analysis on SAP2000 are represented in table 3.5.

Table 3.5. Internal moment and shear force

Internal actions	Value	Units
Bending moment	3.125	KNm
Shear force	2.5	kN

The section of the purlin element under study is an IPE 120 and its properties are presented in table 3.6.

Table 3.6. Properties of IPE 120

Depth (h)	120 mm
Width of web (b)	46 mm
Web thickness (t_w)	4.4 mm
Flange thickness (t_f)	6.3 mm
Fillet radius (r)	7 mm
Weight (G)	10.4 kg/m
Height of the web (h_w)	107.4 mm
Area of section (A)	1320 mm ²
Shear area in z-z direction ($A_{v,z}$)	629.52mm ²
Moment of inertia (I_y)	318000 mm ⁴
Radius of gyration (i_y)	49.0 mm
Plastic section modulus ($W_{pl,y}$)	60700 cm ³
Moment of inertia (I_z)	277000 cm ⁴
Radius of gyration (i_z)	14.5 mm
Plastic section modulus ($W_{pl,z}$)	13600

First, the section is classified as shown in table 3.7 and the design verifications are presented in table 3.8.

Table 3.7. Classification of the purlin cross section

Designation	Verification	Value	Class
Web in bending	$\frac{c}{t_w} \leq 72\varepsilon$	$21.23 \leq 66.24$	Class 1
Flange in compression	$\frac{c}{t_w} \leq 9\varepsilon$	$3.62 \leq 8.28$	Class 1

Table 3.8. Design verification of the purlin

Designation	Verification	Value	Observation
Resistance in bending	$M_{c,Rd} \geq M_{Ed}$	$16.7 \geq 3.125$	Verified
Resistance in shear	$V_{pl,Rd} \geq V_{Ed}$	$99.9 \geq 2.5$	Verified
Shear instability	$\frac{h_w}{t_w} < 72 \frac{\varepsilon}{\eta}$	$17.04 < 46.2$	Verified
Moment-shear interaction	$0.5V_{pl,Rd} \geq V_{Ed}$	$49.95 \geq 2.5$	Verified
Lateral Torsional Buckling	$M_{b,Rd} \geq M_{Ed}$		
Deflection Check (SLS)	$f_{max} < \frac{L}{200}$	$1.2 < 3.0$	Verified

3.5.2. Rafter design verifications

The internal actions gotten from the analysis made in SAP 2000 on rafter are represented on table 3.9.

Table 3.9. Moments and Forces on rafter

Internal actions	Value	Units
Maximum positive bending moment	152	kNm
Maximum negative bending moment	146	kNm
Shear force	78.8	kN
Axial force	268	kN

The sections of the rafter element under study is IPE 300 and its corresponding properties are shown in table 3.10.

Table 3.10. Properties of IPE 300

Depth (h)	300 mm
Width of web (b)	150 mm
Web thickness (t_w)	7.1 mm
Flange thickness (t_f)	10.7 mm
Fillet radius (r)	15.0 mm
Weight (G)	42.2 kg/m
Height of the web (h_w)	278.6 mm
Area of section (A)	5380 mm ²
Shear area in z-z direction ($A_{V,z}$)	25.6697 cm ²
Moment of inertia (I_y)	8356 cm ⁴
Radius of gyration (i_y)	12.5 cm
Plastic section modulus ($W_{pl,y}$)	628 cm ³
Moment of inertia (I_z)	604 cm ⁴
Radius of gyration (i_z)	3.35 cm
Plastic section modulus ($W_{pl,z}$)	125 cm ³

First, we classify the section as shown in table 3.11 and the design verifications are presented in table 3.12

Table 3.11. Classification of the rafter cross section

Designation	Verification	Value	Class
Web subjected to bending and compression	$\frac{c}{t} \leq \frac{36\varepsilon}{\alpha}$	$35.01 \leq 66.24$	Class 1
Flange in compression	$\frac{c}{t} \leq 9\varepsilon$	$5.27 \leq 8.28$	Class 1

Table 3.12. Design verifications of the rafter

Designation	Verification	Value	Observation
Resistance in bending	$M_{c,Rd} \geq M_{Ed}$	$172.7 \geq 141$	Verified
Resistance in shear	$V_{pl,Rd} \geq V_{Ed}$	$407.56 \geq 78.8$	Verified
Shear instability	$\frac{h_w}{t_w} < 72 \frac{\varepsilon}{\eta}$	$39.24 < 55.2$	Verification of shear stability is not required

**FEM ANALYSIS APPLIED TO THE STUDY OF STRESS
DIFFUSION IN THE BASEPLATES OF STEEL STRUCTURES**

Moment and shear interaction	$0.5V_{pl,Rd} \geq V_{Ed}$	$203.78 \geq 78.8$	No shear-moment interaction
Lateral torsional buckling	$M_{b,Rd} \geq M_{Ed}$	$175kNm \geq 141kNm$	Verified
Axial resistance	$N_{pl,Rd} \geq N_{Ed}$	$1479.5 \geq 112kN$	Verified
Buckling resistance	$N_{b,Rd} \geq N_{Ed}$	$1213kN \geq 112kN$	Verified
Axial verifications	$0.25N_{pl,Rd} \geq N_{Ed}$	$369.875kN \geq 112kN$	Axial forces do not affect moments
	$\frac{0.5h_w t_w f_y}{\gamma_{M0}} \geq N_{Ed}$	$271.9kN \geq 112kN$	
Moment and axial interaction	$\frac{N_{Ed}}{N_{pl,Rd}} + \frac{M_{Ed}}{M_{pl,Rd}} \leq 1$	$0.8 \leq 1$	No moment-axial force interaction
Deflection check (SLS)	$f_{max} < \frac{L}{200}$	$47.06 mm < 61.9 mm$	Verified

3.5.3. Column design verification

The IPE 300 and IPE 120 columns found in the structure will be verified according to sections 3.5.3.1 and 3.5.3.2. As explained in the methodology, the criteria of selection of the column to be designed will be the maximum stress on the base plate.

3.5.3.1. IPE 300

IPE 300 columns carry most of the loads in the structure. Table 3.13 shows the axial forces and moments gotten from the static analysis made on SAP2000 on columns.

Table 3.13. Column loadings

Coordinate	N (kN)	M_x (KNm)	M_y (kNm)
4D	-13.545	1.5628	-4.4773
4E	-95.899	-199.617	0.000245
4F	-13.544	-1.563	-4.4778
5B	-11.301	1.7224	23.5715
5C	-66.339	1.8134	87.0995
5D	-94.601	0.9786	139.0139
5E	-94.281	0.6773	140.2576
5F	-71.78	0.1011	94.4762
5G	-11.596	-0.6281	18.6511
8A	-10.119	2.9926	-12.6597
8B	-28.623	30.945	-6.4222
8C	-146.539	3.2309	21.198
8D	-199.301	2.2831	7.3505
8E	-198.273	2.2123	7.6103
8F	-164.706	1.7384	23.4119

**FEM ANALYSIS APPLIED TO THE STUDY OF STRESS
DIFFUSION IN THE BASEPLATES OF STEEL STRUCTURES**

8G	-54.431	1.7574	39.0388
8I	-8.012	1.3903	5.41
11A	-15.551	2.5791	-20.5989
11C	-84.818	0.9878	-110.552
11D	-95.809	0.9099	-139.849
11E	-96.148	0.5619	-138.838
11F	-82.874	-0.1481	-110.894
11G	-50.841	-0.1624	-53.8724
11H	-7.774	-0.3773	-1.2552
12A	-14.026	3.2449	10.9257
12C	-83.752	1.7285	109.4991
12D	-94.69	1.6058	143.1356
12E	-96.221	1.2666	149.6588
12F	-94.513	0.9329	147.2188
12H	-82.935	0.9002	118.7308
12J	-15.687	-0.9478	33.1617
15A	-7.115	1.1056	1.7896
15C	-177.711	-0.8013	-0.33
15D	-193.024	-0.6076	-1.2747
15E	-191.76	-0.7236	-0.4982
15F	-191.646	-0.7872	6.0075
15H	-188.451	-0.8841	29.4871
15J	-94.8	-1.095	76.0259
15L	-14.319	-2.5781	7.9847

From table 3.14, the critical columns are;

Table 3.14. Critical columns

Column	Location	N (kN)	Mx (kNm)	My (kNm)
1 (Max axial)	8D	199.301	2.2831	7.3505
2 (Max Mx)	4E	-95.899	199.617	0.000245
3 (Max My)	12E	-96.221	1.2666	149.6588

Table 3.14 portrays the maximum axial force, maximum moment in x and maximum moment in y acting in the columns. The most critical column is the one which induces more stresses in the base plate – this is the criteria of choice used for the selection of the column which will be designed. The analysis of the three models were performed in ABAQUS and the different values of stresses obtained are displayed in Figure 3.13.

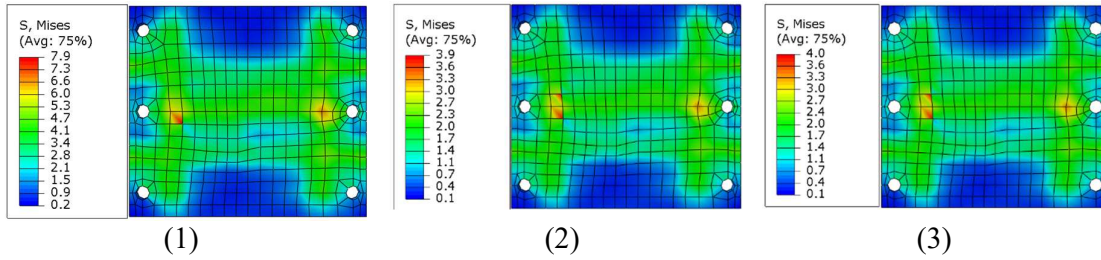


Figure 3.13. Baseplate Stress values for columns 1,2 and 3

Figure 3.10 indicates that the critical column to be considered is column 1 subjected to a greatest axial force.

Table 3.15. Design verifications of the IPE 300 column

Designation	Verification	Value	Observation
Resistance in bending	$M_{c,Rd} \geq M_{Ed}$	147.58kNm $\geq 47.85kNm$	Verified
Resistance in shear	$V_{pl,Rd} \geq V_{Ed}$	407.56kN $\geq 17.48kN$	Verified
Shear instability	$\frac{h_w}{t_w} < 72 \frac{\epsilon}{\eta}$	39.24 < 55.2	Verification of shear stability is not required
Moment and shear interaction	$0.5V_{pl,Rd} \geq V_{Ed}$	203.78kN $\geq 17.48kN$	No shear-moment interaction
Axial resistance	$N_{pl,Rd} \geq N_{Ed}$	1264.3kN $\geq 200kN$	Verified
Buckling resistance	$N_{b,Rd} \geq N_{Ed}$	1202.7kN $\geq 200kN$	Verified
Axial verifications	$0.25N_{pl,Rd} \geq N_{Ed}$	300.675kN $\geq 170.76kN$	Axial forces do not affect moments
	$\frac{0.5h_w t_w f_y}{\gamma_{M0}} \geq N_{Ed}$	271.9kN $\geq 200kN$	
Moment-axial force interaction	$\frac{N_{Ed}}{N_{pl,Rd}} + \frac{M_{Ed}}{M_{pl,Rd}} \leq 1$	0.53 ≤ 1	No moment-axial force interaction
Deflection check (SLS)	$u_{max} < \frac{h}{300}$	18mm < 20mm	Verified

3.5.3.2. IPE 120

The internal moments and forces gotten from the SAP2000 analysis on a column are portrayed in table 3.16.

Table 3.16. Properties of IPE 120

Depth (h)	120 mm
Width of web (b)	64 mm
Web thickness (t_w)	4.4 mm
Flange thickness (t_f)	6.3 mm
Fillet radius (r)	7 mm
Weight (G)	10.4 kg/m
Height of the web (h_w)	107.4 mm
Area of section (A)	13.2 cm ²
Shear area in z-z direction ($A_{V,z}$)	6.3 cm ²
Moment of inertia (I_y)	318 cm ⁴
Radius of gyration (i_y)	4.9 cm
Plastic section modulus ($W_{pl,y}$)	60.7 cm ³
Moment of inertia (I_z)	27.7 cm ⁴
Radius of gyration (i_z)	1.45 cm
Plastic section modulus ($W_{pl,z}$)	13.6 cm ³

First, the section is classified as shown in table 3.17 and the design verifications are presented in table 3.18.

Table 3.17. Classification of the IPE 120 column

Designation	Verification	Value	Observation
Web subjected to bending	$\frac{c}{t} \leq \frac{36\varepsilon}{\alpha}$	$21.23 \leq 66.24$	Class 1
Flange in compression	$\frac{c_f}{t_f} \leq 9\varepsilon$	$3.62 \leq 8.28$	Class 1

Table 3.18. Design verification of the IPE 120 column

Designation	Verification	Value	Observation
Resistance in bending	$M_{c,Rd} \geq M_{Ed}$	$16.69kNm \geq 9.6kNm$	Verified
Resistance in shear	$V_{pl,Rd} \geq V_{Ed}$	$99.9 \geq 10.5$	Verified
Shear instability	$\frac{h_w}{t_w} < 72 \frac{\varepsilon}{\eta}$	$17.04 < 46.2$	Verification of shear stability is not required
Moment and shear interaction	$0.5V_{pl,Rd} \geq V_{Ed}$	$49.95 \geq 10.5$	No shear-moment interaction

**FEM ANALYSIS APPLIED TO THE STUDY OF STRESS
DIFFUSION IN THE BASEPLATES OF STEEL STRUCTURES**

Axial resistance	$N_{pl,Rd} \geq N_{Ed}$	363kN $\geq 63.65kN$	Verified
Buckling resistance	$N_{b,Rd} \geq N_{Ed}$	356kN $\geq 63.65kN$	Verified
Axial verifications	$0.25N_{pl,Rd} \geq N_{Ed}$	90.75kN $\geq 63.65kN$	Axial forces do not affect moments
	$\frac{0.5h_w t_w f_y}{\gamma_{M0}} \geq N_{Ed}$	65kN $\geq 63.65kN$	
Moment-axial force interaction	$\frac{N_{Ed}}{N_{pl,Rd}} + \frac{M_{Ed}}{M_{pl,Rd}} \leq 1$	0.7 \leq 1	No moment-axial force interaction
Deflection check (SLS)	$u_{max} < \frac{h}{300}$	22mm < 29mm	Verified

3.5.4. Braces design verifications

The building has only horizontal braces on the roof. They will be verified according to sections 3.5.4.1 and 3.5.4.2. The axial force gotten from the analysis on SAP2000 on the roof braces are portrayed in table 3.19.

Table 3.19. Axial force on braces

Action	Value	Units
Axial force	63	kN

Table 3.20. Properties of L60×60×5

	Depth (h)	60 mm
	Width (b)	60 mm
	Thickness (t)	5 mm
	Fillet radius (r)	8 mm
	Weight (G)	4.65 kg/m
	Area (A)	5.82 cm²
	Moment of Inertia ($I_y = I_z$)	193700 mm⁴
	Elastic section modulus ($W_{el,y} = W_{el,z}$)	4450 mm³
	Radius of gyration ($i_x = i_y$)	18.2 mm
	Moment of inertia (I_u)	307100 mm⁴
	Radius of gyration (i_u)	23 mm
	Moment of inertia (I_v)	80300 mm⁴
	Elastic section modulus ($W_{el,v}$)	
	Radius of gyration (i_v)	11.7 mm

L60×60×5 is a cross section of class 1 and its design verifications according to the case study are portrayed in table 3.21.

Table 3.21. Design verification of the horizontal braces

Designation	Verification	Value	Observation
Tensile resistance	$N_{t,Rd} \geq N_{Ed}$	196.4kN \geq 63.5kN	Verified

3.5.5. Connection design verifications

The connections were verified according to the equations from section 2.5.6

3.5.5.1. Rafter column connections

The type of connection used for this joint is an eave moment connection used to connect a rafter with a column since the building is made of a portal frame with eave haunches. The internal moments and forces gotten from the analysis on SAP2000 of this connection are portrayed in table 3.23.

Table 3.22. Internal moments and forces in the rafter to column connection

Internal actions	Value	Units
Bending moment	256.4	kNm
Shear force	58.6	kN
Axial force	58.6	kN

The results obtained from the verification are presented in table 3.23.

Table 3.23. Design verifications of the rafter-column connection

Designation	Value/Verification	Observation
Number of bolts	12	/
Bolts diameter	16 mm	/
Ultimate tensile strength of the bolt f_{ub}	800 N/mm ²	/
Plate thickness	20 mm	/
Yielding strength of the steel profile, f_y	275 N/mm ²	Verified
Shear resistance per bolt, $F_{v,Rd}$	161.5 kN > 8.51 kN	Verified
Traction resistance per bolt, $F_{t,Rd}$	182kN > 7.24 kN	Verified
Shear and traction Interaction of one bolt	0.07 < 1	Verified

Bearing resistance per bolt, $F_{b,Rd}$	301 kN > 8.19 kN	Verified
Total resisting moment,	270 kNm > 251 kNm	Verified

3.5.5.2. Rafter-Rafter connection

The type of connection used for this joint connecting two rafters is an apex connection since the building is made of a portal frame with an apex haunch. The internal actions gotten from the analysis made on SAP2000 on this connection are portrayed in table 3.24.

Table 3.24. Internal actions on rafter to rafter connection

Internal actions	Value	Units
Bending moment	256.4	kNm
Shear force	58.6	kN
Axial force	58.6	kN

The results obtained from the verification are presented in table 3.25.

Table 3.25. Design verifications of the rafter-rafter connection

Designation	Value/Verification	Observation
Number of bolts	12	/
Bolts diameter	22 mm	/
Ultimate tensile strength of the bolt f_{ub}	800 N/mm ²	/
Plate thickness	20	/
Yielding strength of the steel profile, f_y	275 N/mm ²	/
Shear resistance per bolt, $F_{v,Rd}$	161.5 kN > 8.51 kN	Verified
Traction resistance per bolt, $F_{t,Rd}$	182 kN > 7.24 kN	Verified
Shear and traction Interaction of one bolt	0.07 < 1	Verified
Bearing resistance per bolt, $F_{b,Rd}$	122.1 kN > 7.4 kN	Verified
Total resisting moment,	215 kN > 7.4 kN	Verified

3.5.5.3. Brace connection

These connections are used at the joints between the braces and the column/beam. The connection here is a shear connection, so there is no moment transmission. The axial forces present in the connection are represented in table 3.26.

Table 3.26. Axial forces in the beam to beam connection

Internal actions	Value	Units
Axial force	52	kN

The results obtained from the verification are presented in the table 3.27.

Table 3.27. Design verifications of the brace connection

Designation	Value/Verification	Observation
Number of bolts	2	/
Bolts diameter	16 mm	/
Ultimate tensile strength of the bolt, f_{ub}	800 N/mm ²	/
Plate thickness	10 mm	/
Yielding strength of the steel profile, f_y	235 N/mm ²	/
Shear resistance per bolt, $F_{v,Rd}$	38.5kN > 22kN	Verified
Bearing resistance per bolt, $F_{b,Rd}$	50kN > 22kN	Verified

3.5.5.4. Column base connection

Geometry

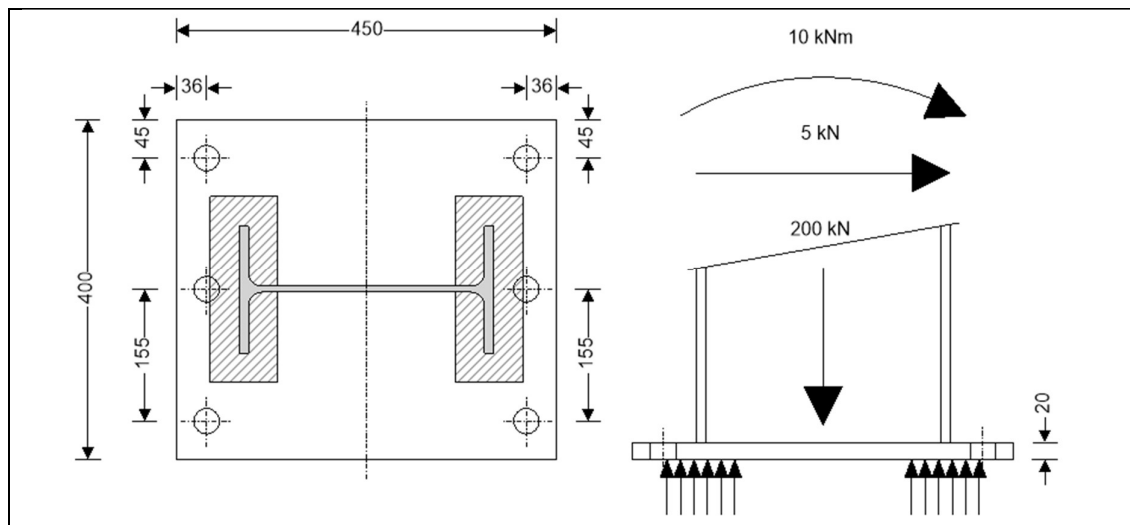


Figure 3.14. Column base connection geometry

Table 3.28. Column base design forces

Design axial force (compression)	$N_{Ed} = 200kN$
Design shear force	$V_{Ed} = 5kN$
Design moment	$M_{Ed} = 10kNm$

Table 3.29. Column Details

Column section	IPE 300
Depth	D = 300 mm
Width	B = 150 mm
Flange thickness	T = 10.7 mm
Web thickness	t = 7.1 mm

Table 3.30. Base plate details

Length	$h_p = 450$ mm
Width	$b_p = 400$ mm
Thickness	$t_p = 20$ mm
Column eccentricity in x-axis	$e_{pbx} = 0$ mm

Table 3.31. Anchor details

Number of anchors in the left	$n_1 = 3$
Edge distance in x-axis	$e_{x1} = 36$ mm
Edge distance in the y-axis	$e_{y1} = 45$ mm
Number of anchors in the right	$n_2 = 3$
Edge distance in x-axis	$e_{x2} = 36$ mm
Edge distance in the y-axis	$e_{y2} = 45$ mm
Anchor diameter	d = 27 mm

Table 3.32. Concrete base details

Concrete strength class	C25/30
Characteristic compressive cylinder strength	$f_{ck} = 25N/mm^2$
Characteristic compressive cube strength	$f_{ck,cube} = 30 N/mm^2$
Partial factor for concrete	$\gamma_c = 1.50$
Compressive strength coefficient	$\alpha_{cc} = 0.85$
Design compressive concrete strength	$f_{cd} = \alpha_{cc} \times (f_{ck} / \gamma_c) = 14.17 N/mm^2$

Table 3.33. Steel details

Base plate steel grade	S275
------------------------	-------------

**FEM ANALYSIS APPLIED TO THE STUDY OF STRESS
DIFFUSION IN THE BASEPLATES OF STEEL STRUCTURES**

Base plate nominal yield strength	$f_{yp} = 265 \text{ N/mm}^2$
Base plate nominal ultimate tensile strength	$f_u = 410 \text{ N/mm}^2$
Column steel grade	S275
Column nominal yield strength	$f_{yp} = 265 \text{ N/mm}^2$
Column nominal ultimate tensile strength	$f_u = 410 \text{ N/mm}^2$
Partial safety factor cross sections	$\gamma_{M0} = 1.50$
Partial safety factor welds	$\gamma_{M2} = 1.25$

Table 3.34. Tension and compressive lever arms

LHS compressive lever arm	$z_{C,l} = (D - T) / 2 = 144.7 \text{ mm}$
RHS compressive lever arm	$z_{C,r} = (D - T) / 2 = 144.7 \text{ mm}$
LHS tension lever arm	$z_{T,l} = h_p / 2 + e_{pbx} - e_{x1} = 189 \text{ mm}$
RHS tension lever arm	$z_{T,r} = h_p / 2 + e_{pbx} - e_{x2} = 189 \text{ mm}$

Table 3.35. Design forces in T-stubs

Force in left hand T-stub	$N_{L,T} = N_{Ed} \times \frac{z_{C,r}}{(z_{C,l} + z_{C,r})} - \frac{M_{Ed}}{(z_{C,l} + z_{C,r})}$ $= 55.4 \text{ kN (Comp)}$
Force in right hand T-stub	$N_{R,T} = N_{Ed} \times \frac{z_{C,l}}{(z_{C,l} + z_{C,r})} - \frac{M_{Ed}}{(z_{C,l} + z_{C,r})}$ $= 124.6 \text{ kN (Comp)}$

Table 3.36. Concrete base bearing strength under left hand flange – EN1992-1-1 Section 6.7

Additional bearing width	$c_{LF} = t_p \times \sqrt{\frac{f_{yp}}{3 \times f_{jd,LF} \times \gamma_{M0}}}$ $= 39.5 \text{ mm}$
Effective width of T-stub flange	$b_{eff1,LF} = 89.6 \text{ mm}$
Effective length of T-stub flange	$l_{eff1,LF} = 228.9 \text{ mm}$
Loaded area	$A_{c0,LF} = b_{eff1,LF} \times l_{eff1,LF} = 20516 \text{ mm}^2$
Design distribution width	$b_{eff2,LF} = 215.3 \text{ mm}$
Design distribution length	$l_{eff2,LF} = 550 \text{ mm}$
Maximum design distribution area	$A_{c1,LF} = b_{eff2,LF} \times l_{eff2,LF}$ $= 118427 \text{ mm}^2$
Concentrated design resistance force	$F_{Rdu,LF} = \min \left(A_{c0,LF} \times f_{cd} \times \sqrt{\frac{A_{c1,LF}}{A_{c0,LF}}}, 3 \right.$ $\left. \times f_{cd} \times A_{c0,LF} \right) = 698.3 \text{ kN}$
Foundation joint material coefficient	$\beta_j = 0.67$

**FEM ANALYSIS APPLIED TO THE STUDY OF STRESS
DIFFUSION IN THE BASEPLATES OF STEEL STRUCTURES**

Design bearing strength of the joint	$f_{jd,LF} = \beta_j \times F_{Rdu,LF} / (b_{eff1,LF} \times l_{eff1,LF})$ $= 22.69 \text{ N/mm}^2$
---	---

Table 3.37. Concrete base bearing strength under right hand flange – EN1992-1-1 Section 6.7

Additional bearing width	$c_{LF} = t_p \times \sqrt{\frac{f_{yp}}{3 \times f_{jd,LF} \times \gamma_{M0}}}$ $= 39.5 \text{ mm}$
Effective width of T-stub flange	$b_{eff1,LF} = 89.6 \text{ mm}$
Effective length of T-stub flange	$l_{eff1,LF} = 228.9 \text{ mm}$
Loaded area	$A_{c0,LF} = b_{eff1,LF} \times l_{eff1,LF} = 20516 \text{ mm}^2$
Design distribution width	$b_{eff2,LF} = 215.3 \text{ mm}$
Design distribution length	$l_{eff2,LF} = 550 \text{ mm}$
Maximum design distribution area	$A_{c1,LF} = b_{eff2,LF} \times l_{eff2,LF}$ $= 118427 \text{ mm}^2$
Concentrated design resistance force	$F_{Rdu,LF} = \min \left(A_{c0,LF} \times f_{cd} \times \sqrt{\frac{A_{c1,LF}}{A_{c0,LF}}}, 3 \right.$ $\left. \times f_{cd} \times A_{c0,LF} \right) = 698.3 \text{ kN}$
Foundation joint material coefficient	$\beta_j = 0.67$
Design bearing strength of the joint	$f_{jd,LF} = \beta_j \times F_{Rdu,LF} / (b_{eff1,LF} \times l_{eff1,LF})$ $= 22.69 \text{ N/mm}^2$

Table 3.38. Equivalent T-stub in compression under right hand flange – Section 6.2.5

Design compression resistance of T-stub flange	$F_{C,Rd2} = f_{jd,RF} \times b_{eff1,RF} \times l_{eff1,RF}$ $= 465.5 \text{ kN}$
---	--

Table 3.39. Equivalent T-stub in compression under left hand flange – Section 6.2.5

Design compression resistance of T-stub flange	$F_{C,Rd1} = f_{jd,RF} \times b_{eff1,RF} \times l_{eff1,RF}$ $= 465.5 \text{ kN}$
---	--

Table 3.40. Concrete in compression under right hand flange – Section 6.2.6.9

Design resistance of concrete in compression	$F_{c,pl,Rd2} = F_{C,Rd2} = 465.5 \text{ kN}$
---	---

Table 3.41. Concrete in compression under left hand flange – Section 6.2.6.9

Design resistance of concrete in compression	$F_{c,pl,Rd1} = F_{c,Rd1} = 465.5 \text{ kN}$
--	---

Table 3.42. Bending resistance of column – EN1993-1-1 Section 6.2.5

Design resistance for bending	$M_{c,Rd} = M_{pl,Rd} = \frac{W_{pl,y} \times f_{yp,col}}{\gamma_{M0}} = 172.8 \text{ kNm}$
-------------------------------	---

Table 3.43. Column bases subjected to axial forces and bending moments – Section 6.2.8.3

Design compression resistance LHS of joint	$F_{c,l,Rd} = \min(F_{c,pl,Rd1}, F_{c,fc,Rd}) = 465.5 \text{ kN}$
Design compression resistance RHS of joint	$F_{c,r,Rd} = \min(F_{c,pl,Rd2}, F_{c,fc,Rd}) = 465.5 \text{ kN}$

Table 3.44. Design moment resistance of column base

Relative eccentricity of load	$e = \frac{M_{Ed}}{-N_{Ed}} = -55.6 \text{ mm}$
Loading type	Left side and right side compression
Lever arm	$z = z_{c,l} + z_{c,r} = 289.3 \text{ mm}$
Design moment resistance	$\text{Min}((-F_{c,l,Rd} \times z / (z_{c,r} / e + 1)) , (-F_{c,r,Rd} \times z / (z_{c,l} / e - 1))) = 37.4 \text{ kNm}$

The design moment resistance exceeds the applied moment, the column base is verified!

Table 3.45. Frictional shear resistance

Base plate friction coefficient	$C_{f,d} = 0.2$
Design frictional shear resistance	$F_{t,Rd} = C_{f,d} \times (N_{L,T} + N_{R,T}) = 36 \text{ kN}$

Table 3.46. Shear weld resistance

Force in shear weld	$F_{w,v,Ed} = 5 \text{ kN}$
Weld leg length	$s_w = 8 \text{ mm}$
Weld throat size	$a_w = \frac{1}{\sqrt{2}} \times s_w = 5.7 \text{ mm}$
Length of weld	$L_{w,v} = 2 \times (D - 2 \times (T + r)) = 497.2 \text{ mm}$
Correlation factor for fillet welds	$\beta_w = 0.85$
Design shear strength	$f_{vw,d} = \frac{f_{u,plt}}{\sqrt{3} \times \beta_w \times \gamma_{M2}} = 222.8 \text{ N/mm}^2$

Design resistance per unit length	$f_{w,Rd} = f_{vw,d} \times a_w = 1260.3 \text{ N/mm}^2$
Design resistance	$F_{w,v,Rd} = f_{w,Rd} \times L_{w,v} = 626.6 \text{ kN}$

The available strength of weld exceeds the force acting in the weld. It is verified!

Upon analysis, design and verification of the base plate, it was noticed that the Eurocode requirements regarding bolt spacings and distances with respect to the plate edges were not respected. The required specifications are provided in table 3.47.

Table 3.47. Limitations for bolt spacings and distances.

Distances		Spacing	
e1 end distance		p1 parallel to the force	
e2 edge distance		p2 perpendicular to the force	
min e1	1.2·d ₀	min p1	2.2·d ₀
min e2	1.5·d ₀	min p1	2.4·d ₀ or 1.2·d ₀ for staggered
min e3	1.5·d ₀	min L	2.4·d ₀
min e4	1.5·d ₀		
max e1	Steel exposed to weather or corrosive influences	max p1	Compression members {14 t; 200mm} Tension members:
max e2	40 mm + 4 t Otherwise not applicable	max p2	Outer rows min {14 t; 200mm} Inner rows min {28 t; 400mm }

The minimum end distance proposed by the Eurocode is $e_1 = 1.2 \cdot d_0 = 1.2 \cdot 30 = 36 \text{ mm}$. Contrary to this, the end distance used in the case study was 25mm. This indicates that to satisfy the Eurocode requirements, the anchor bolt position needed to be moved at least by **11mm** away from the base plate edge. The required modification was performed and as such the sub-model was modified as shown in figure.

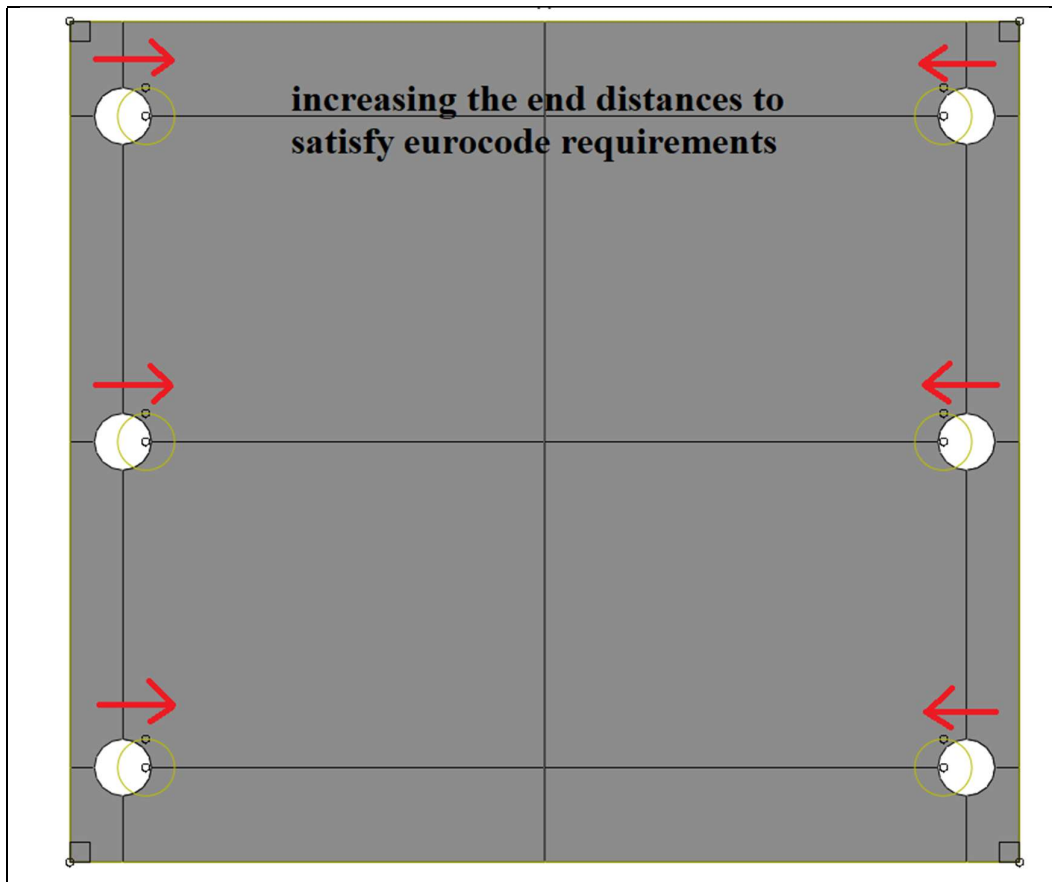


Figure 3.15. New position of anchor bolts with respect to the Eurocode

In this section, the design and verification of the steel members were the main objectives and they were accomplished. Following the design and verification of the column base plate, a new column model which satisfies the Eurocode requirements was modeled to perform the non-linear study of stress diffusion.

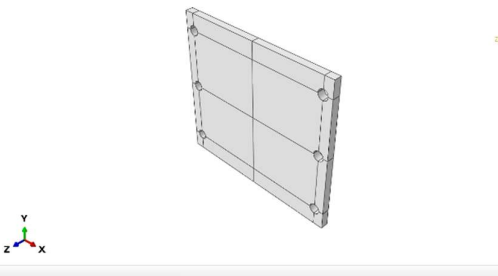

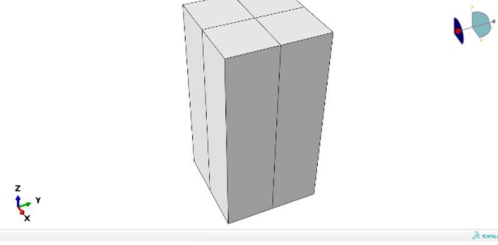
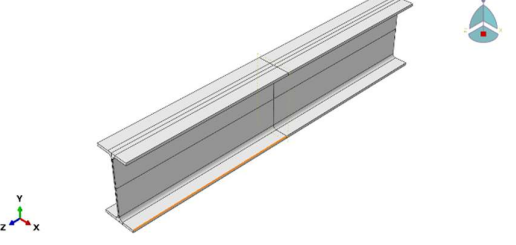
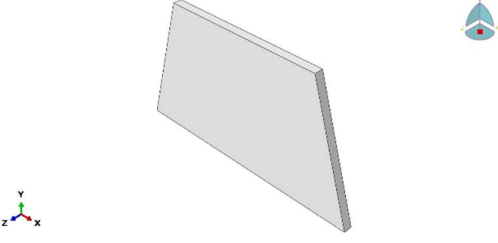
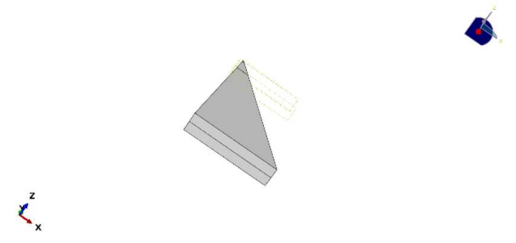
3.6. Results Obtained from the Sub-model Study in ABAQUS

The analysis on ABAQUS was performed considering all the steps explained in the methodology and the results will be presented in compliance to the analysis performed.

3.6.1. Parts module results

The model of the different parts of the column base plate are represented on table...

Table 3.48. Components of the column base connection

	
<p>40*45 cm² Base plate</p>	<p>M27 anchor bolts with washers</p>
	
<p>50*50 cm² Concrete column</p>	<p>IPE 300</p>
	
<p>Stiffener</p>	<p>Stiffener</p>

3.6.2. Property module results

The different properties attributed to the model are expressed in this section.

3.6.2.1. Steel

The material behavior is assumed to be perfectly elastic up to the yield strength f_y which is 275 MPa for all steel elements except stiffeners and 235 MPa for the stiffeners. The values considered were from construction documents and no coupon test were performed on ABAQUS.

3.6.2.2. Concrete

The concrete compressive test was performed on ABAQUS and the failure values obtained accurately represented the behavior of the concrete as shown in table

Table 3.49. Concrete cylinder compression test performed on ABAQUS

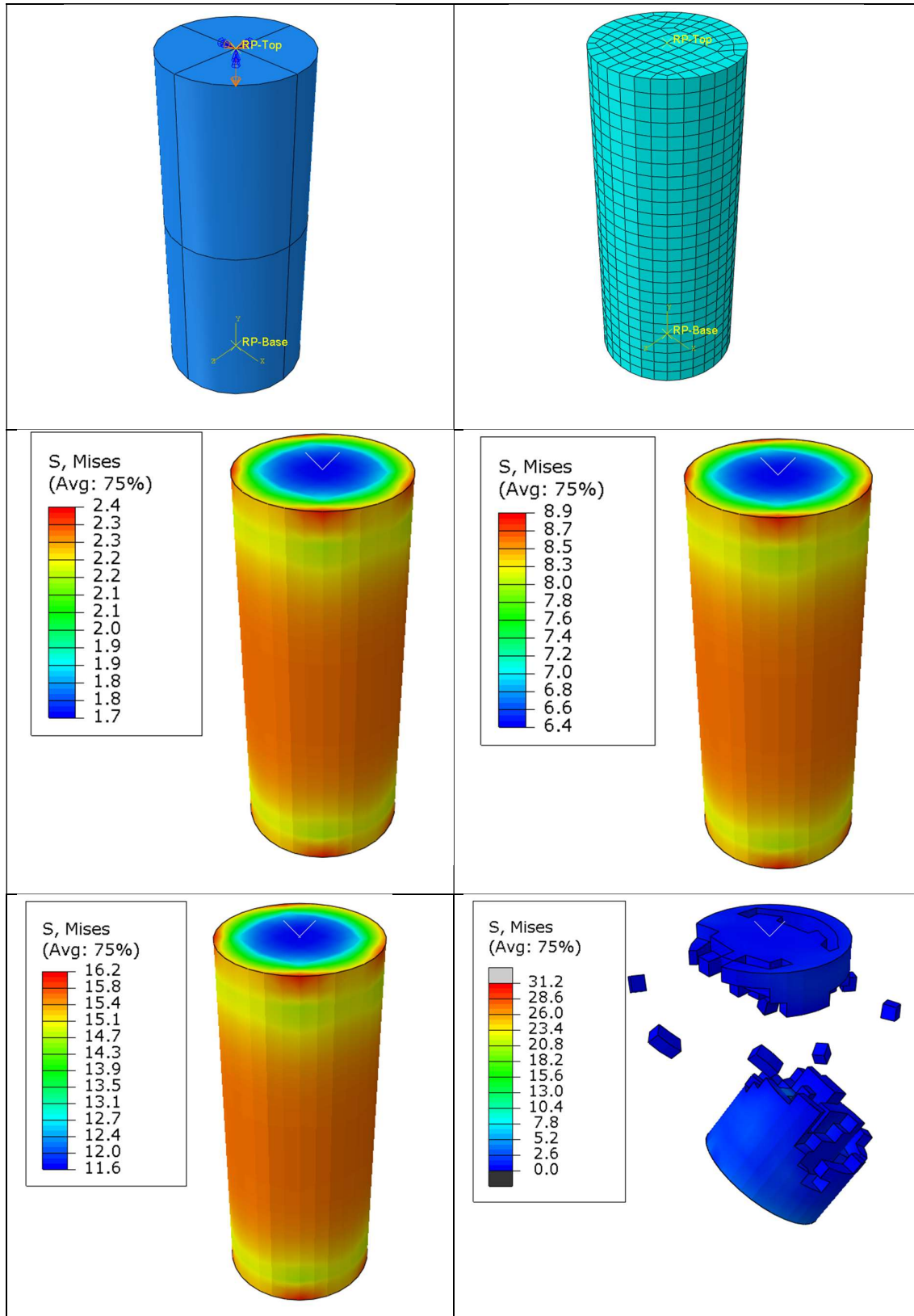


Table 3.50. Concrete main properties in compression and tension

Concrete	$\varepsilon_{c1}(0/00)$	$f_{ctm}(MPa)$	$\delta_{t1}(mm)$
C25/30	2.1	2.6	0

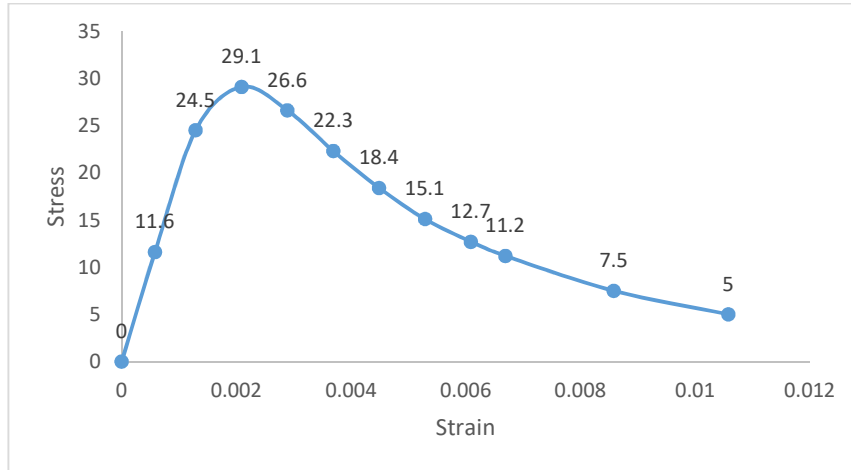


Figure 3.16. Concrete stress-strain law for compression

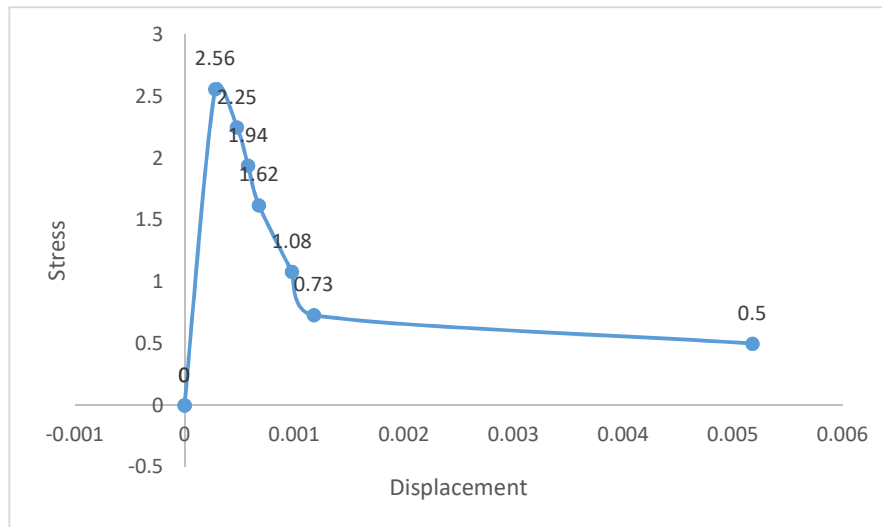


Figure 3.17. Stress-displacement law for tension

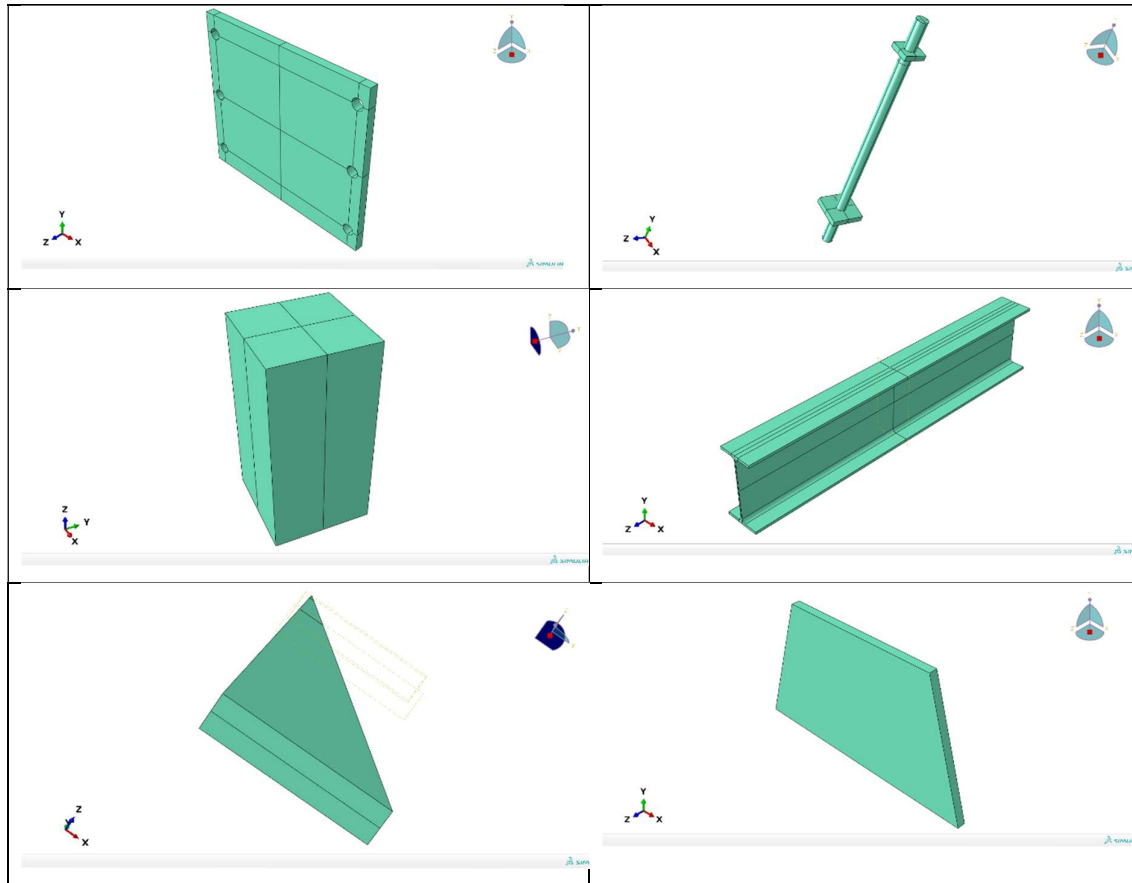
The CDP values considered are shown in table 3.51.

Table 3.51. Concrete damaged plasticity parameters

Dilation angle(°)	Eccentricity	f_{b0}/f_{c0}	K	Viscosity parameter
40	0.1	1.16	0.667	0

The definition of properties in ABAQUS and their assignment to components in ABAQUS confer a green color to the individual parts indicating that the part considered has acquired a property. Table 3.52 show the different parts when their properties have been assigned.

Table 3.52. Column base components with assigned properties



3.6.3. Assembly module

This module involves the combination of all the parts created to obtain the column base connection as shown in figure 3.18.

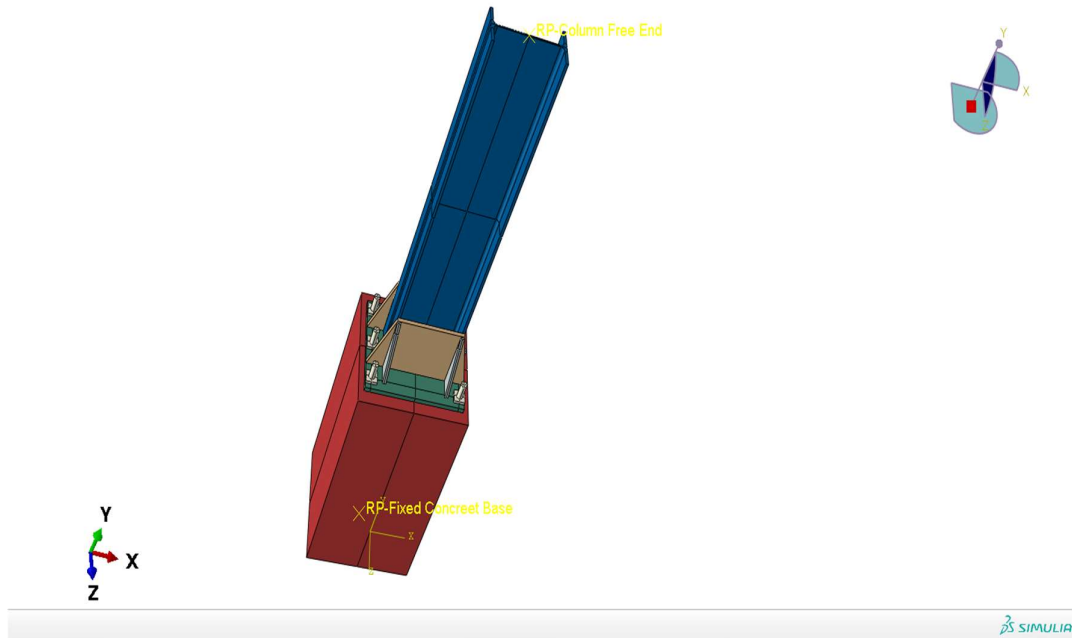


Figure 3.18. Column base connection

3.6.4. Step module

Steps are created as static general. This type of analysis has been found to be the most suitable for the considered case since it can be linear and nonlinear and is assumed when the inertia and time-dependent material effects (such as creep, swelling or viscoelasticity) can be ignored. Option Nlgeom is activated to consider nonlinearities inherent to large displacements.

3.6.5. Interactions

The interactions in the model were created as explained in section 2.9.2.5 as shown in figure 3.19.

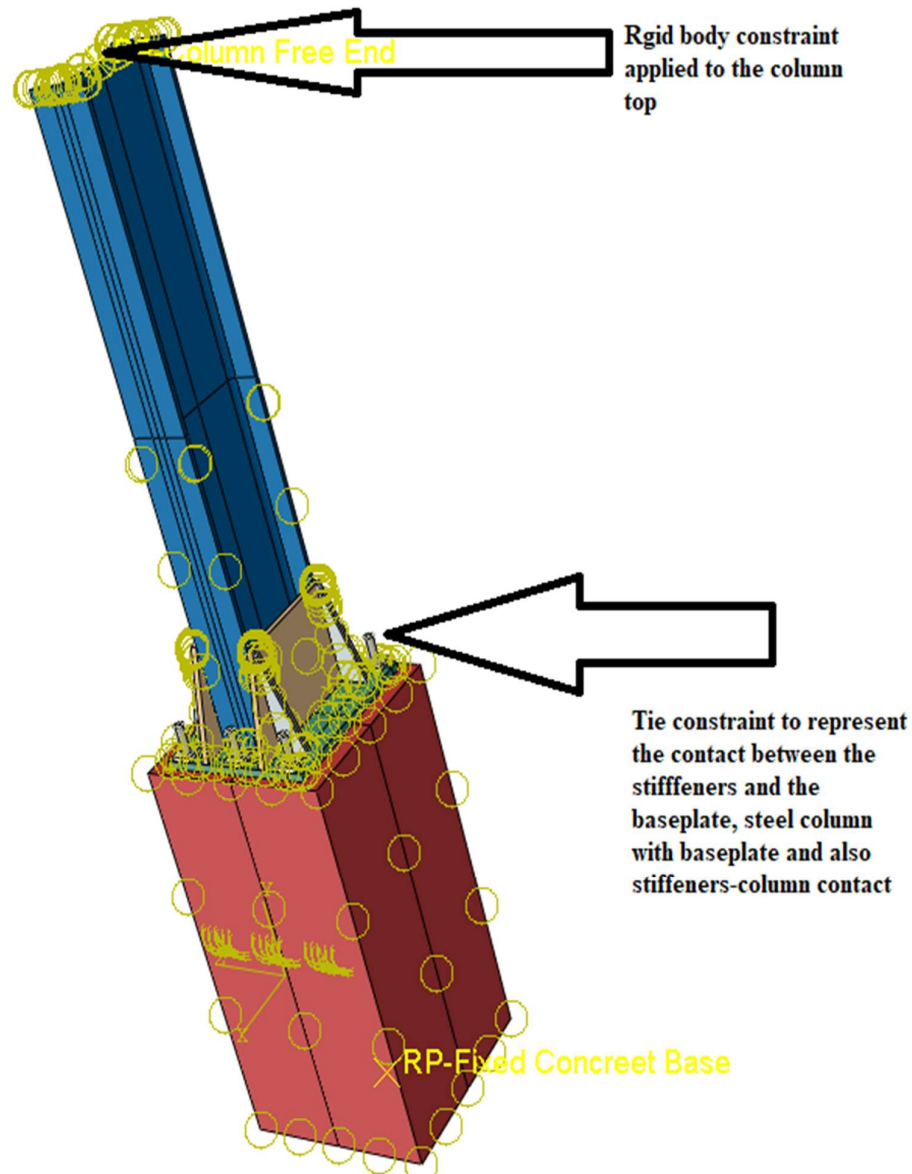


Figure 3.19. Interactions in the column base plate

The contact between the anchor bolts and the concrete block is of paramount importance since the way these elements interact with each other strongly affects the overall stiffness of the specimens. For that, it is necessary to create a constrain at the interface between them known as an “embedded region”. This region is showed in figure 3.20.

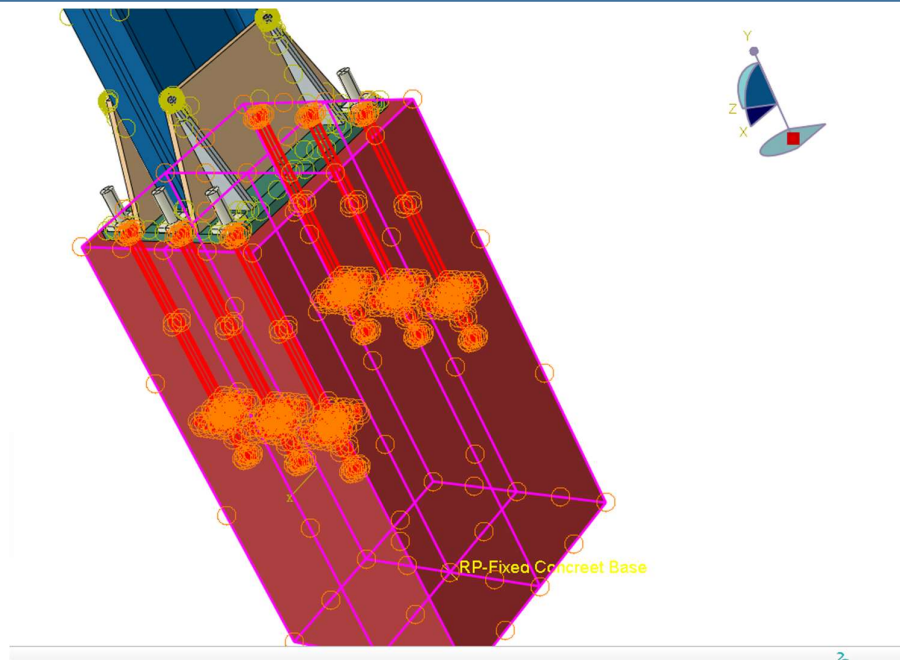


Figure 3.20. Anchor embedded region

3.6.6. Load module

As mentioned above, the specimen was subjected to axial compressive forces and moments. In a force-controlled simulation, the externally applied load is simulated by imposing a vertical force, which is increased until the desired value is attained. This force is applied at the reference point created at the geometric center of the column cross-section, to which all nodes from the surface are rigidly connected.

Boundary conditions are set for the concrete base, the column base plate and the column-to-concrete base connection models in order to create support conditions similar to the real one.

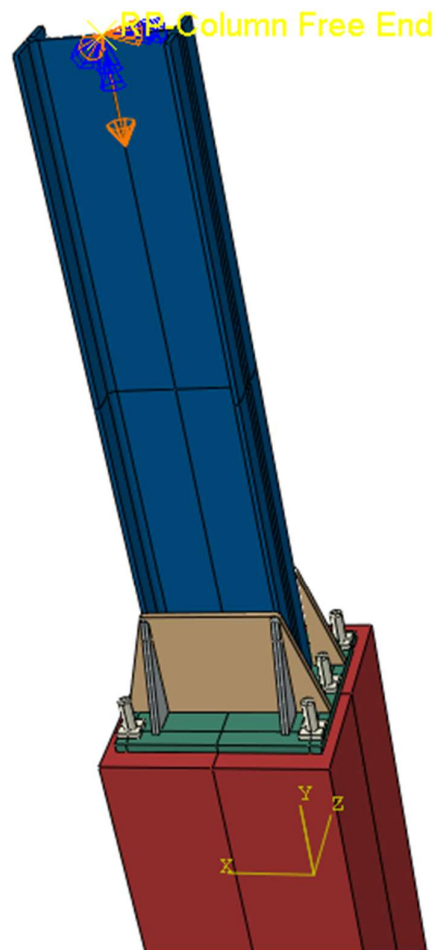


Figure 3.21. Axial Force application on column base

3.6.7. Mesh

The different element meshes are shown in figure 3.22

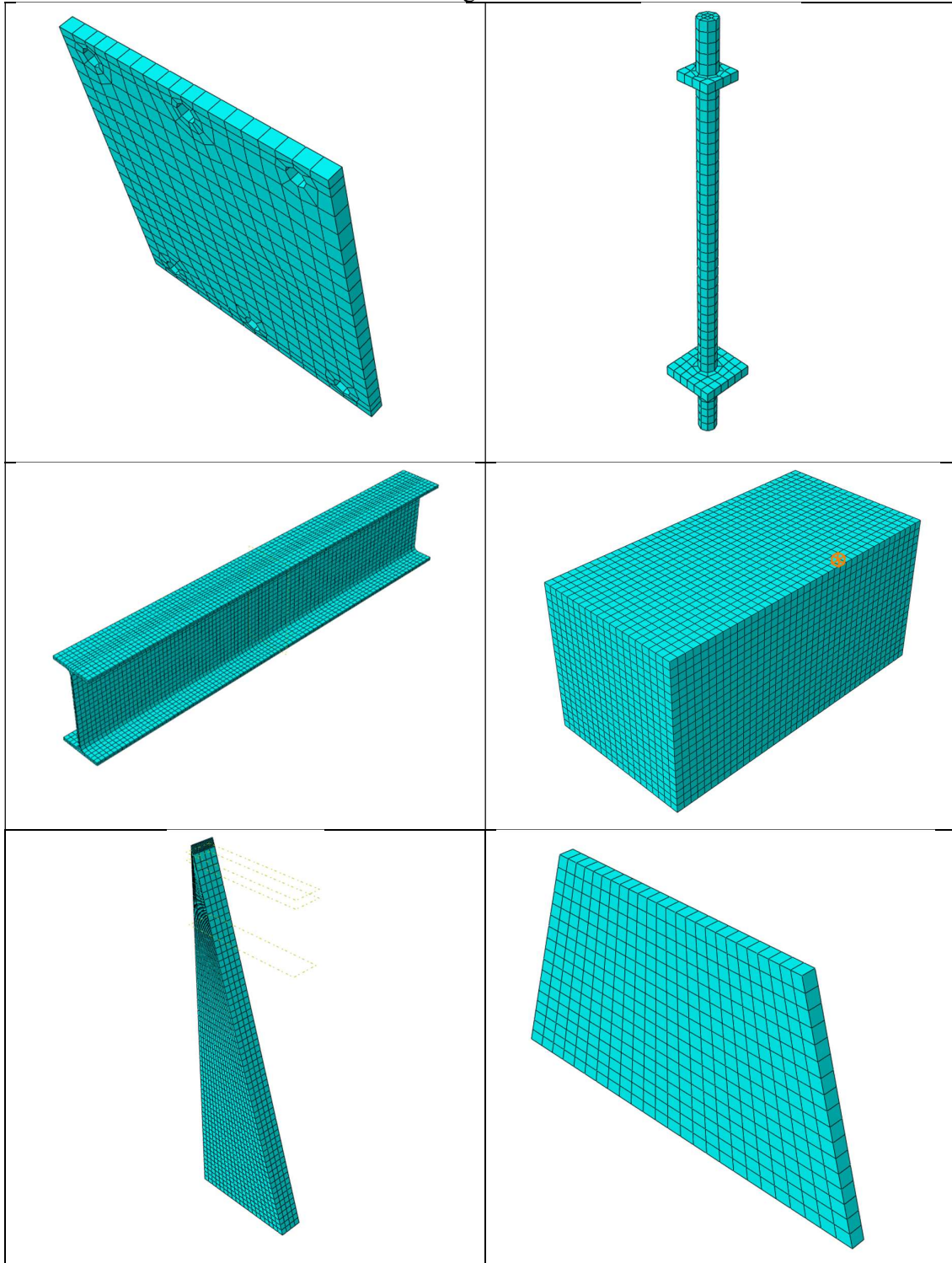


Figure 3.22. Individual part meshes

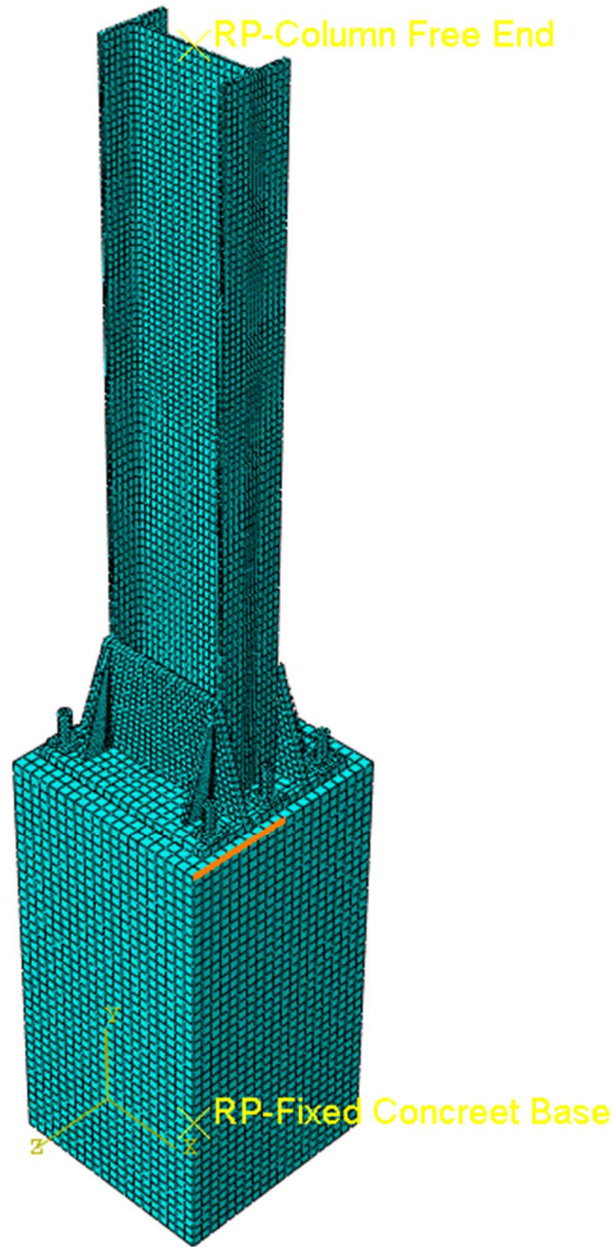


Figure 3.23. Mesh view of the overall model

3.7. Stress analysis of the column base plate connection subjected to the design axial loads

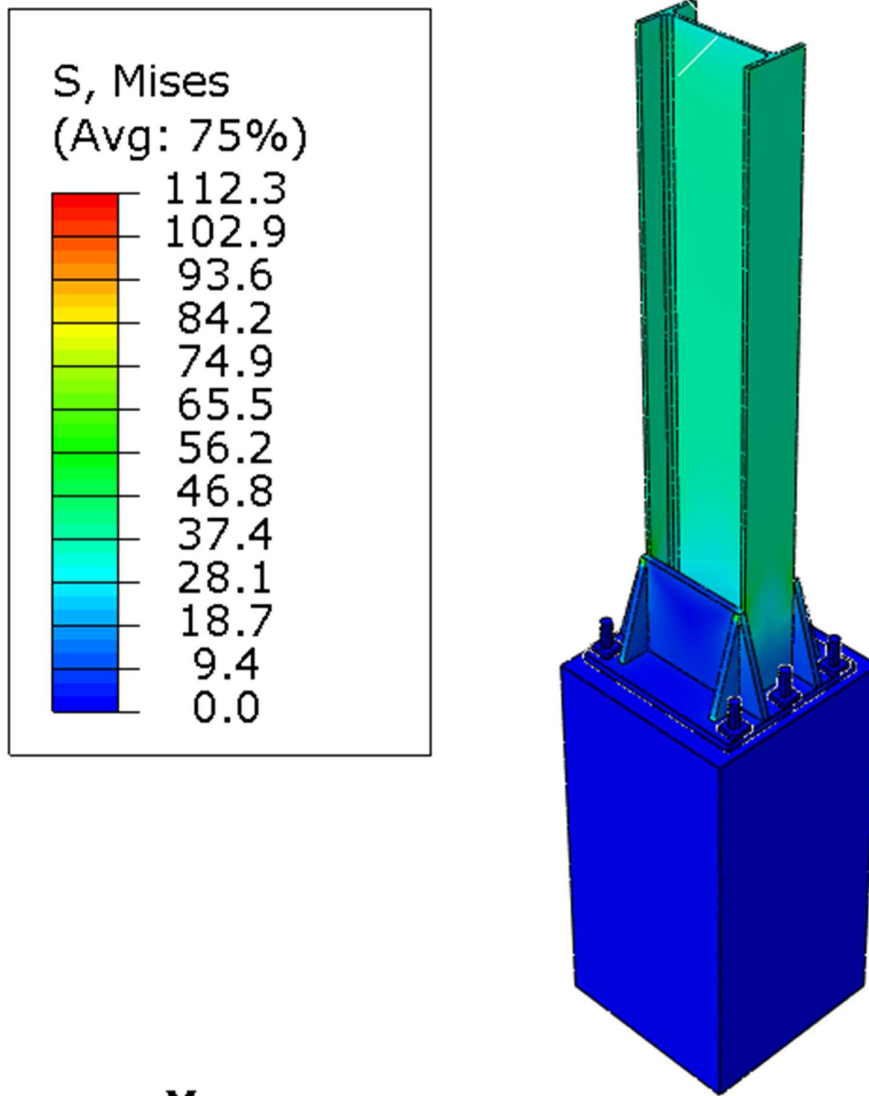


Figure 3.24. Result of stress distribution in the overall model when subjected to design axial force.

From the diagram the progressive transmission of the axial load from the column top cross-section surface to the base plate can be observed.

The maximum stress within the model is 112.3 MPa and the yield strength of the steel element is 275 MPa. From the von-mises stress distribution obtained, it can be seen that none of the steel elements reached the yield point. This further confirms that the designed column base connection supports the loads subjected to it with respect to the unfavorable loading condition considered in chapter 2.

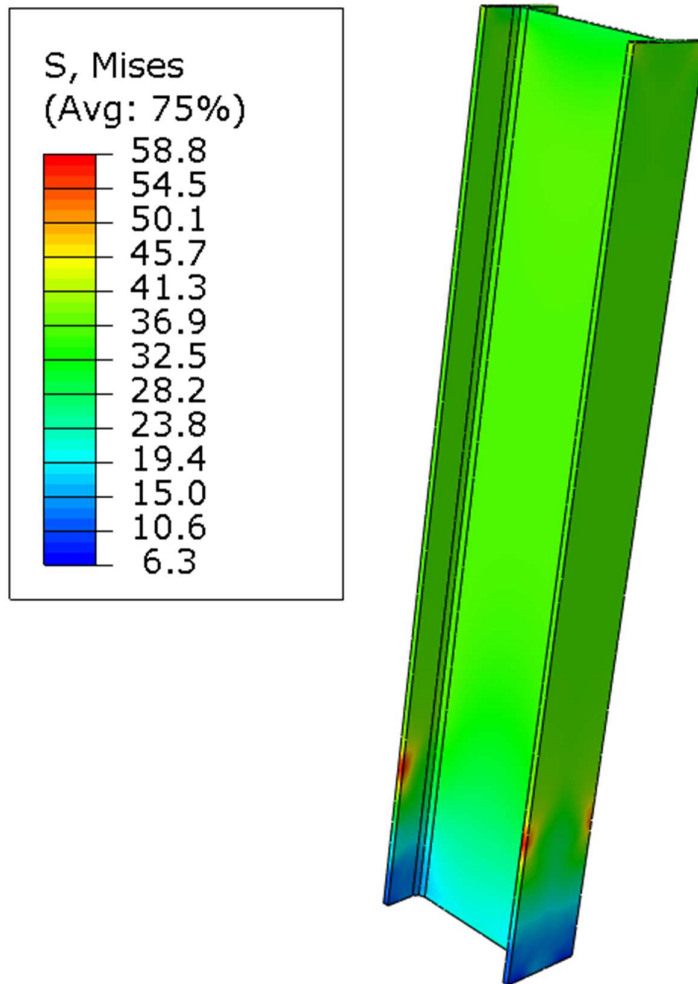


Figure 3.25. stress distribution in the IPE column

The stress distribution obtained primarily indicates that the IPE column is very far from reaching the yielding condition due to the fact that the maximum mises stress obtained is 58.8 MPa which is lower than 275 MPa corresponding to the yield strength of the IPE column.

In addition, it can be observed that the maximum stress on the IPE column is located at the weld points linking the IPE column to the stiffeners. This suggests that in the event of failure, the first plastic hinge appearance will be at those connection points.

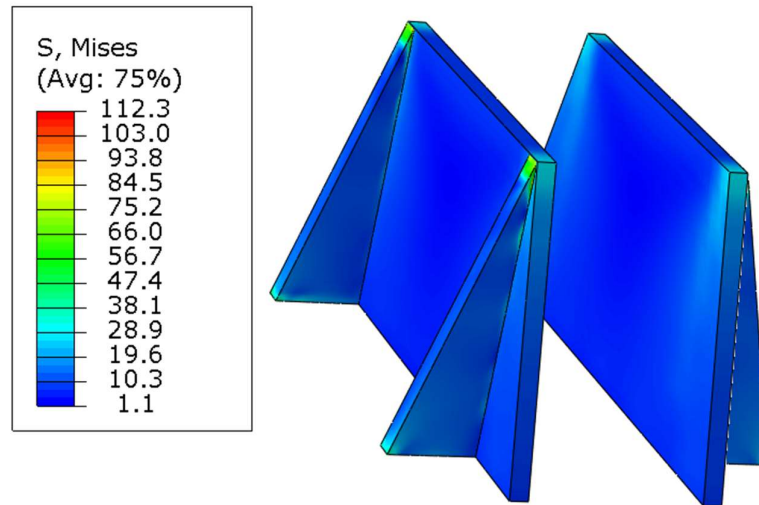


Figure 3.26. Stress distribution in stiffeners

From the von mises distribution and values obtained, it is observed that the maximum stress transferred to the whole model is actually transmitted to the stiffeners. This indicates that the stiffeners retake a greater percentage of the stress transmitted to the column base connection. This is further understood due to the fact that the most stressed point of the stiffener corresponds to the column-stiffener contact point.

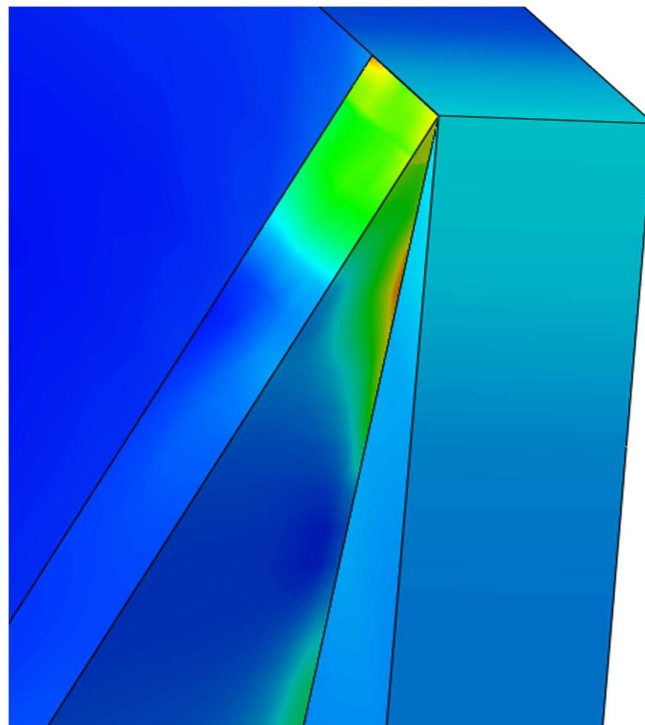


Figure 3.27. The most stressed point of the stiffener

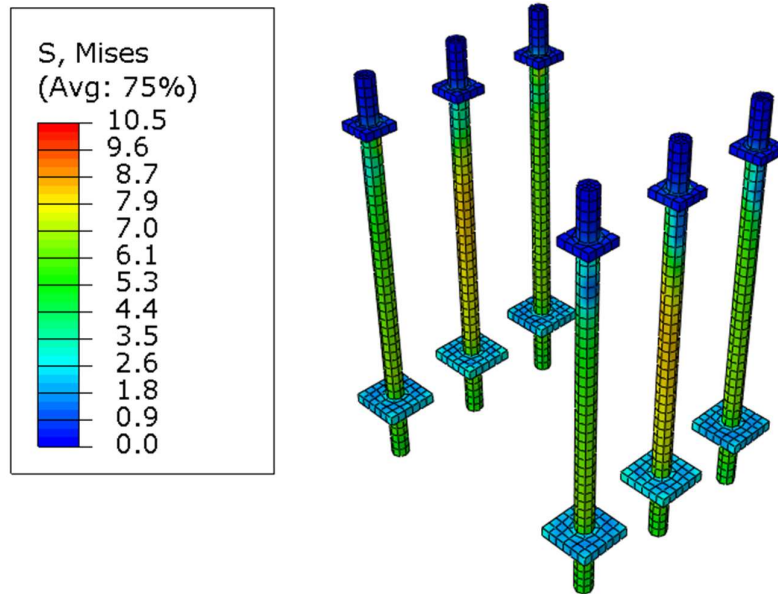


Figure 3.28. Stress distribution in the anchor bolts of the connection

From the von mises stress distribution portrayed in the figure, a maximum value of 10.5 MPa is noticeable in the anchor bolts closest to the flange-web intersection. This indicates that the vertical axial stress from the column acts preponderantly on the flange web intersection of the IPE section. The anchor bolts of class 8.8 and yield strength 640 MPa will not attain rupture with respect to the acting stress.

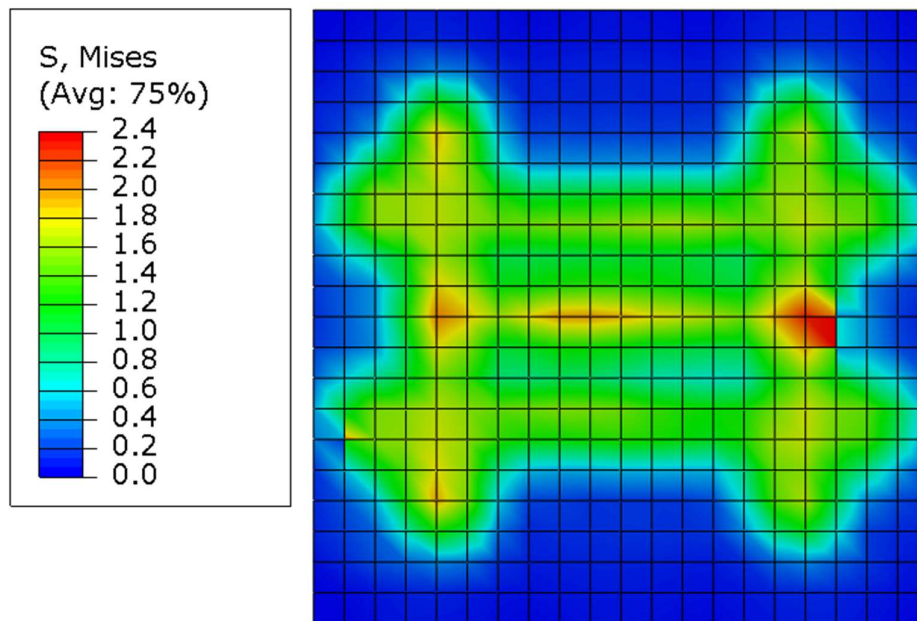


Figure 3.29. 2D Stress distribution on the concrete base

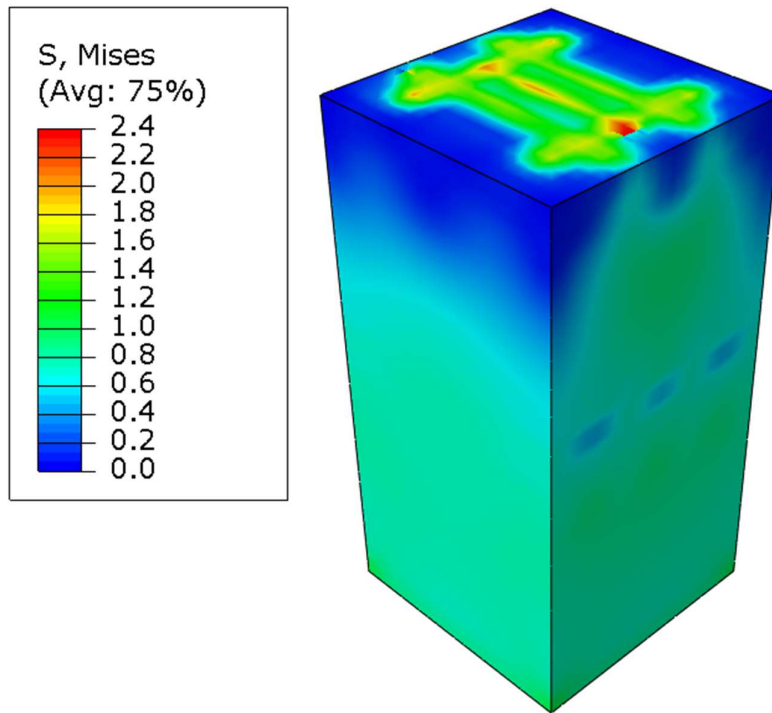


Figure 3.30. 3D stress distribution in the concrete base

Figures 3.29 and 3.30 portray the average distribution of stress in the concrete base. Observation of the top part of the concrete base reveals that; the stress concentration points are located along the line found directly under the steel web. In addition to this observation, lower stress concentration points can be observed along the concrete area directly below the stiffeners.

Regarding the 3D schematic representation on figure 3.31 it can be observed that, the distribution of normal stress under the effective base plate takes place in an angular radial pattern (idealized concrete cone). According to the European norm, the normal stress distribution below the effective base plate takes place at an angle of 45° . From the observed results, it could be conclusively said that the concrete base is in accordance with the norm.

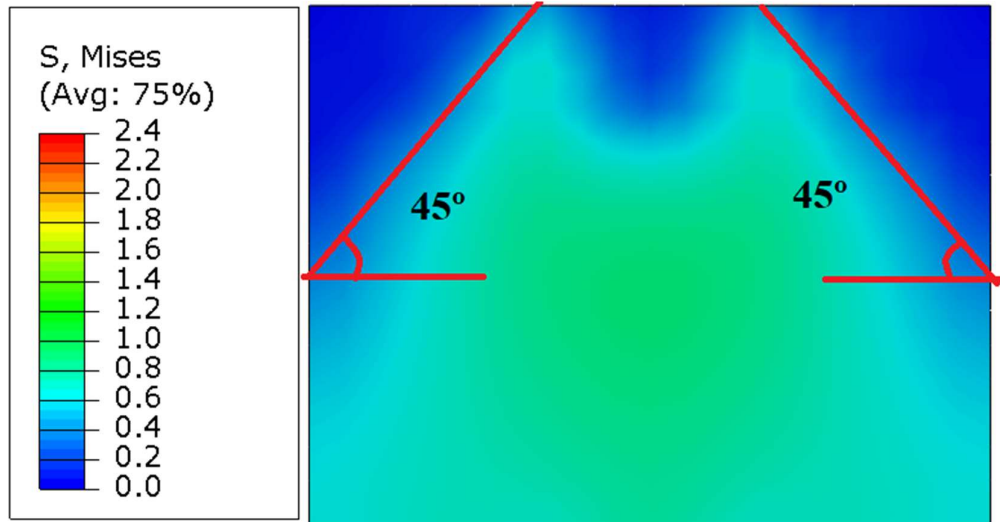


Figure 3.31. Cone Stress distribution in the concrete base

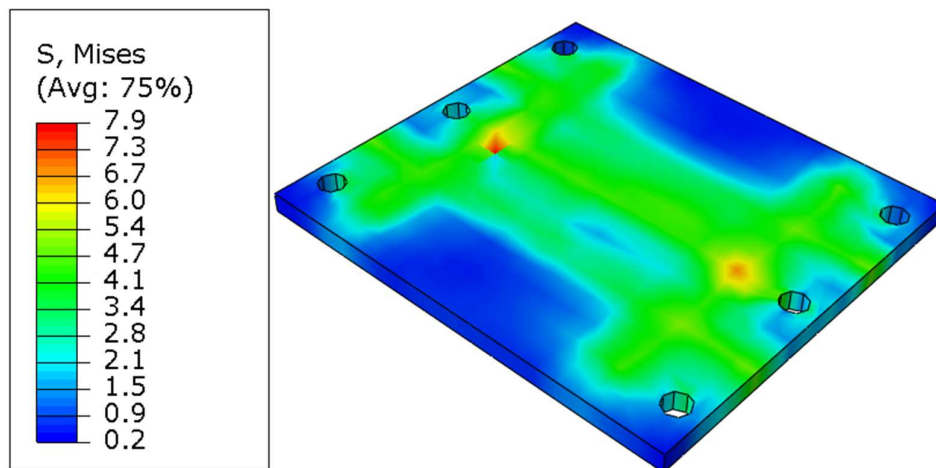


Figure 3.32. Von-mises stress distribution on the base plate

The maximum von-mises stress transmitted to the base plate is 7.9 MPa which is less than the yield strength 275 MPa. This is quite understandable because most of the axial stress distribution is transmitted to the stiffeners as explained earlier. From the results obtained, it can be observed that the range of distribution in the base plate is symmetric with respect to both the web and the flange and the stress distribution range in the vicinity of the flange is more than that surrounding the web.

Stress concentration points can be observed at contact points where the flange-web intersection's pressure is exerted on the base plate. The mises stress variation along the central line passing through the stress concentration points is presented in Figure 3.22. Figure 3.23 shows the center line considered.

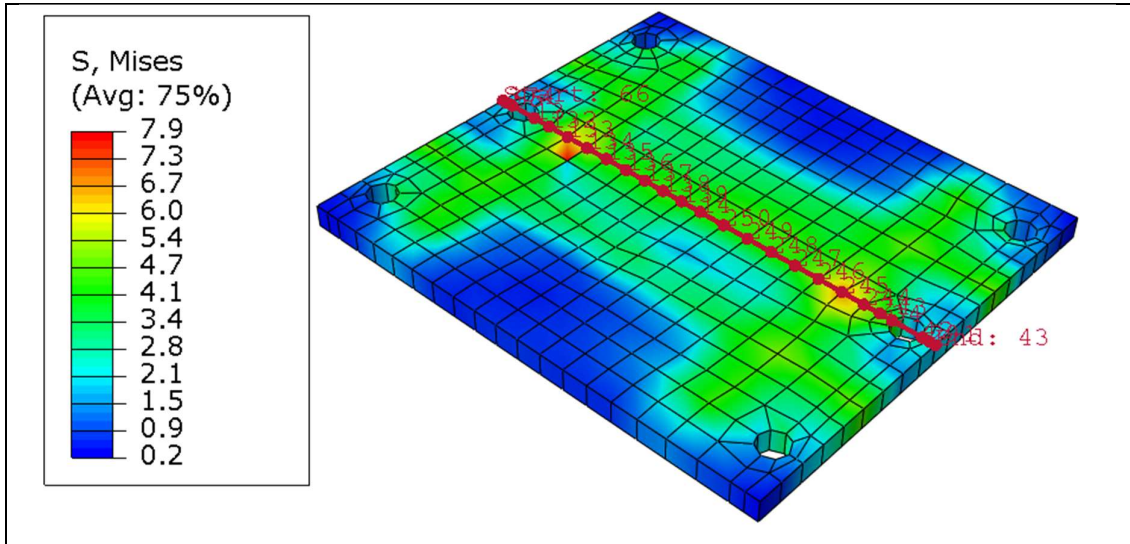


Figure 3.33. Central path under study

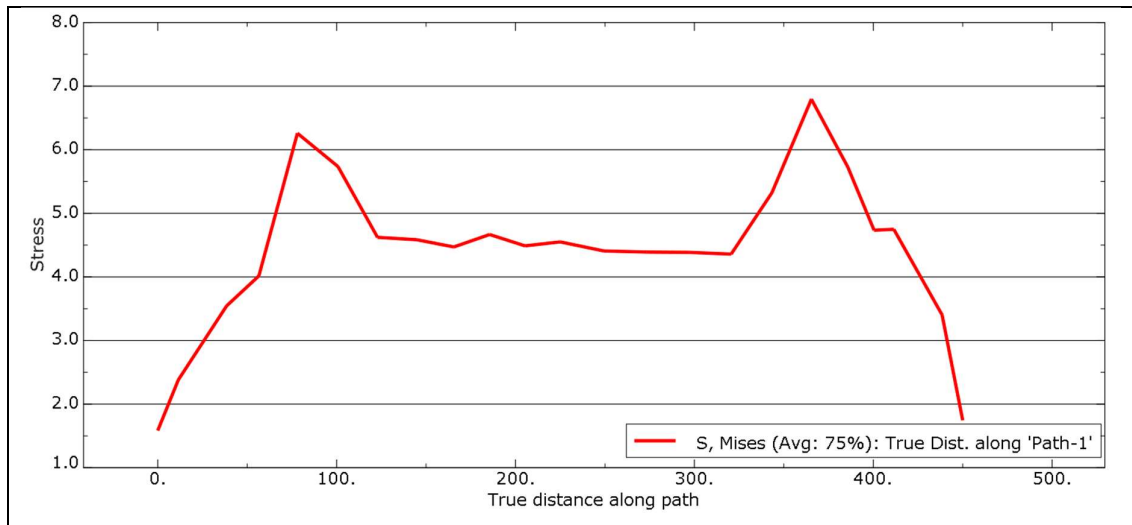


Figure 3.34. Mises stress variation along the central path

The two peaks in figure 3.34 represent the stress concentration points at the flange-web intersection mentioned in the previous paragraph. There is a progressive decrease in stress concentration away from the flange area towards the edges of the base plate in both directions. The variation of stress along the web is constant for a pure axial force as shown in figure 3.34. After observation of the graph, the symmetric nature of stress distribution can be observed.

3.7.1. Parametric study of the stress diffusion in a stiffened baseplate

A study was performed to evaluate the stress diffusion under various loading conditions for the base plates and the results are displayed in the following lines.

FEM ANALYSIS APPLIED TO THE STUDY OF STRESS DIFFUSION IN THE BASEPLATES OF STEEL STRUCTURES

3.7.1.1. Axial loading study

Five different axial loads were loaded to the column base connections with more details regarding the base plate and its stress results. The axial loads considered here were; 200kN, 250kN, 300kN, 350kN and 400kN.

Table 3.53. Stress diffusion results along central path

Axial load	Von mises stress distribution	Stress-distance graph
200kN		
250kN		
300kN		
350kN		

FEM ANALYSIS APPLIED TO THE STUDY OF STRESS DIFFUSION IN THE BASEPLATES OF STEEL STRUCTURES

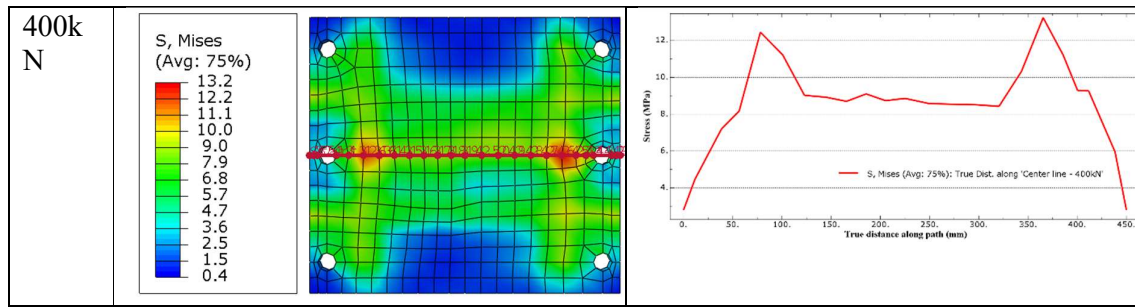


Table 3.53 shows the variation of stress along the geometric central line of the base plate for different loading conditions.

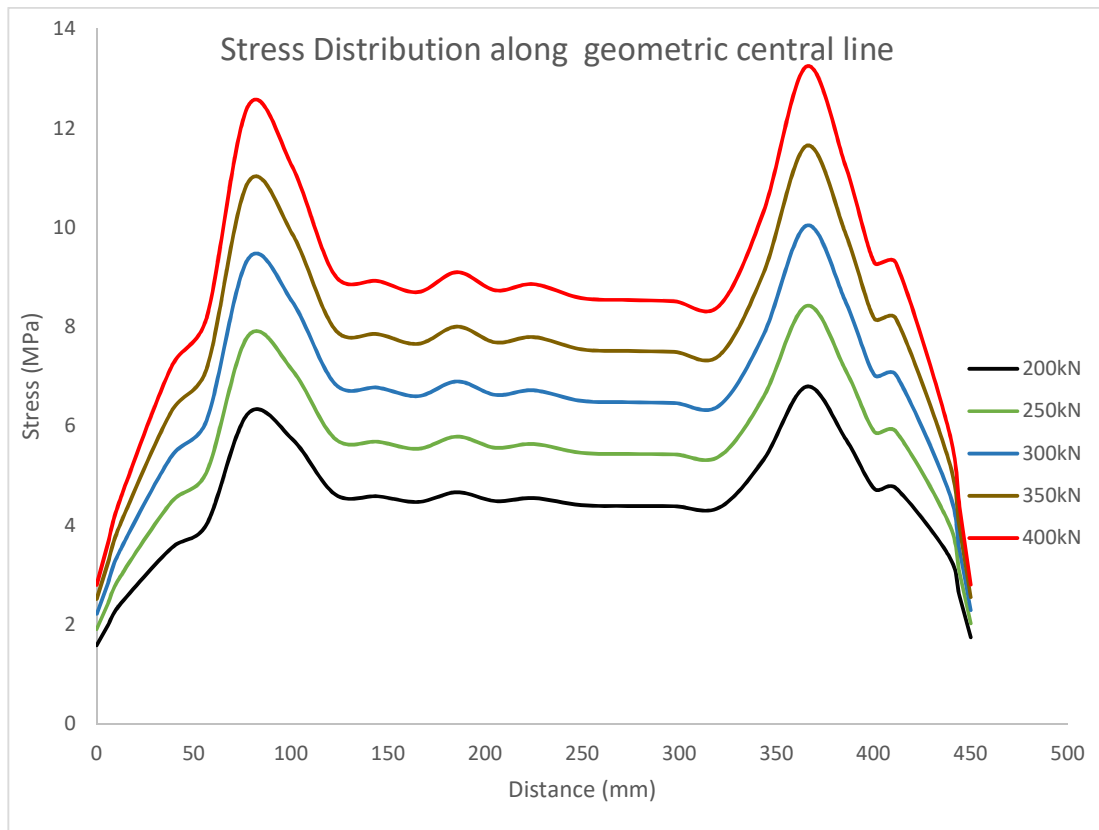


Figure 3.35. Stress distribution along the geometrical central line of the base plate

The five analysis performed allowed us to verify that the pattern of stress distribution in a base plate subjected to axial loading is the same no matter the magnitude of the load. The stress concentration points revealed could be a starting point to predict the possible failure mechanism that the base plate could suffer.

In addition to this, the variation of the maximum von mises stress (peak point) in the base plate with respect to the axial loads was studied with the help of a graph displayed on figure 3.36.

Figure 3.36 shows that the stress and the strain of the base plate varies linearly with the applied force. This suggests that the plate is still in the elastic state. This is quite understandable since the axial force plastic resistance is 1264.3 kN and it was not reached.

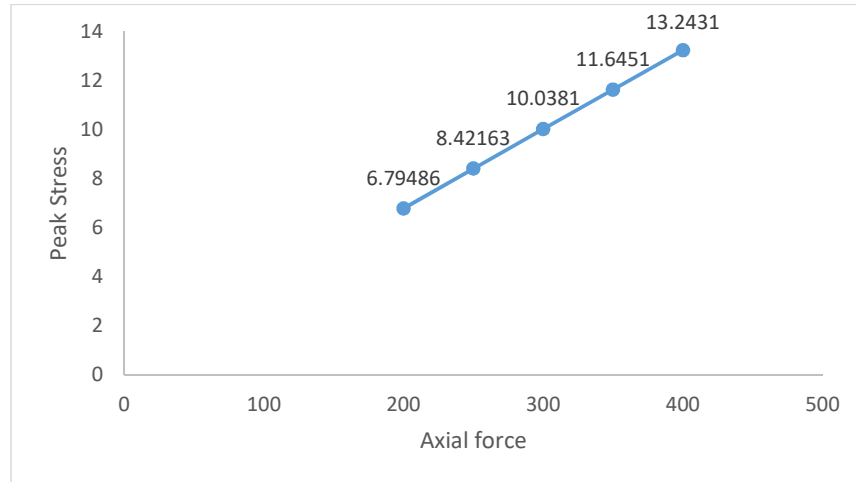


Figure 3.36. Variation of mises peak stress with axial force

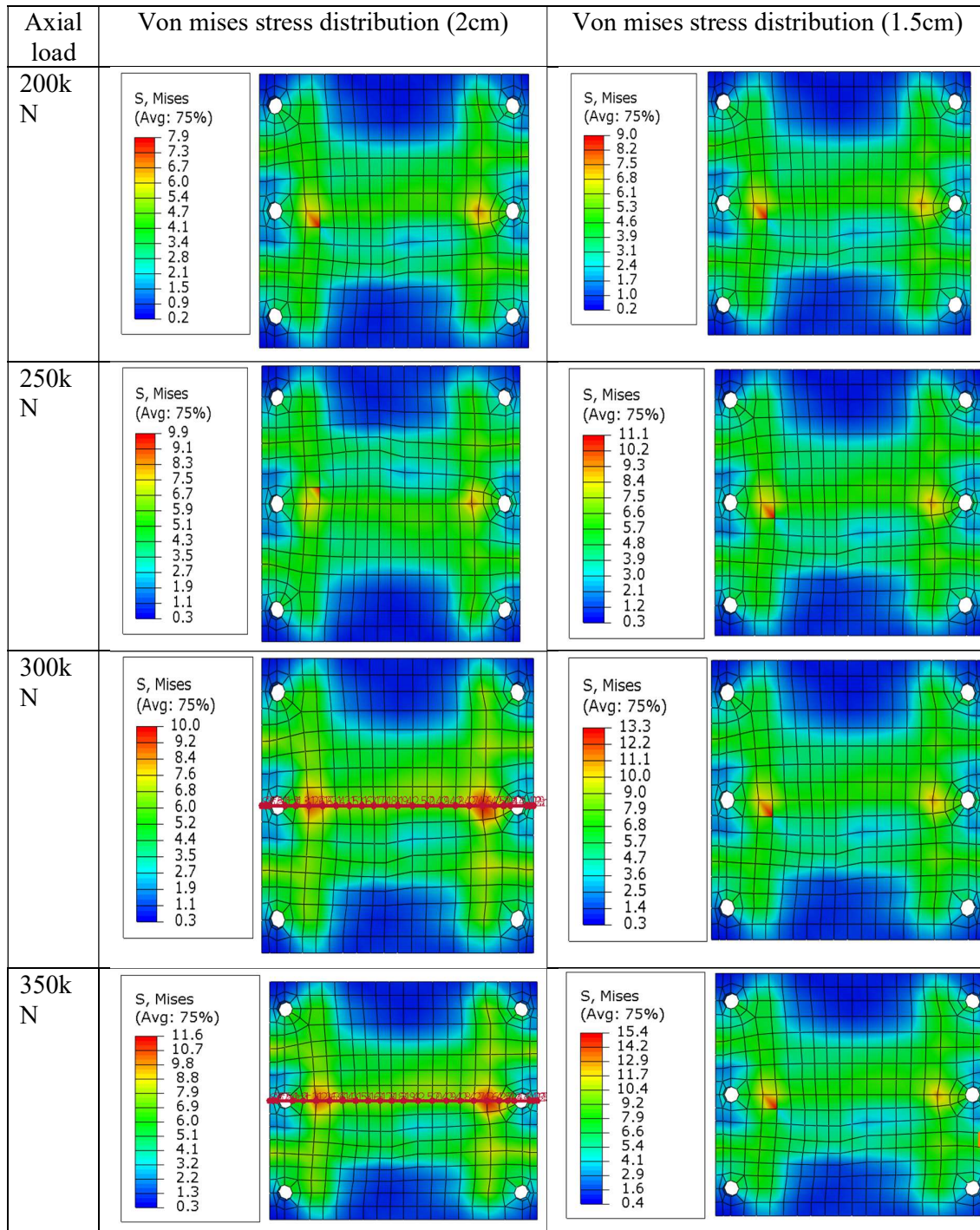
The percentage of stress absorbed by the most stressed zone (the flange-web intersection area) with respect to zone where the stresses are averagely distributed was determined in each loading case. From the 200 kN loading case, it was observed that the stress concentration zone in the flange-web vicinity absorbed 92.7% of stress more than the average zone. The results obtained were 94.1%, 92.3%, 93.3% and 94.1% of stress in the flange vicinity respectively for 250 kN, 300 kN, 350 kN and 400 kN. This shows that, the base plate area around the flange-web absorbs about 93.3% more of compressive stress than the averagely stressed zones.

3.7.1.2. Axial loading with variation of the thickness of the base plate

The reduction in the thickness of the steel base plate leads to an increase in the amount of stress in the base plate. This is quite understandable since the volume of distribution reduces. This variation can be witnessed on table 3.54 which shows how the stress is distributed in steel base plates of thicknesses 1cm, 1.5cm and 2cm.

**FEM ANALYSIS APPLIED TO THE STUDY OF STRESS
DIFFUSION IN THE BASEPLATES OF STEEL STRUCTURES**

Table 3.54. Effect of baseplate thickness variation on the stress diffusion (2 cm and 1.5 cm)



**FEM ANALYSIS APPLIED TO THE STUDY OF STRESS
DIFFUSION IN THE BASEPLATES OF STEEL STRUCTURES**

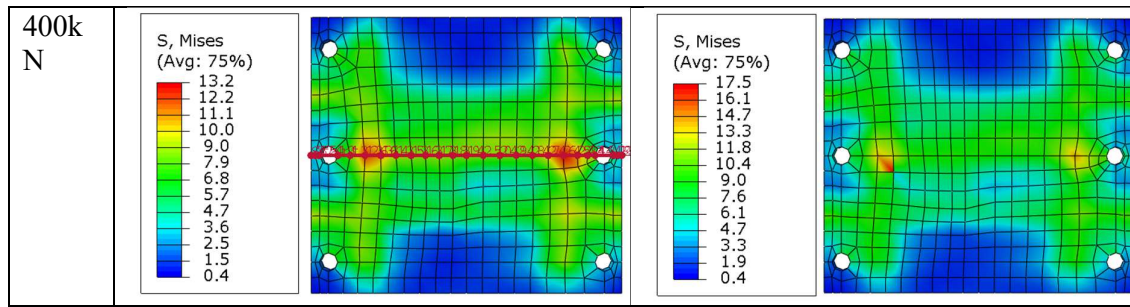
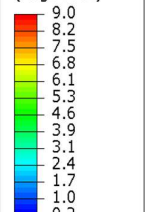
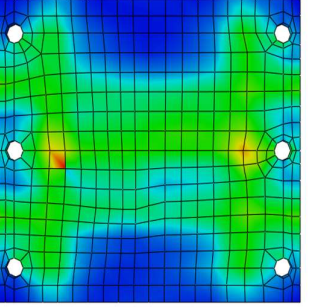
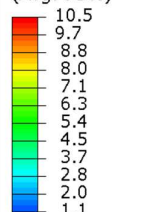
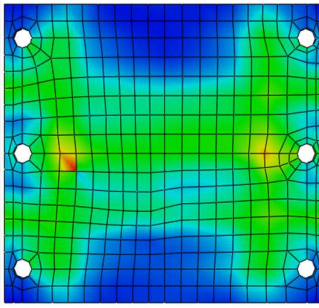
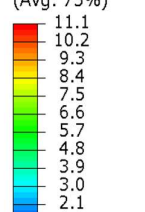
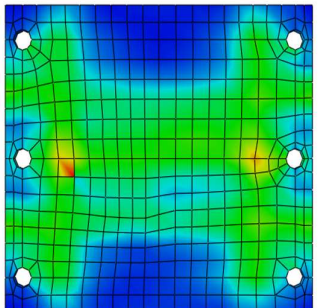
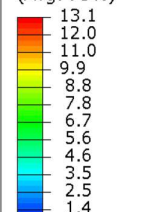
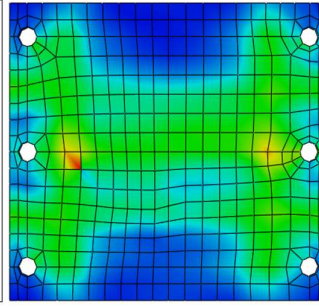
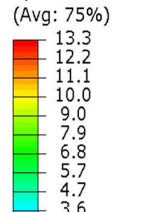
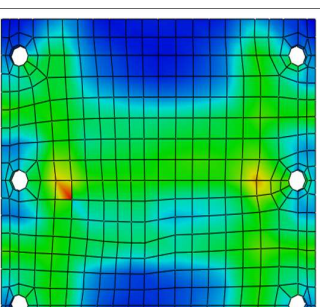
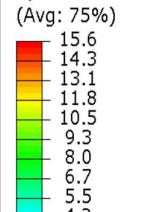
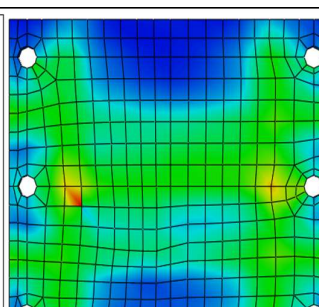
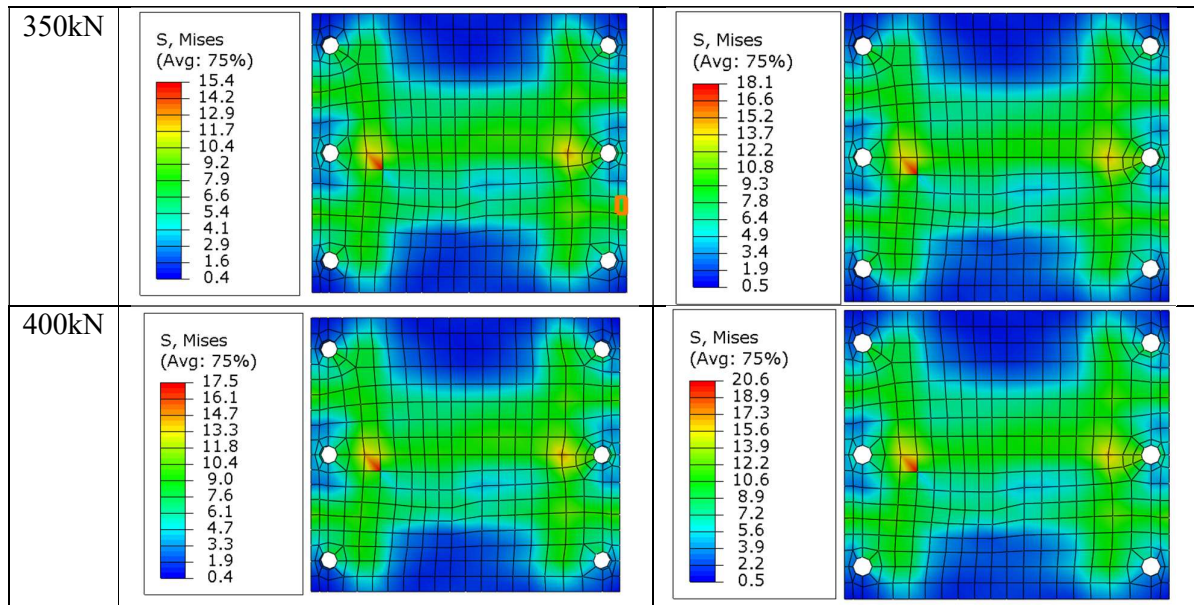


Table 3.55. Effect of baseplate thickness variation on the stress diffusion (1.5 cm and 1.0 cm)

Axial load	Von mises stress distribution (1.5 cm)	Von mises stress distribution (1 cm)
200kN	<p>S, Mises (Avg: 75%)</p>  	<p>S, Mises (Avg: 75%)</p>  
250kN	<p>S, Mises (Avg: 75%)</p>  	<p>S, Mises (Avg: 75%)</p>  
300kN	<p>S, Mises (Avg: 75%)</p>  	<p>S, Mises (Avg: 75%)</p>  

**FEM ANALYSIS APPLIED TO THE STUDY OF STRESS
DIFFUSION IN THE BASEPLATES OF STEEL STRUCTURES**



To have a better understanding of this variation, a representative plot shown in figure 3.37 has been drawn.

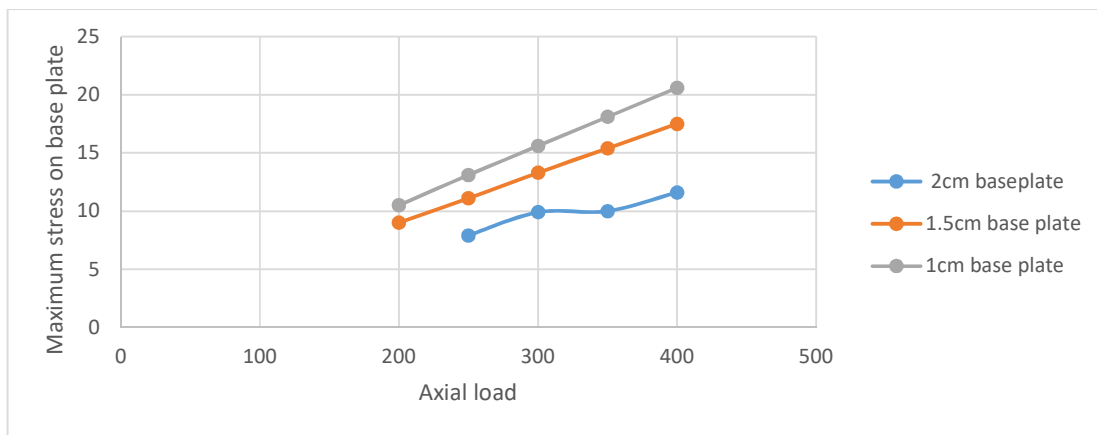


Figure 3.37. Maximum stress variation with baseplate thickness

The pattern of variation of stress with axial load was studied with the help of trend lines and it was observed that when the axial load is below a certain threshold value, the increment of the stress with the reduction of the base plate thickness does not take place, rather, the thicker base plate receives a greater stress, and this continues until the acting axial force goes above the threshold value as shown in figure 3.38. Above this value, the increment in axial stress induces an increment in the base plate. This behavior suggests that the stress could be locally concentrated in thick base plates and that with the reduction of the thickness, the stress gets more uniformly distributed.

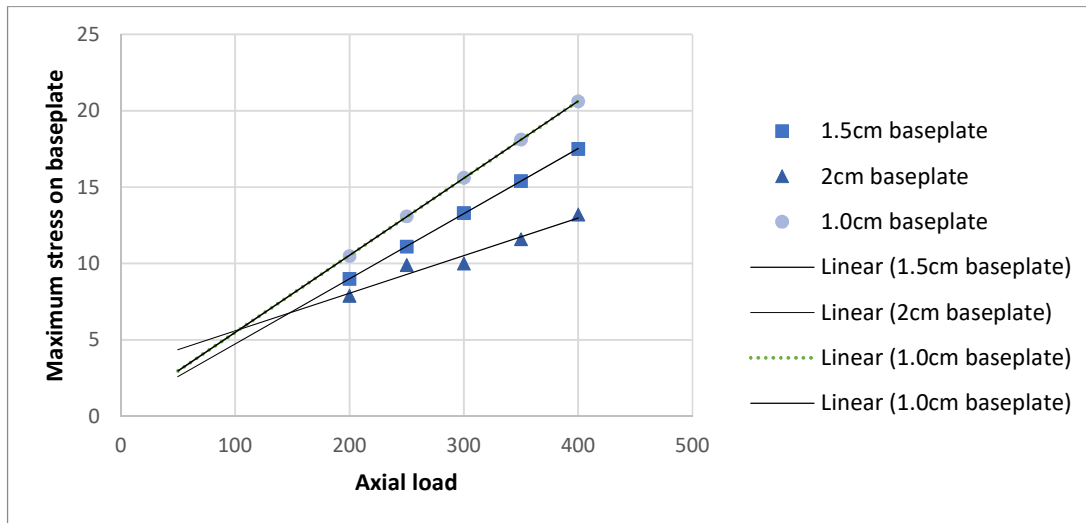


Figure 3.38. Trend lines indicating the behavior of baseplates under axial loads

3.7.1.3. Displacement-driven moment study of the base plate

The imposed lateral displacement induces a rotation along the strong axis of the IPE 300 column. A brief overview of the behavior of all the components of the column base plate connection subjected to bending is presented within the following lines.

Column bending

Column bending study was performed about the strong axis

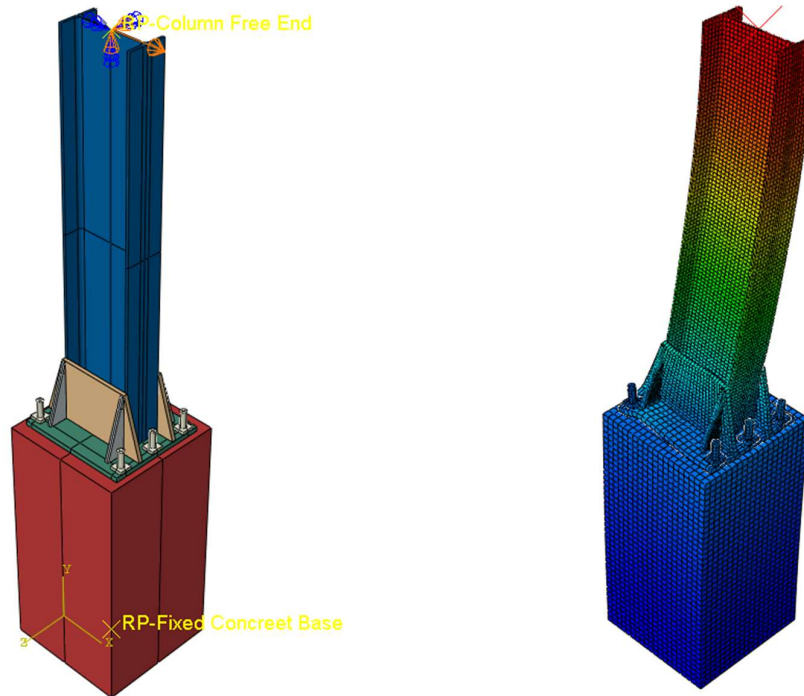


Figure 3.39. Rotation of the IPE column with respect to its strong axis

Baseplate

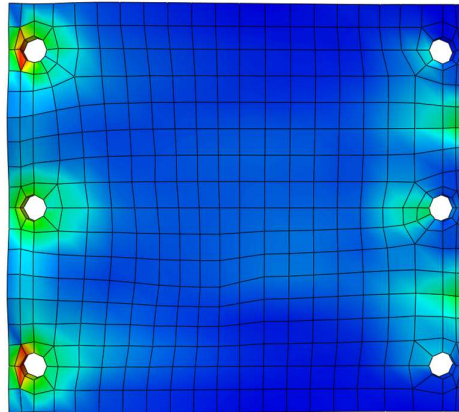


Figure 3.40. Stress distribution on a base plate subjected to bending

From figure 3.38, the von mises stress distribution indicate that in the tension zone (left part of the base plate), the stress concentration points are located at the bolt openings whereas in the compression zone, stress concentration points are mostly located in between anchor bolts openings with a small proportion found at the center anchor bolt.

Anchor bolts

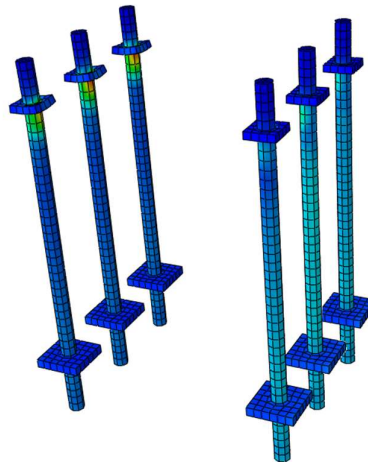


Figure 3.41. Stress distribution in anchor bolts when subjected to bending

Figure 3.39 depicts the tension and compressive stress distribution along the left and right anchor bolts respectively. The tensioned anchor bolts have stress concentrations at their interface with the base plate; this is due to the pulling force acting on them during the rotation of the column. The compressed anchor bolts do not show a distinguished stress concentration. Rather, they show a progressive increase of the stress from the top to bottom parts; this is a clear indication of compressive stress diffusion.

Stiffeners

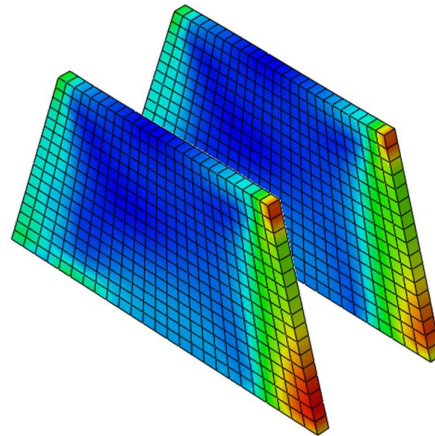


Figure 3.42. Stress distribution in stiffeners subjected to bending

Stress concentration points within stiffeners are mostly located at their base, at their interface with the base plate. It should be noted that they receive the majority of the stress transmitted during a bending moment action.

Concrete under bending action

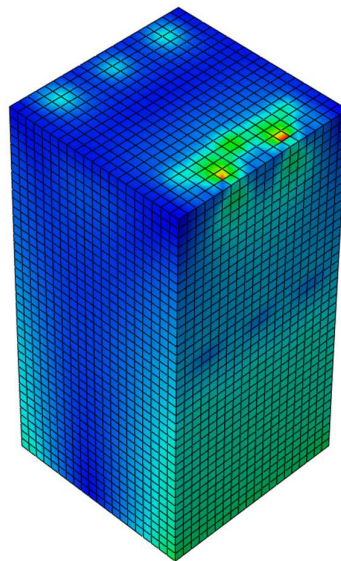


Figure 3.43. Stress distribution in concrete under bending moment action of column base connection

From figure 3.29, the major stress concentration points observed are located below the compression zones of the base plate. The minor 3 concentration points observed are located below the tension zone of the base plate. If the tensile stress values within the concrete base

exceed the maximum tensile resistance of concrete, 2.6 MPa, the concrete base may fail due to anchor bolt pull out.

3.7.1.4. Bending stress distribution in a stiffened base plate

A bending moment study was performed on the base plate by varying the horizontal cantilever deflection of the column generated by an imposed displacement. This was performed so as to witness the evolution of stress diffusion with the progressive increment of the horizontal displacement.

This study was performed for both the previous column base model used on the case study (it will be called model 1) and the newly designed column base model (It will be called model 2) which satisfies the Eurocode recommendations so as to notice the influence of the position of anchor bolts in the diffusion of stress in base plates.

For each case of bending, the stress diffusion along the 3 lines portrayed in figure 3.42 was studied.

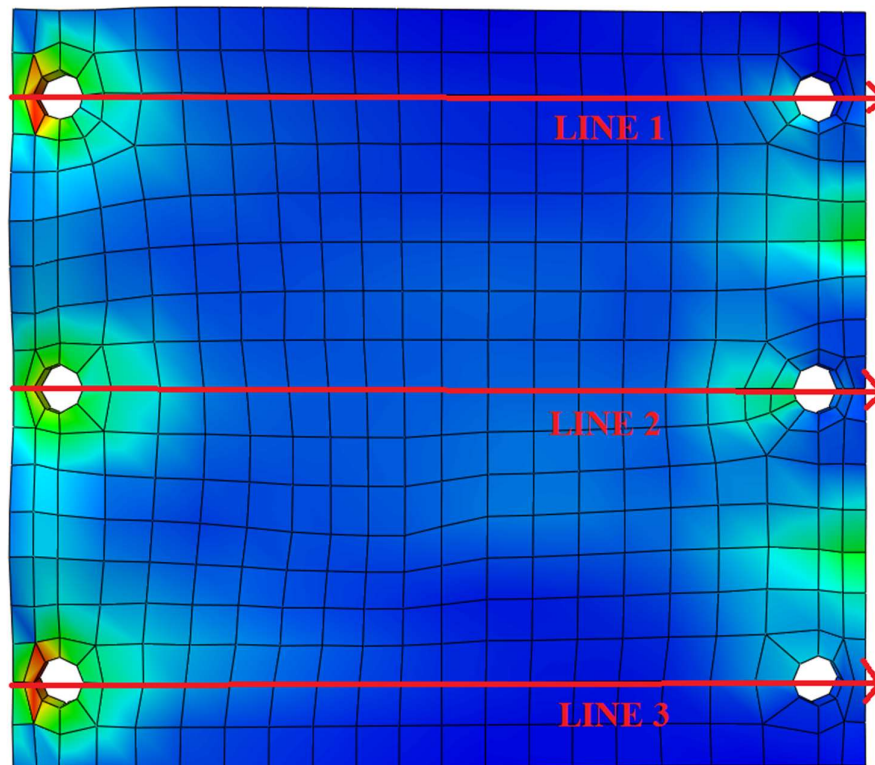


Figure 3.44. Paths considered for the stress diffusion study under bending action

a. Results obtained from the first column base plate model (Model 1)

Figures 3.45, 3.46 and 3.47 represent respectively the stress variation for lines 1, 2 and 3 under 1mm, 1.5mm, 2mm, 2.5mm and 3mm imposed displacements. The two distinct peaks shown

**FEM ANALYSIS APPLIED TO THE STUDY OF STRESS
DIFFUSION IN THE BASEPLATES OF STEEL STRUCTURES**

in each figure indicates the stress concentration points which coincide with the position of the anchor bolts. The left higher peak and the right lower peak indicate respectively the tensile and compressive zones of the base plate. Higher peaks observed at the left of the graphs are due to the elevated tensile stress transmitted to the base plate from the anchor bolts. The comparatively lower peak portrays the compressive stresses acting on the base plate. A large percentage of that stress is transmitted to the concrete foundation which works in compression, this explains why the base plate stress concentration at that point is comparatively lower.

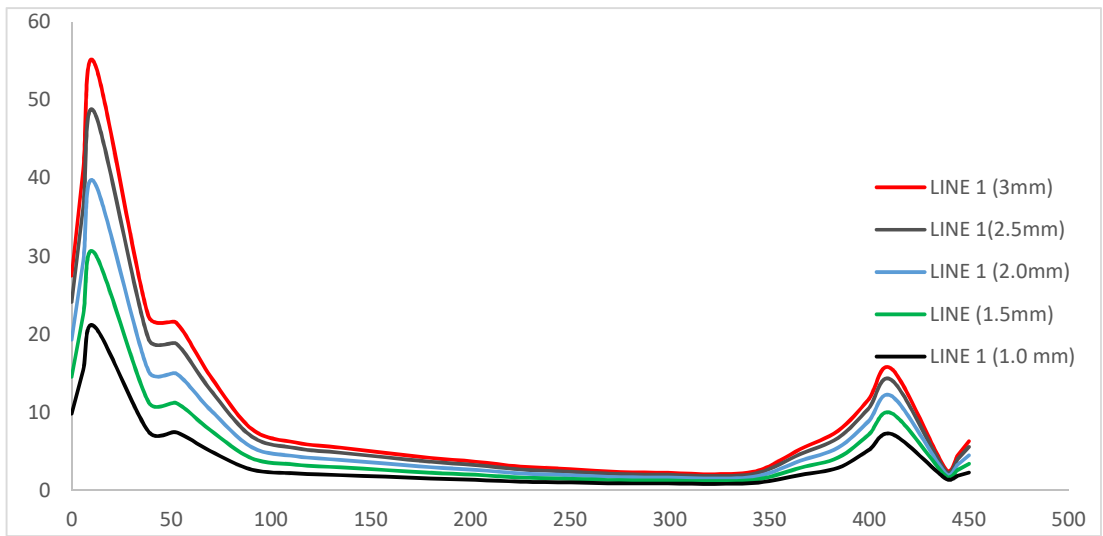


Figure 3.45. Variation of stress along line 1 under different bending conditions

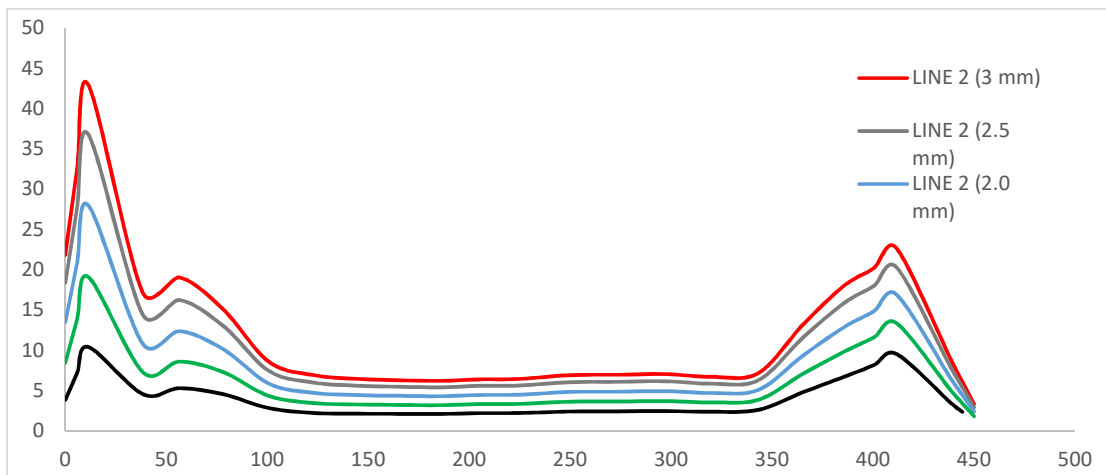


Figure 3.46. Variation of stress along line 2 under different bending conditions

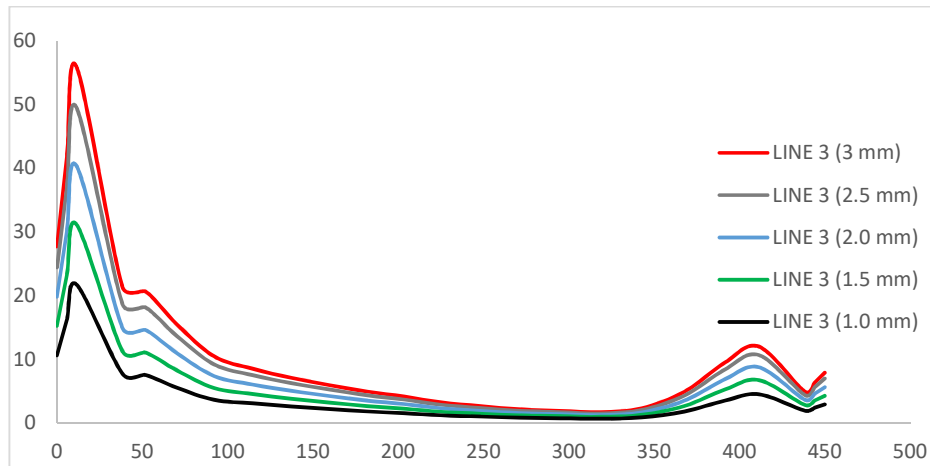


Figure 3.47. Variation of stress along line 3 under different bending conditions

The fact that the shapes of the different curves are homothetic indicate that the manner of stress distribution along the paths do not change no matter the magnitude of the bending moment. The only noticeable change observed is that of the von mises stress value.

The distribution of stress in figures 3.45 and 3.47 are similar and different from the distribution in figure 3.46. This indicates that the variation of stress along lines 1 and 3 are similar whereas the stress variation along line 2 which is the median of the base plate is different with lower stress concentration values compared to the lines closer to the edges. This indicates that the tensile areas of the base plate closer to the top and bottom anchor bolts are more stressed than the tensile area close to the middle bolt.

b. Results obtained from the second base plate model (Model 2)

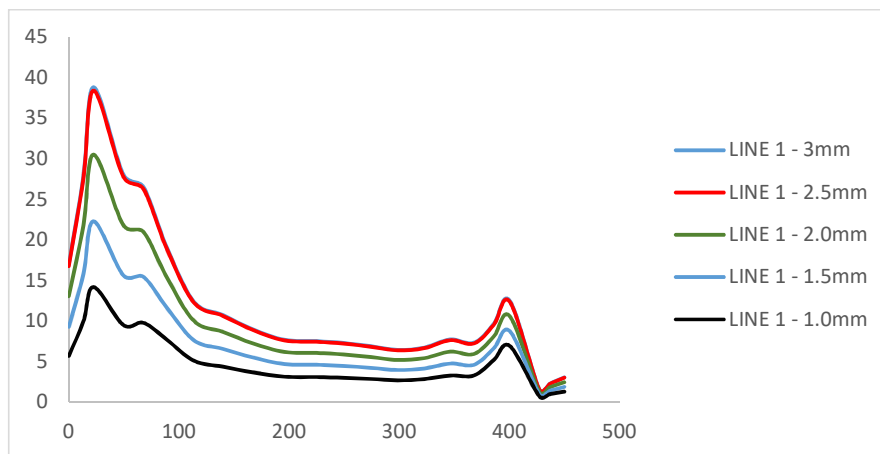


Figure 3.48. Stress variation along line 1 in model 2

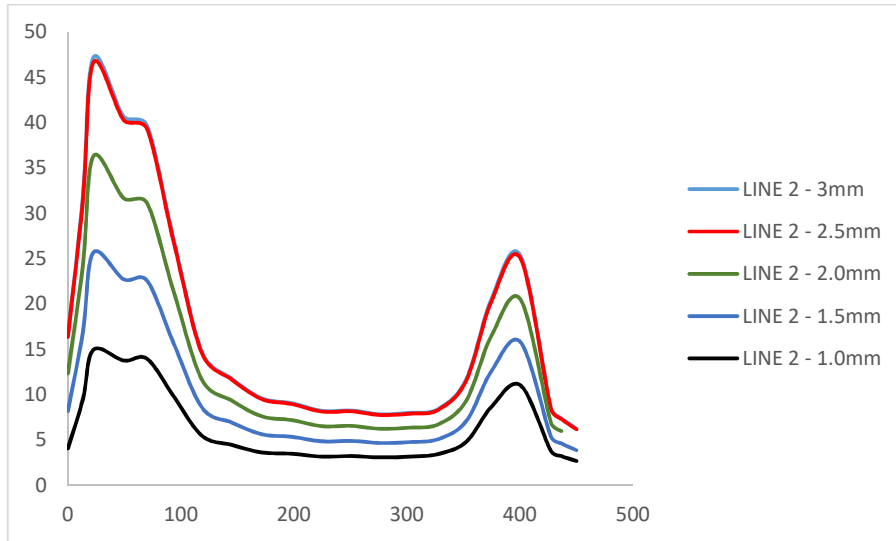


Figure 3.49. Stress variation along line 2 in model 2

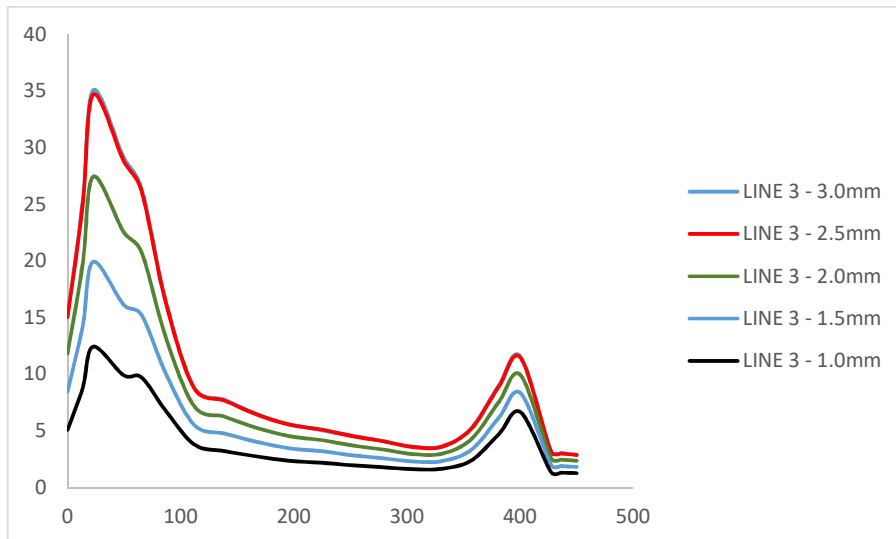
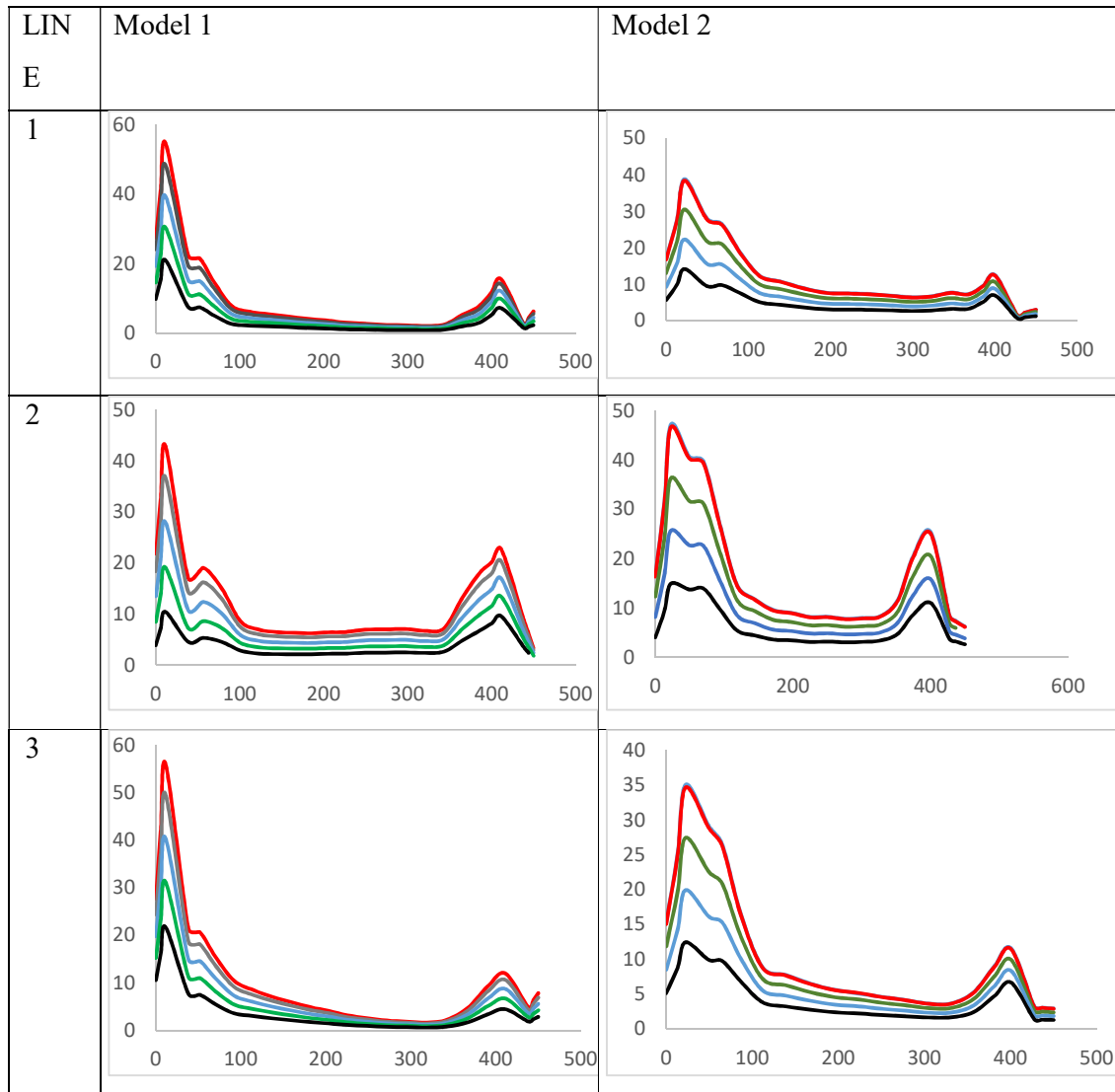


Figure 3.50. Stress variation along line 3 in model 2

Table 3.56. Stress diffusion disparity between model 1 and 2



The graphs obtained reveal that the stress peaks in model 2 are of comparatively lower magnitude with respect to those in model 1. This indicates that the closer the anchor bolts are to the column flange, the lower the stresses subjected to the base plates. Also, the peaks in model 1 are sharper than those observed in model 2; this indicates that the stress is more uniformly distributed in model 2 than in model 1. Another remarkable observation is that the maximum stress in model 2 is along the central line; line 2 whereas in model 1 the maximum stresses are observed along lines 1 and 3; the lines closer to the edges. This further accounts for the increase in uniformity of stress distribution in the base plate.

The stress displacement curves along lines 1,2 and 3 for both models were studied to have a clearer idea of the proportion of stress distributed in each case.

In Figure 3.51, the symmetric distribution of high stress along lines 1 and 3 can be reconfirmed since they have closely similar stress-displacement curves. The stress-displacement curve along line 2 is comparatively lower since it receives a lower amount of stress. It has been found that lines 1 and 3 receive about 28.8% of stress more than line 2.

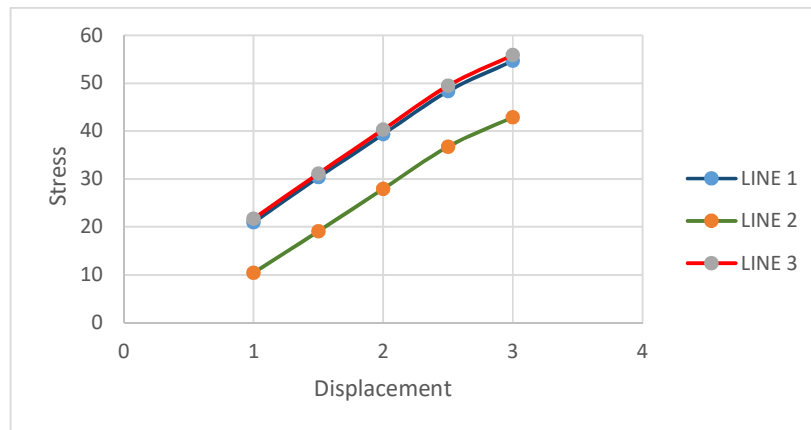


Figure 3.51. Stress-displacement curves along lines 1, 2 and 3 for model 1

Figure 3.52 shows the stress-displacement curves for lines 1, 2 and 3 for model 2 (Eurocode compliant). These curves reconfirm the fact that in model 2, the maximum stress is exerted along the central line (line 2). It has been found that line 2 receives 21.5% of stress more than line 1 and 34.5% of stress more than line 3.

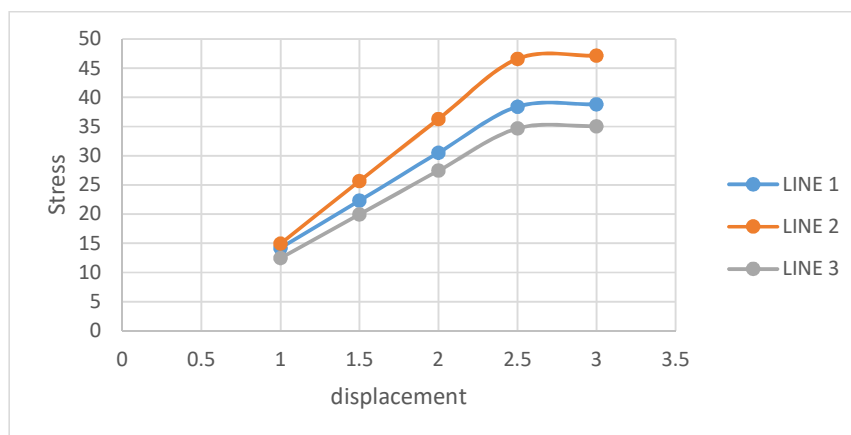


Figure 3.52. Stress-displacement curves along lines 1, 2 and 3 for model 2

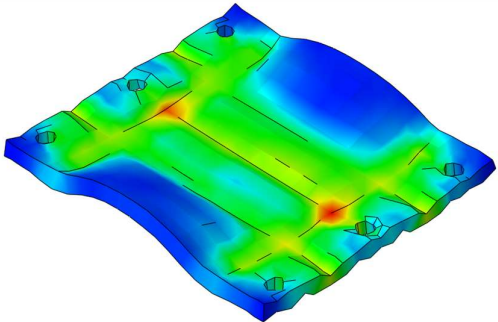
Comparing the stresses on the baseplate between model 1 and model 2, results shows that from model 1 to model 2 there is a reduction of stress in line 1 by 40.85% (54.6752 MPa to 38.8162 MPa), an increase in stress in line 2 by 9.8% (from 42.9116 MPa to 47.153 MPa) and a reduction in stress by 59.5% (from 55.9087 MPa to 35.0368 MPa). Globally, there is a reduction of stress from model 1 to model 2 by 26.8%. It can be conclusively said that; the Eurocode compliant baseplate is more efficient from a stress analysis point of view.

3.7.2. Prediction of possible failure mechanisms with respect to stress concentrations observed

3.7.2.1. Under axial loading condition

The subjection of the steel base plate to different axial loading conditions allows the observation of stress concentration points particularly at the flange-web intersection. The repetitive nature of these concentration points under the different axial loading conditions is considered as a validation of the stress diffusion path. From stress mechanics and studies, stress concentration points can be used as basis to predict the type of failure mechanism that shall be undergone. In table 3.57, the deformed shape under axial loading is portrayed with the possible failure mechanism explained.

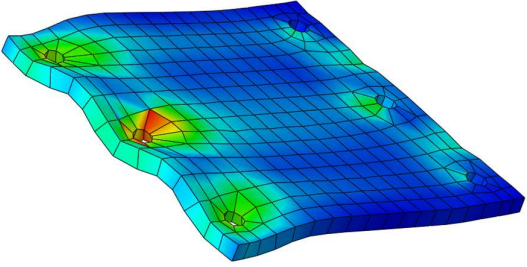
Table 3.57. Failure mechanisms under axial loads

Deformed shape	Failure mechanism
	<p>The deformation and stress concentration witnessed on this plate suggests that the first mechanisms of failure could be initiated by the local yielding of the base plate which is followed by the crushing of concrete due to the high compressive forces.</p>

3.7.2.2. Under bending condition

The subjection of the base plate under different bending moments display stress concentration points around anchor bolts found in the tensile region whose distribution follows a similar pattern for the different load cases. This repetitive pattern of stress distribution and stress concentration points serves as a basis for the estimation/determination of the possible failure mechanism. Table 3.58 presents the deformed shape of the base plate under bending condition.

Table 3.58. Failure mechanisms under bending moment

Deformed shape	Failure mechanism
	<p>The stress concentration on this plate suggests that the first mechanisms of failure could be initiated by anchor bolt pull out due to the tensile forces, particularly for the baseplate in model 1 where the stresses were more concentrated along the anchor bolts area. Also, this could lead to the tearing and yielding of the base plate at the tension side.</p>

Conclusion

The aim of this chapter was to present and interpret the results obtained from the static analysis and verification of the case study. More importantly, results and interpretations of the finite element analysis performed on the column base connection sub model were equally presented. Initially, the structural members within the considered case study were proven to be statically verified according to the Eurocode prescriptions. Then, results from the finite element analysis performed on the column base sub-model showed the stress diffusion on a steel base plate when subjected to axial and bending loading conditions. The FEM analysis performed served as a basis to obtain a pattern of stress distribution in the base plate whose validity was justifiable due to its repetitive nature at different loading magnitudes. The pattern obtained under axial loads were characterized by high stress concentrations range at the flange and web vicinity. The bending moment study expressed a resulting pattern with high stress concentrations at the tensile zone of the baseplate precisely at the vicinity of the anchor bolts. In conjunction to these,

***FEM ANALYSIS APPLIED TO THE STUDY OF STRESS
DIFFUSION IN THE BASEPLATES OF STEEL STRUCTURES***

a parametric study with respect to the thickness of the baseplate was performed; from this, it was observed that the von mises stress transmitted to the base plate increases with the reduction of the thickness after a certain threshold value. These stress patterns and stress concentrations were used as a basis for deciding the possible failure mechanism which shall incur on the base plate. Finally, the effect of the anchor bolt position on the stress diffusion was observed considering the initial and modified base plate. It could be observed that the redistribution of the stress is better in the base plate which is compliant with the Eurocode where the anchor bolts are closer to the flange of the IPE column.

GENERAL CONCLUSION

The main objective of this work was to perform by finite element method a study of the stress diffusion in base plates of steel structures. In order to achieve this objective, a study of the behavior of base plates and a review on past studies performed with respect to base plates was carried out. Then, followed the presentation of the research methodology, the static analysis and design of the different structural elements of the steel ware house. Three parametric studies were performed; axial load parametric study, bending moment parametric study and base plate thickness parametric study. In addition to this, the effect of the position of anchor bolts on the stress diffusion on base plates was also studied. The static analysis was performed on SAP 2000 and the stress study under which the parametric studies were performed was carried out in ABAQUS. The results of the parametric studies showed that; (1) The distribution of stress on a baseplate whose column is subjected to concentrated axial loads follows the same pattern without regard to the magnitude of the force. (2) The stress distribution on base plates have stress concentration points corresponding to the flange web intersection of the IPE column which receive about 93.3% of stress more than the averagely stressed zone. (3) The distribution of stress on a baseplate subjected to bending is highly dependent on the position of anchor bolts; The closer the anchor bolt is to the center of the base plate, the lower the average stress on the base plate and the more uniform it is distributed. It was observed that displacing the anchor bolts towards the center of the base plate by a distance of 11mm granted a reduction of stress of about 26.8%. (4) The thinner the base plate, the more stress is distributed on it.

With the results and observations made, an attempt to predict the mechanism of failure which will ensue with respect to the loading history was made. They are; (a) Crushing of the concrete base due to high compressive stresses, with the crushing initiated below the stress concentration points. (b) Anchor bolt pull out due to high tensile forces. (d) Possibility of tearing of the base plate at its edge especially when the edge distances of the anchor bolts are not compliant to the Eurocode or are too small.

In order to ensure an objective continuity of this study, the following perspectives are formulated; (i) Given that the study was centered on the stress diffusion on base plates, the study could be enhanced to studying the diffusion within the concrete base. (ii) Also, more studies should be made regarding design methodologies of base plates with stiffeners considering their position and geometry. This is because the presence or absence of a stiffener greatly affects the pattern of stress distribution. The method proposed by Marcin Gorski in his article entitled “Design procedure for steel column bases with stiffeners” could serve as a

starting point. (iii) Finally, the study was performed in a non-seismic zone. Investigation of the column base plate behavior considering seismic actions need to be performed,

BIBLIOGRAPHY

- Abdollahzadeh, G. R. and Ghobadi, F. (2013) 'Mathematical modeling of column-base connections under monotonic loading', *Civil Engineering Infrastructures journal*.
- Akiyama, H., Kurosawa, M., Wakuni, N., and Nishinura, I. (1984). Strength and Deformation of Exposed Type of Steel Column Bases. *Journal of Structural and Construction Engineering*.
- Akiyama, H., Yamada, S., Takahashi, M., Katsura, D., Kumura, K., and Yahata, S. (1998). Full Scale Shaking Test of the Exposed-Type Column Bases. *Journal of Structural and Construction Engineering*.
- Amaral, P. M. (2014) *Steel column bases under biaxial loading conditions*. University of Porto. American Institute of Steel Construction (1990) *Steel design guide series: Column base plates*.
- Astaneh, A., Bergsma, G., and Shen, J.H. (1992). Behavior and Design of Base Plates for Gravity, Wind and Seismic Loads. *Proceedings of the National Steel Construction Conference, Las Vegas, Nevada, AISC, Chicago, Illinois*.
- American Institute of Steel Construction (AISC). (2017). Load and Resistance Factor Design. *Manual of Steel Construction, 15th Ed., AISC, Chicago, Illinois*.
- Balut, N. and Moldovan, A. (1997). A Model for the Behavior of Column Base Connections. *Proceedings of the Second Conference STESSA, Kyoto, Japan*.
- Borzouie, J. (2016). Low Damage Steel Base Connections. *PhD Thesis, Department of Civil and Natural Resources Engineering, University of Canterbury, Christchurch, New Zealand*.
- Dewolf, J. T., and Sarisley, E. F. (1980). Column base plates with axial loads and moments. *ASCE Journal of Structural Division*.
- Ermopolous, J. C. and Stamatopoulos, G. N. (1996) 'Mathematical modelling of column baseplate connections', *Journal of Constructional Steel Research*.
- EN 1990. (2002). *Eurocode 0: Basis of structural design*.
- EN 1991-1-1. (2002). *Eurocode 1: Actions on structures — Part 1-1: General actions — Densities, self-weight, imposed loads for buildings*.
- EN 1991-1-4. (2002). *Eurocode 1: Actions on structures — Part 1-4: General actions — Windactions*.
- EN 1993-1-1. (2005). *Eurocode 3: Design of steel structures — Part 1-1: General rules and rules for buildings*.

EN 1993-1-2. (2005). *Eurocode 3: Design of steel structures — Part 1-2: General rules — Structural fire design.*

EN 1993-1-5. (2006). *Eurocode 3: Design of steel structures — Part 1-5: Plated structural elements.*

EN 1993-1-8. (2005). *Eurocode 3: Design of steel structures — Part 1-8: Design of joints.*

Fahmy, M., Stojadinovic, B., and Goel, S. C. (1999). Analytical and experimental behavior of steel column bases. *Proceedings of 8th Canadian Conference on Earthquake Engineering, Canadian Association for Earthquake Engineering, Ottawa, ON, Canada.*

Fahmy, M. (1999). Seismic Behavior of Moment-resisting Steel Column Bases. *Ph.D. Dissertation, Department of Civil and Environmental Engineering, University of Michigan, Ann Arbor, Michigan, USA.*

Fisher, J.M., and Kloiber, L.A. (2006). Design Guide 1: Base Plate and Anchor Rod Design. *2nd Ed. American Institute of Steel Construction (AISC), Chicago, USA.*

Grauvilardell, J.E., Lee, D., Hajjar, J.F., and Dexter, R.J. (2005). Synthesis of design, testing and analysis research on steel column base plate connections in high seismic zones. *Structural Engineering Rep. No. T-04-02, Dept. of Civil Engineering, University of Minnesota, Minneapolis, USA.*

Grilli, D.A., and Kanvinde, A.M. (2015). Embedded Column Base Connections Subjected to Flexure and Axial Load: Tests and Strength Models. *Final Report (3-11) University of California, Davis, CA, USA.*

Goldman, C. (1983). Design of Column Base Plates and Anchor Bolts for Uplift and Shear. *Structural Engineering Practice, 2.*

Gomez, I.R., Kanvinde, A., Smith, C., and Deierlein, G.G. (2009). Shear Transfer in Exposed Column Base Plates. *Technical Report submitted to the American Institute of Steel Construction (AISC), Chicago, USA.*

Gomez, I. R., Kanvinde, A. and Deierlein, G. G. (2010) *Exposed column base connections subjected to axial compression and flexure, Final Report AISC.* Chicago.

Guisse, S., Vandegans, D. and Jaspart, J. P. (1996) *Application of the component method to column bases - experimentation and development of a mechanical model for characterization, Report No. MT195.*

Heisinuo, M., Laine, V. and Lehtimaki, E. (2009) 'Enlargement of the component method into 3D', in *Nordic Steel Construction Conference 2009.*

Jacob Fish, Ted Belytschko - A first course in finite elements (2007, John Wiley & Sons Ltd).

Jaspart, J. P. and Vandegans, D. (1998). Application of Component Method to Column Bases. *Journal of Constructional Steel Research*.

Jaspart, J. P. (1990) *Étude de la semi-rigidité des noeuds poutre-colonne et son influence sur la résistance et la stabilité des ossatures en acier*. University of Liège.

Jaspart, J. P. (1997) *Recent advances in the field of steel joints column bases and further configurations for beam-to-column joints and beam splices*. University of Liège.

Jaspart, J. P. and Vandegans, D. (1998) 'Application of the component method to column bases', *Journal of Constructional Steel Research*.

Kanvinde, A.M., Jordan, S. J., and Cooke, R. J. (2013). Exposed column baseplate connections in moment frames—Simulations and behavioral insights. *Journal of Constructional Steel Research*.

Kanvinde, A.M., Grilli, D.A., and Zareian, F. (2012). Rotational stiffness of exposed column base connections - experiments and analytical models. *ASCE Journal of Structural Engineering*.

Kavoura, F. and Genvturk, B. (2018) 'Evaluation of existing provisions for design of pinned column base-plate connections', *Journal of Constructional Steel Research*.

Khodaie, S., Mohamadi-shooreh, M. R. and Mofid, M. (2012) 'Parametric analyses on the initial stiffness of the SHS column base plate connections using FEM', *Engineering Structures*.

Krishnamurthy, N. and Thambiratnam, D. P. (1990) 'Finite element analysis of column baseplates', *Computers & Structures*.

Kawano, A. and Matsui, C. (1998). On the Effect of Restoring Force Characteristics of ColumnBase on Inelastic Response Behavior of Weak-Beam Steel Frame under Earthquake GroundMotion. *Journal of Structural and Construction Engineering*.

Laura da Silva Seco, (2019) 'Column base plates under 3D loading. Structures', *INSA de Rennes, 2019*.

Lee, D. Y., Goel, S. and Stojadinovic, B. (2008a) 'Exposed column-base plate connections bending about weak axis: I. Numerical parametric study', *Steel Structures*.

Lee, D. Y., Goel, S. and Stojadinovic, B. (2008b) 'Exposed column-base plate connections bending about weak axis: II. Experimental study', *Steel Structures*.

- Lescouarc'h, Y. (1988) *Les pieds de poteaux encastrés en acier*. France: CTICM.
- Lim, W., Lee, D. Y. and You, Y. (2017a) 'Cyclic loading tests on exposed column-base plate weak-axis connections of small-size steel structures', *Engineering Structures*.
- Midorikawa, M., Nishiyama, I., Tada, M., and Terada, T. (2012). Earthquake and tsunami damage on steel buildings caused by the 2011 tohoku japan earthquake. *International Symposium on Engineering Lessons Learned from the 2011 Great East Japan Earthquake, March. Tokyo, Japan*.
- Márai, P. *et al.* (2014) 'Resistance model for fixed column bases', in *EUROSTEEL*. Naples.
- O. C. Zienkiewicz, R. L. Taylor and J.Z. Zhu (Auth.) - *The Finite Element Method_ its Basis and Fundamentals* (2013, Butterworth-Heinemann).
- Picard, A. and Beaulieu, D. (1985) 'Behavior of a simple column base connection', *Canadian Journal of Civil Engineering*.
- Picard, A., Beaulieu, D., and Perusse, B. (1987). Rotational Restraint of a Simple Column Base Connection. *Canadian Journal of Civil Engineering*.
- Sato, K. (1987). A Research on the Aseismic Behavior of Steel Column Base for Evaluating Its Strength Capacity and Fixity. *Report No. 69, Kajima Institute of Construction Technology, Tokyo, Japan*.
- Simões da Silva, L. (2008) 'Towards a consistent design approach for steel joints under generalized loading', *Journal of Constructional Steel Research*.
- Simões da Silva, L. and Santiago, A. (2003) *Manual de ligações metálicas*.
- Stamatopoulos, G. N. and Ermopolous, J. C. (1997) 'Interaction curves for column base plate connections', *Journal of Constructional Steel Research*.
- Stamatopoulos, G. N. and Ermopolous, J. C. (2011) 'Experimental and analytical investigation of steel column bases', *Journal of Constructional Steel Research*.
- Thambiratnam, D.P., Paramasivam, P. (1986). Base Plates under Axial Loads and Moments. *Journal of Structural Engineering*.
- Tronzo, T. M. (1984). Design of Heavy Steel Column Bases: Handling Forces- Some Practical Procedures. *Structural Engineering Practice, 2*.
- Wald, F. and Jaspert, J. (1998). Stiffness Design of Column Bases. *Journal of Constructional Steel Research*.

Wald, F., Sokol, Z., and Steenhuis, M. (1995). Proposal of the Stiffness Design Model of the Column Bases. *Proceedings of the Third International Workshop on Connections in Steel Structures, Trento, Italy.*

Wald, F. (1995) *Patky Sloupù - Column bases.* CVUT Praha.

Wald, F., Sokol, Z. and Steenhuis, M. (2000) *Proposal of the stiffness design of column bases, COST Project C1.*

Yamada, S. and Akiyama, H. (1997). Influence of the Rigidity of Column Bases on the Ultimate Earthquake Resistance of Multi-Story Steel Moment Frames. *Journal of Structural and Construction Engineering.*

ANNEXES

Annex 1: Comprehensive summary of column base connection studies

Investigator	Year	Loading Type	Number of Tests	Main Test Parameters	Main Failure Modes
Akiyama et al.	1984	Axial moment (cyclic)	5	End detail and depth of anchor rod Shape of column and base plate	Concrete crushing Anchor rod pull-out
Thambiratnam & Paramasivam	1986	Axial plus moment (from eccentricity)	12	Base plate thickness Eccentricity of axial load	Concrete block failure Base plate yielding Anchor rod yielding
Picard & Beaulieu	1987	Axial plus moment	14	Shape of column Base plate area and thickness Number of anchors	Column buckling in the direction of weak axis
Sato	1987	Axial plus moment (cyclic)	6	Size of base plate Column axial load Yield strength of anchor rod	Anchor rod fracture Concrete failure Anchor rod yielding
Hon & Melchers	1988	Axial plus moment (from eccentricity)	26	Base plate thickness Anchor rod size	Anchor rod failure Base plate yielding
Astaneh et al.	1992	Axial plus moment (cyclic)	6	Base plate thickness Column axial load	Column and plate yielding Rod and weld fracture Grout crushing
Igarashi et al.	1992	Moment (cyclic)	4	Type of anchor rod	Concrete riser and grout cracking and crushing Anchor rod yielding
Melchers	1992	Moment (cyclic)	10	Base plate thickness Number and size of anchor rod Anchor rod yield strength	Base plate yielding Anchor rod yielding
Targowski et al.	1993	Moment	12	Column section Base plate thickness	Base plate yielding Anchor rod elongation

**FEM ANALYSIS APPLIED TO THE STUDY OF STRESS
DIFFUSION IN THE BASEPLATES OF STEEL STRUCTURES**

Kallolil et al	1998	Axial plus moment (from eccentricity)	3	Anchor bolt size Base plate thickness Ratio of the moment to the axial load	Yielding and fracture of anchor rods Yielding of base plate
Akiyama et al.	1998	Moment (shaking table)	2	Base plate thickness	Anchor rod elongation Base plate yielding
Jaspart & Vandegans	1998	Axial plus moment	12	Base plate thickness Number of anchor rods	Failure of anchor rod and concrete Yielding of base plate and column
Burda & Itani	1999	Axial plus moment	12	Base plate area Base plate thickness	Fracture of the weld between column and base plate
Fahmy	1999	Moment (cyclic)	3	Number of anchor rods Weld material	Fracture of the weld between column and base plate
Adany et al.	2000	Moment (cyclic)	5	End-plate thickness Anchor bolt pretensioning	Base plate yielding Anchor rod yielding Column local buckling
Li et al.	2000	Axial plus moment (cyclic)	7	Column section Concrete filing Anchor rod strength	Anchor rod yielding Buckling of steel tube
Lee & Goel	2001	Moment (cyclic)	4	Number of anchor rods Weld material	Fracture of the weld between column and base plate
Miyasaka et al.	2001	Moment	8	Base plate thickness Location of anchor rods	Base plate deformation and yielding
Liu	2001	Moment	8	Base plate thickness Number of anchor rods	Plate yielding Anchor yielding
Somiya et al.	2002	Axial and moment	12	Different initial axial load and load rate Plate and tube thickness	Base plate yielding Anchor rod yielding
Takamatsu & Tamai	2005	Axial plus moment (cyclic)	9	Number of anchor rods Level of axial load	Yielding of anchor rods

**FEM ANALYSIS APPLIED TO THE STUDY OF STRESS
DIFFUSION IN THE BASEPLATES OF STEEL STRUCTURES**

				Moment application (monotonic/cyclic) Use of wedge device	
Kim et al.	2007	Axial plus moment (cyclic)	9	Number of anchor rods full scale frame	Plastic hinging at column top Inelastic flexural- torsional buckling.
Di Sarno et al.	2007	Axial plus moment	4	Axial load level Connection type	Fracture of anchor bolts Plastic hinging of column
Lee et al.	2008	Moment (cyclic)	4	Number of anchor bolt Relative strength between base plate & anchor rod Weld detail	Plastic hinging of column Weld failure
Myers et al.	2009	Moment (cyclic)	5	Weld detail Loading history	Weld failure
Cui et al.	2009	Axial plus moment	8	Column embedment type	Fracture of anchor bolts
Gomez et al.	2009	(1) Moment (monotonic/ cyclic) (2) Axial plus moment (cyclic)	7	Number of anchor rods Anchor rod strength Base plate thickness Level of axial load Cyclic/monotonic moment	Anchor rod yielding and fracture Grout crushing Plate yielding
Kanvinde et al.	2012	Axial load plus moment	9	Base plate size & thickness Axial load level level Anchor rod dimension Column size	Base plate yielding Anchor rod yielding
Kanvinde et al.	2013	Axial load plus moment	6	Base plate thickness Axial load ratio Moment	Base plate yielding Anchor rod yielding
Choi & Choi	2013	Axial load plus moment	14	Base plate thickness Uniaxial & cyclic moment	Base plate yielding Anchor rod yielding
Trautner et al.	2015	Cyclic load	8	Anchor rod selection	Crack in grout &

**FEM ANALYSIS APPLIED TO THE STUDY OF STRESS
DIFFUSION IN THE BASEPLATES OF STEEL STRUCTURES**

				Setting arrangement Stretch length	concrete Base plate yielding Anchor rod yielding
Shaheen et al.	2017	Lateral load	-	Grout thickness	Crack in grout Anchor rod yielding
Fasaee et al.	2018	Axial load plus biaxial bending	7	Base plate thickness Biaxial moment	Base plate yielding Anchor rod yielding
Trautner & Hutchinson	2018	Axial & Lateral load	6	Number of anchor rods Anchor rod size Base plate thickness Cyclic/monotonic moment	Base plate yielding Anchor rod yielding
Elkady & Lignos	2018	Axial load plus uniaxial/biaxial bending	10	Column section Loading protocol	Local buckling & axial shortening of column Plastic hinge formation near column base

Annex 2: Building usage categories

Table 6.1 - Categories of use

Category	Specific Use	Example
A	Areas for domestic and residential activities	Rooms in residential buildings and houses; bedrooms and wards in hospitals; bedrooms in hotels and hostels kitchens and toilets.
B	Office areas	
C	Areas where people may congregate (with the exception of areas defined under category A, B, and D ¹⁾)	<p>C1: Areas with tables, etc. e.g. areas in schools, cafés, restaurants, dining halls, reading rooms, receptions.</p> <p>C2: Areas with fixed seats, e.g. areas in churches, theatres or cinemas, conference rooms, lecture halls, assembly halls, waiting rooms, railway waiting rooms.</p> <p>C3: Areas without obstacles for moving people, e.g. areas in museums, exhibition rooms, etc. and access areas in public and administration buildings, hotels, hospitals, railway station forecourts.</p> <p>C4: Areas with possible physical activities, e.g. dance halls, gymnastic rooms, stages.</p> <p>C5: Areas susceptible to large crowds, e.g. in buildings for public events like concert halls, sports halls including stands, terraces and access areas and railway platforms.</p>
D	Shoppings areas	<p>D1: Areas in general retail shops</p> <p>D2: Areas in department stores</p>
<p>¹⁾ Attention is drawn to 6.3.1.1(2), in particular for C4 and C5. See EN 1990 when dynamic effects need to be considered. For Category E, see Table 6.3</p> <p>NOTE 1 Depending on their anticipated uses, areas likely to be categorised as C2, C3, C4 may be categorised as C5 by decision of the client and/or National annex.</p> <p>NOTE 2 The National annex may provide sub categories to A, B, C1 to C5, D1 and D2</p> <p>NOTE 3 See 6.3.2 for storage or industrial activity</p>		

Table 6.3 -Categories of storage and industrial use

Category	Specific use	Example
E1	Areas susceptible to accumulation of goods, including access areas	Areas for storage use including storage of books and other documents.
E2	Industrial use	

Annex 3: Safety factors for permanent and variable actions

Table A2.4(A) - Design values of actions (EQU) (Set A)

Persistent and transient design situation	Permanent actions		Prestress	Leading variable action (*)	Accompanying variable actions (*)	
	Unfavourable	Favourable			Main (if any)	Others
(Eq. 6.10)	$\gamma_{G,\text{sup}} G_{k,j,\text{sup}}$	$\gamma_{G,\text{inf}} G_{k,j,\text{inf}}$	$\gamma_p P$	$\gamma_{Q,1} Q_{k,1}$		$\gamma_{Q,i} \psi_{0,i} Q_{k,i}$
(*) Variable actions are those considered in Tables A2.1 to A2.3.						
NOTE 1 The γ values for the persistent and transient design situations may be set by the National Annex.						
<p>For persistent design situations, the recommended set of values for γ are:</p> <p>$\gamma_{G,\text{sup}} = 1,05$ $\gamma_{G,\text{inf}} = 0,95^{(1)}$ $\gamma_Q = 1,35$ for road and pedestrian traffic actions, where unfavourable (0 where favourable) $\gamma_Q = 1,45$ for rail traffic actions, where unfavourable (0 where favourable) $\gamma_Q = 1,50$ for all other variable actions for persistent design situations, where unfavourable (0 where favourable). ψ_0 = recommended values defined in the relevant design Eurocode.</p> <p>For transient design situations during which there is a risk of loss of static equilibrium, $Q_{k,1}$ represents the dominant destabilising variable action and $Q_{k,i}$ represents the relevant accompanying destabilising variable actions.</p> <p>During execution, if the construction process is adequately controlled, the recommended set of values for γ are:</p> <p>$\gamma_{G,\text{sup}} = 1,05$ $\gamma_{G,\text{inf}} = 0,95^{(1)}$ $\gamma_Q = 1,35$ for construction loads where unfavourable (0 where favourable) $\gamma_Q = 1,50$ for all other variable actions, where unfavourable (0 where favourable)</p>						

Annex 4: Recommended values of Ψ factors for buildings

Table A1.1 - Recommended values of ψ factors for buildings

Action	ψ_0	ψ_1	ψ_2
Imposed loads in buildings, category (see EN 1991-1-1)			
Category A : domestic, residential areas	0,7	0,5	0,3
Category B : office areas	0,7	0,5	0,3
Category C : congregation areas	0,7	0,7	0,6
Category D : shopping areas	0,7	0,7	0,6
Category E : storage areas	1,0	0,9	0,8
Category F : traffic area, vehicle weight $\leq 30\text{kN}$	0,7	0,7	0,6
Category G : traffic area, $30\text{kN} < \text{vehicle weight} \leq 160\text{kN}$	0,7	0,5	0,3
Category H : roofs	0	0	0
Snow loads on buildings (see EN 1991-1-3)*			
Finland, Iceland, Norway, Sweden	0,70	0,50	0,20
Remainder of CEN Member States, for sites located at altitude $H > 1000$ m a.s.l.	0,70	0,50	0,20
Remainder of CEN Member States, for sites located at altitude $H \leq 1000$ m a.s.l.	0,50	0,20	0
Wind loads on buildings (see EN 1991-1-4)	0,6	0,2	0
Temperature (non-fire) in buildings (see EN 1991-1-5)	0,6	0,5	0
NOTE The ψ values may be set by the National annex. * For countries not mentioned below, see relevant local conditions.			

Annex 5: Classification of steel cross section

Table 5.2 (sheet 1 of 3): Maximum width-to-thickness ratios for compression parts

Internal compression parts						
Class	Part subject to bending	Part subject to compression		Part subject to bending and compression		
1						
	$c/t \leq 72\varepsilon$	$c/t \leq 33\varepsilon$	when $\alpha > 0,5$: $c/t \leq \frac{396\varepsilon}{13\alpha - 1}$ when $\alpha \leq 0,5$: $c/t \leq \frac{36\varepsilon}{\alpha}$			
2						
	$c/t \leq 83\varepsilon$	$c/t \leq 38\varepsilon$	when $\alpha > 0,5$: $c/t \leq \frac{456\varepsilon}{13\alpha - 1}$ when $\alpha \leq 0,5$: $c/t \leq \frac{41,5\varepsilon}{\alpha}$			
3						
	$c/t \leq 124\varepsilon$	$c/t \leq 42\varepsilon$	when $\psi > -1$: $c/t \leq \frac{42\varepsilon}{0,67 + 0,33\psi}$ when $\psi \leq -1^*)$: $c/t \leq 62\varepsilon(1 - \psi)\sqrt{-\psi}$			
$\varepsilon = \sqrt{235/f_y}$	f_y	235	275	355	420	460
	ε	1,00	0,92	0,81	0,75	0,71

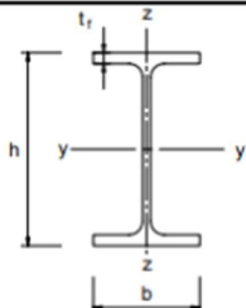
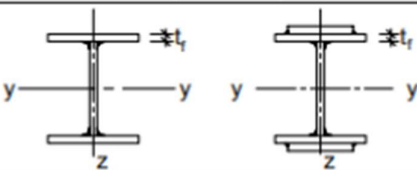

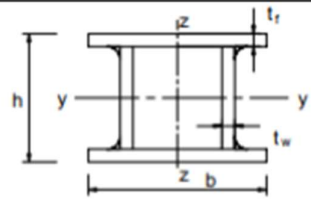
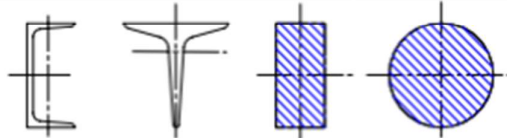

*) $\psi \leq -1$ applies where either the compression stress $\sigma \leq f_y$ or the tensile strain $\varepsilon_y > f_y/E$

Annex 6: Imperfection factor and buckling curve's selection tables

Table 6.1: Imperfection factors for buckling curves

Buckling curve	a_0	a	b	c	d
Imperfection factor α	0,13	0,21	0,34	0,49	0,76

Table 6.2: Selection of buckling curve for a cross-section

Cross section	Limits	Buckling about axis	Buckling curve		
			S 235 S 275 S 355 S 420	S 460	
Rolled sections 	$h/b > 1,2$	y-y z-z	$t_f \leq 40$ mm	a b	a_0 a_0
			$40 < t_f \leq 100$	b c	a a
	$h/b \leq 1,2$	y-y z-z	$t_f \leq 100$ mm	b c	a a
			$t_f > 100$ mm	d d	c c
Welded I-sections 	$t_f \leq 40$ mm	y-y z-z	b c	b c	
	$t_f > 40$ mm	y-y z-z	c d	c d	
Hollow sections 	hot finished	any	a	a_0	
	cold formed	any	c	c	
Welded box sections 	generally (except as below)	any	b	b	
	thick welds: $a > 0,5t_f$ $b/t_f < 30$ $h/t_w < 30$	any	c	c	
U-, T- and solid sections 		any	c	c	
L-sections 		any	b	b	

Annex 7: Effective length of the T-stub

Bolt-row Location	Bolt-row considered individually		Bolt-row considered as part of a group of bolt-rows	
	Circular patterns $\ell_{\text{eff,cp}}$	Non-circular patterns $\ell_{\text{eff,nc}}$	Circular patterns $\ell_{\text{eff,cp}}$	Non-circular patterns $\ell_{\text{eff,nc}}$
Inner bolt-row	$2\pi m$	$4m + 1,25e$	$2p$	p
End bolt-row	The smaller of: $2\pi m$ $\pi m + 2e_1$	The smaller of: $4m + 1,25e$ $2m + 0,625e + e_1$	The smaller of: $\pi m + p$ $2e_1 + p$	The smaller of: $2m + 0,625e + 0,5p$ $e_1 + 0,5p$
Mode 1:	$\ell_{\text{eff,1}} = \ell_{\text{eff,nc}}$ but $\ell_{\text{eff,1}} \leq \ell_{\text{eff,cp}}$		$\sum \ell_{\text{eff,1}} = \sum \ell_{\text{eff,nc}}$ but $\sum \ell_{\text{eff,1}} \leq \sum \ell_{\text{eff,cp}}$	
Mode 2:	$\ell_{\text{eff,2}} = \ell_{\text{eff,nc}}$		$\sum \ell_{\text{eff,2}} = \sum \ell_{\text{eff,nc}}$	

Annex 8: Real view of the column base connection

